UNIVERSITY OF SOUTHAMPTON

UNSHIELDED APPLICATIONS OF HIGH TEMPERATURE SUPERCONDUCTING QUANTUM INTERFERENCE DEVICES.

By Gordon Macmillan.

Submitted for the qualification of Master of Philosophy.

Physics Department, Faculty of Science.

August 2001.

UNIVERSITY OF SOUTHAMPTON

ABSTRACT

FACULTY OF SCIENCE

PHYSICS

Master of Philosophy

UNSHIELDED APPLICATIONS OF HIGH TEMPERATURE SUPERCONDUCTING QUANTUM INTERFERENCE DEVICES.

By Gordon Macmillan.

We have tested the performance of several different SQUID magnetometers in both laboratory and field environments. The performance was compared to that of other magnetic field measurement devices.

This thesis describes the principle of operation of the SQUID magnetometer. It also explains some principles behind other types of magnetic field measuring devices. The differences between magnetometer and gradiometer are also explained.

Many potential and existing applications for the high temperature SQUID magnetometer are discussed. The report pays particular attention to the applications of deep sea magnetometry, land mine detection and geophysical prospecting.

A chapter is devoted to the issue of noise. Both intrinsic sensor noise and external ambient noise are discussed in detail.

During the project many pieces of equipment were designed, fabricated and developed. Description is given of the various sensor holders and cryostats that were constructed along with the electrical circuits that were designed to collect and process data.

Experimental data confirmed the magnetically shielded specification of the sensors that were supplied. The unshielded performance was measured and compared to the shielded performance. Experiments were also carried out to detect land mines and make geophysical prospecting measurements.

The research confirmed the potential of a high temperature SQUID for the application in geophysical prospecting. It was concluded that further research should be conducted to assess the suitability of this technique for future application.

Thankyou to my supervisor, Peter de Groot, and all the staff at the University of Southampton who provided me with the wonderful opportunity that is higher education.

My heartfelt thanks thanks go out to all those who helped me through the highs and the lows of my university career – you know who you are.

'Always look on the bright side of life'

The work contained in this thesis is the result of research undertaken mainly by the author whilst in registered postgraduate candidature. Collaboration with the University of Wales Swansea was undertaken for the field tests in south Wales. The collaboration consisted of the sharing of equipment to gather data and perform geomagnetic measurements.

CONTENTS

1. INTRODUCTION.

The SQUID was discovered in the 1960s after the discovery of the Josephson junction. The low temperature SQUID required liquid helium as coolant to operate. Since the discovery of the SQUID, many applications have been found for the device, from aircraft wheel testing to brain wave studies. This project began with the aim of finding new applications for the relatively new high temperature superconducting quantum interference devices, which require the easier to handle coolant, liquid nitrogen. During the research, particular attention was paid to applications in a magnetically non-shielded environment.

The following report begins with an explanation of the different types of SQUID that are available and their construction. Description is also given of some of the principles of operation. The difference between magnetometer and gradiometer are discussed. Several potential and existing unshielded applications are discussed, including deep sea surveying, geophysical prospecting and biomagnetometry.

There are many different types of magnetic field measurement devices. These are discussed in some detail, beginning with the high temperature SQUID and followed by the low temperature SQUID. The commercially successful fluxgate magnetometer is discussed in context of its operation and performance in comparison to the SQUID magnetometer. Other high precision magnetometers that are discussed include the proton precession, optically pumped magnetometers, hall probe and induction coils.

The research concentrated on obtaining the measurement resolution of a SQUID magnetometer. All magnetometers are limited by the noise that is generated, both internally and externally. Chapter 5 is used to discuss the different aspects and issues that surround the subject of noise. Many techniques that may be used to minimise noise are discussed in this chapter.

During the project many pieces of apparatus were designed constructed and tested. Cryostats, sensor holders and a Helmholtz coil were built during the project. Electronic circuits were designed to reduce noise and increase sensitivity. Analysis was made of analogue to digital converters and electronic filters that were used in the collection of data. Methods used for data processing, calculation and manipulation are explained in chapter 6.

Many tests were conducted with seven different magnetometers during the project. Calibration tests in magnetic shielding were conducted to confirm the specifications of the various sensors used in the project. Tests were then conducted in an unshielded environment within a park in the city of Southampton. This lent familiarity to working in an unshielded environment. The research concludes in chapter 7 with several geophysical prospecting runs in the remote environment of the Gower in west Wales.

At the end of the project several SQUID sensors had been tested for their specification in the laboratory. The experience gained from these tests enabled the system to be modified for portable use in the unshielded environment. Further experience was gained with field operation, culminating in geophysical measurements being made with a high temperature superconducting SQUID.

Although conclusive results were not obtained in the geophysical measurements, the SQUID system showed great promise. As a result this research has provided the basis from which further development in SQUID applications may progress.

CHAPTER 2.

2. THE SQUID

2.1. INTRODUCTION

The purpose of this chapter is to give an overview of how the SQUID works, its history and development. Because an intimate knowledge of how a SQUID works is not critical for this project the emphasis will always be kept towards an air of practical application. The electronic circuits that form a working magnetometer will also be mentioned in the context of system integration. The many different types of high T_c SQUID magnetometer and their construction will also be discussed.

2.2. HISTORY OF THE SQUID

Since superconductivity was first observed in 1911 when a sample of mercury lost all measurable resistance at 4.2 K people have searched for new and useful devices to create from superconducting materials. The SQUID is a result of such research and has shown itself to be one of the most popular small-scale superconducting devices discovered to date. It was twenty years after the discovery of superconductivity before the Meissner effect was discovered. The Meissner effect is crucial in the working of a SQUID and involves the expelling of magnetic flux from penetrating the body of the superconductor when it is in the superconducting state. Another integral aspect of SQUID operation, that was not predicted until 1950, was that of flux quantisation, observation of which had to wait until 1961. It was a few years later that the Josephson effect was predicted and experimentally verified, and hence the Josephson junction was born. SQUIDs were first studied in the mid-1960's soon after the first Josephson junctions were made [2.1]. The 1960's were a time of great progress in the world of superconductivity because practical and useful superconducting wire became commercially available, allowing

superconducting magnets to be made. But it was not until 1986 that the next step forward occurred in the field when a new class of 'high' temperature superconductors was discovered. These new superconductors facilitated the use of liquid nitrogen as coolant, a cryogen that is a lot cheaper, a lot more efficient and easier to handle than the previously used liquid helium. This very brief history plots the progress made to allow the discovery of the modern day high T_c SQUIDs that are presently in use.

In the simplest definition, a SQUID is a flux to voltage transducer. For a given change in magnetic flux incident upon the SQUID ring there is a corresponding change in the voltage output from the SQUID. A SQUID obtains its record of being the most sensitive detector of any kind by taking advantage of three quantum mechanical effects:

1. Superconductivity
2. The Josephson junction
3. Flux quantisation

Before the discovery of high temperature superconductivity it was estimated that the maximum possible temperature for superconductivity would be about 30 K before the Cooper pairs would break up. Hence it was a great surprise in 1986 when possible high temperature superconductivity was published by Bednorz and Muller [2.2] in a new class of copper oxide material. A whole new class of high temperature superconducting materials was discovered, having critical temperatures above the all-important threshold of 77 K, the boiling point of liquid nitrogen. BCS theory does not explain high temperature superconductivity, and to date none of the many theories proposed to explain high temperature superconductivity have been generally accepted.

The next quantum mechanical effect that is exploited in the SQUID is the Josephson effect. Brian Josephson was working at the University of Cambridge as a research student when he predicted the effect that was subsequently named after him. Consider two superconductors separated by a thin insulating layer, which will act as a barrier to the conduction electrons. The wave function associated with the Cooper pairs is able to 'leak' into this region from each side. As long as the barrier is thin enough, the two wave functions will overlap, if they overlap sufficiently, the phases of the two wave functions

lock together. Under these conditions, Cooper pairs can tunnel through the barrier without being broken up. The net effect of this is that the insulating region acts as a superconductor, but with a much lower critical current than the regions either side of it.
The Josephson effect can take two forms, depending on the current flowing across the junction. The first, the dc Josephson effect occurs when the current across the junction is below its critical level. The other effect is the ac Josephson effect, where a voltage is generated across the junction because the current is now above the critical current of the junction, but below that of the superconducting sandwich either side. Josephson showed:

$$I = I_c \sin(\Phi_2 - \Phi_1)$$

Where $\Phi_2 - \Phi_1$ is the quantum mechanical phase difference across the junction.

Flux quantisation is the third quantum mechanical phenomenon exploited in the SQUID. Flux quantisation stems from the discrete energy levels that are allowed in nature. Just as there are discrete energy levels available to an electron in orbit around the nucleus, there are discrete amounts of magnetic flux that are allowed to exist in nature. This effect can be observed on a macroscopic scale in a superconducting ring. If a current flows around the ring, it will produce a magnetic field inside the ring. The magnetic flux (magnetic field times area) in the ring has to take a specific value, i.e. it cannot take any arbitrary value: it must take an integral number of flux quanta. The value of the flux quantum being, $\Phi_o = h/2e = 2.07\times10^{-15}$ Wb. A SQUID is able to detect the effect from a magnetic flux the magnitude of a millionth of a flux quantum or less.

2.3. PRINCIPLE OF OPERATION

The physical make up of a dc SQUID is rather simple in design, as previously stated it consists of two Josephson junctions connected in parallel on a closed superconducting loop. Figure 2.1 shows the schematic layout of a dc SQUID. The output voltage of the SQUID is a periodic function of the applied magnetic flux, going through one complete cycle for every flux quantum applied. Whilst it would be possible to obtain a reasonably

sensitive measure of magnetic field change just by counting the number of flux quanta leaving or entering the SQUID ring, the addition of control electronics that interpolate between whole numbers of flux quanta increases the sensitivity. It is important to note the point that was made in the last sentence, that is, a SQUID only measures the change in magnetic field. Hence if the magnitude of the field were required then it would be necessary to zero the SQUID in a known field and count the number of flux quanta entering or leaving from there. This gives the SQUID the advantage of having a dynamic range that is only limited by the number of times the scale is reset.

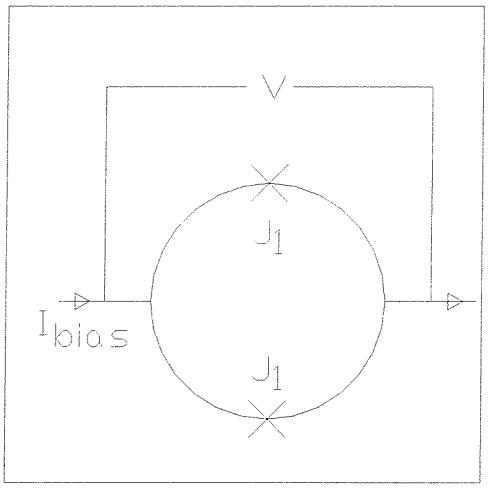

Figure 2.1. Schematic representation of a SQUID.

The SQUID ring is biased with a constant current across it. If the two Josephson junctions are identical then the current will divide equally across them as it travels through the ring. A superconducting current will flow through the SQUID so long as the total current flowing does not exceed the critical current of the two junctions combined. This implies that if each Josephson junction remains superconducting up until 10 μA, then a total of 20 μA can be passed through the SQUID ring with superconductivity still being maintained. The value of 20 μA thus becomes the critical current (I_c) of the SQUID. The critical current of the SQUID is measured in practice by increasing the current across the Josephson junctions until a voltage develops across the SQUID. A

current voltage plot of this behaviour is shown in figure 2.2. There is the characteristic flat region in which the SQUID is still superconducting and the knees that show the point at which a voltage develops across the SQUID (current moving in both positive and negative directions.)

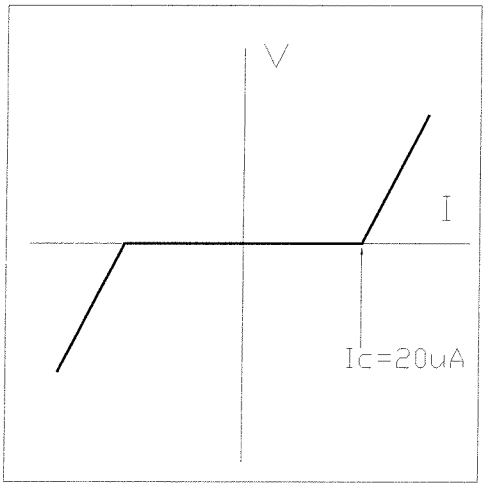

Figure 2.2. I-V characteristic of a DC SQUID.

If a magnetic field is applied to the SQUID ring when it is biased at a level below its critical current, screening currents are set up within the body of the superconducting material. The screening current (I_s) acts to oppose the effect of the magnetic field. This has the effect of adding to the bias current within the body of the SQUID ring, as seen in figure 2.3. The screening current creates a magnetic field equal and opposite to the applied field, effectively cancelling out the flux in the ring. This applied magnetic field has the effect of lowering the critical current of the SQUID itself. As the screening current now adds to the bias current flowing through one of the Josephson junctions, this lowers the total bias current that can be passed through the SQUID before a voltage is produced. When the magnetic flux incident upon the SQUID ring is increased to the point at which the effect of half a flux quantum is present within the SQUID ring an interesting event takes place. When the ring reaches half a flux quantum it is no longer energetically favourable for the screening currents to shield the ring from the incident flux. In fact the screening current changes direction and allows a flux quantum to enter

the SQUID ring. Figure 2.4 shows a graph of how this effect would develop over several flux quanta entering the SQUID loop. Hence it can be seen that the screening current changes direction at every half a flux quantum and reaches zero at every whole number of flux quanta.

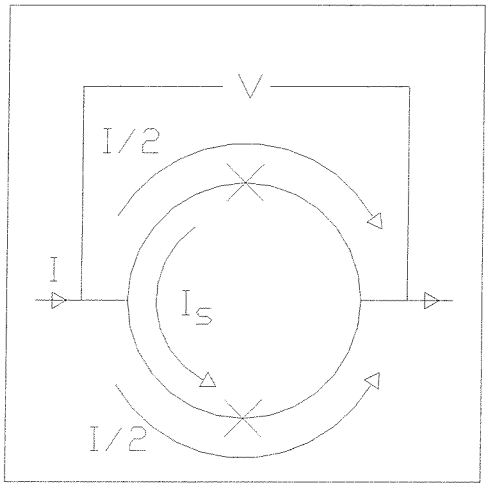

Figure 2.3. Creation of screening currents due to the addition of a magnetic field.

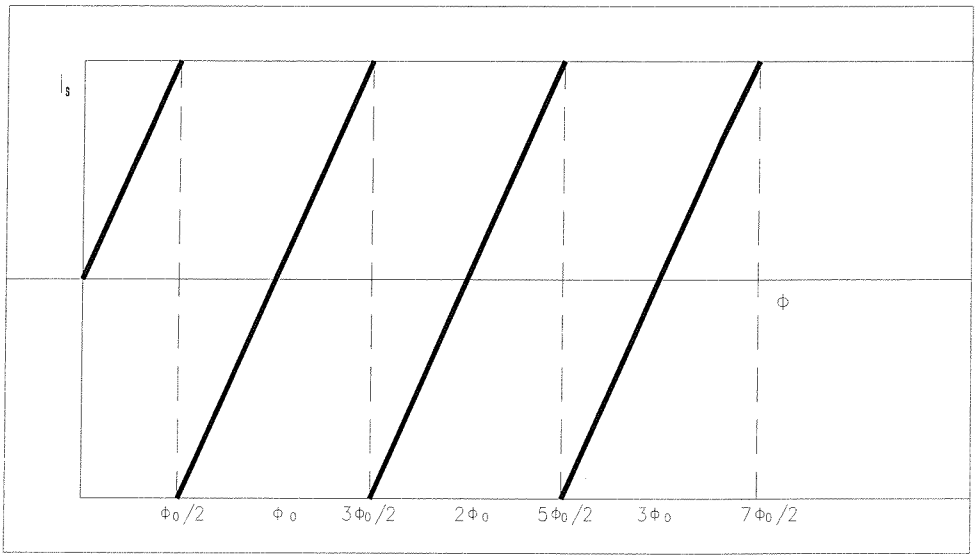

Figure 2.4. Dependence of screening current upon applied magnetic field.

Two main facts have been established so far.

1. The screening current of the SQUID is periodic in the applied flux
2. The critical current of the SQUID depends on the screening current

Hence a further point can be implied from points 1 and 2.

3. The SQUIDs critical current is also periodic in the applied magnetic flux.

Hence the critical current goes through a maximum when the applied magnetic flux is an integer multiple of a flux quantum, I_s is a minimum. It correspondingly goes through a minimum when the applied flux is an integer multiple plus one half of a single flux quantum, I_s is a maximum. As a result of these two states the I-V curve can be modified to that of figure 2.5 in which the applied current to produce a voltage changes depending on magnetic flux present.

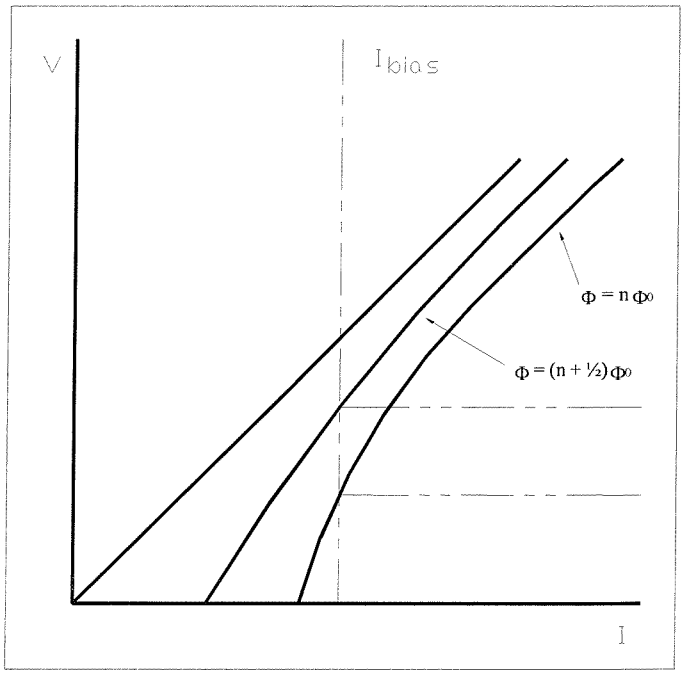

Figure 2.5. Modified I-V curve due to applied current.

An actual magnetometer, is operated with the bias current at a level above the critical current of the Josephson junctions to ensure they are permanently resistive. Under these conditions there is a periodic relationship between the voltage across the SQUID and the applied magnetic flux, with a period of one flux quantum. It is possible to note from figure 2.5 that at constant bias current the voltage across the SQUID is at a maximum when the critical current is at a minimum, and vice versa. The corresponding relationship between flux input and the voltage output can be viewed in figure 2.6.

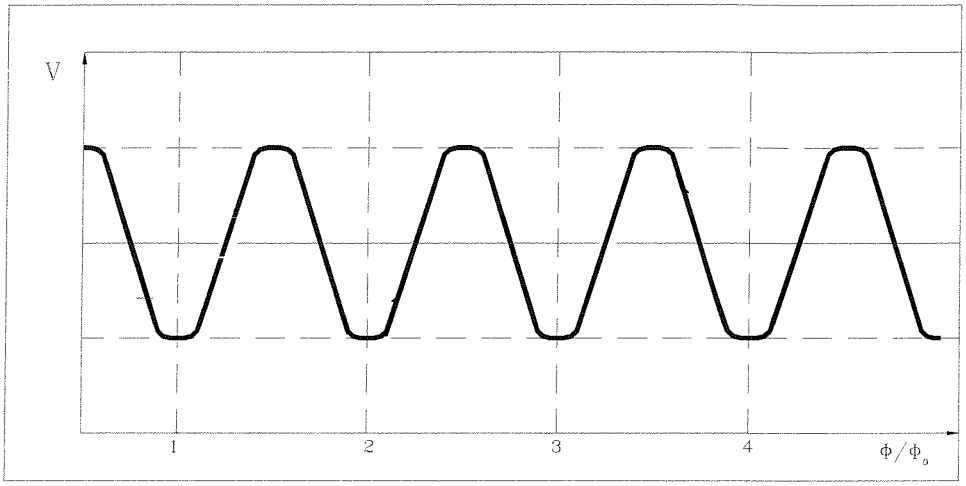

Figure 2.6. Periodic relationship between voltage and applied flux.

Although the model presented here is by no means rigorous it presents the main aspects of how a SQUID works. The main weakness of the model is that it does not really convey the phenomenon of quantum interference. Figure 2.6 shows the variation of critical current with applied flux as an interference pattern analogous to an optical interference pattern. If light is shone through two slits on to a screen it is possible to view a pattern of maxima and minima of intensity because the two sources of light interfere with each other. If a current is passed through a dc SQUID then maxima and minima of critical current can be observed as the incident flux is raised and lowered, because the macroscopic quantum wave functions at the two junctions interfere with each other.

It is not necessary to measure a whole period in the SQUID modulation to perform a flux measurement. Accurate measurement of a small fraction of a flux quantum is possible. This is achieved by biasing the SQUID to a point in figure 2.6 where $dV/d\Phi$ is at its steepest slope, to maximise the output voltage for minimum input magnetic flux change. A SQUID is usually operated in a flux-locked mode, where an external coil is used to generate a magnetic field in such a manner as to keep the total flux through the SQUID loop constant. The current required to keep the SQUID loop at a constant level is measured and calibrated to correspond to the value of the incident magnetic flux.

2.4. SQUID ELECTRONICS

2.4.1. FLUX LOCKED SQUID

Most practical applications use the SQUID in a feedback circuit as a null detector of magnetic flux. As stated in section 2.3, a SQUID can be operated in a flux locked loop (FLL), and as all work in this project was carried out with a FLL it is worthy of some explanation as to its general construction and operation. A schematic representation of a flux locked loop can be seen figure 2.7.

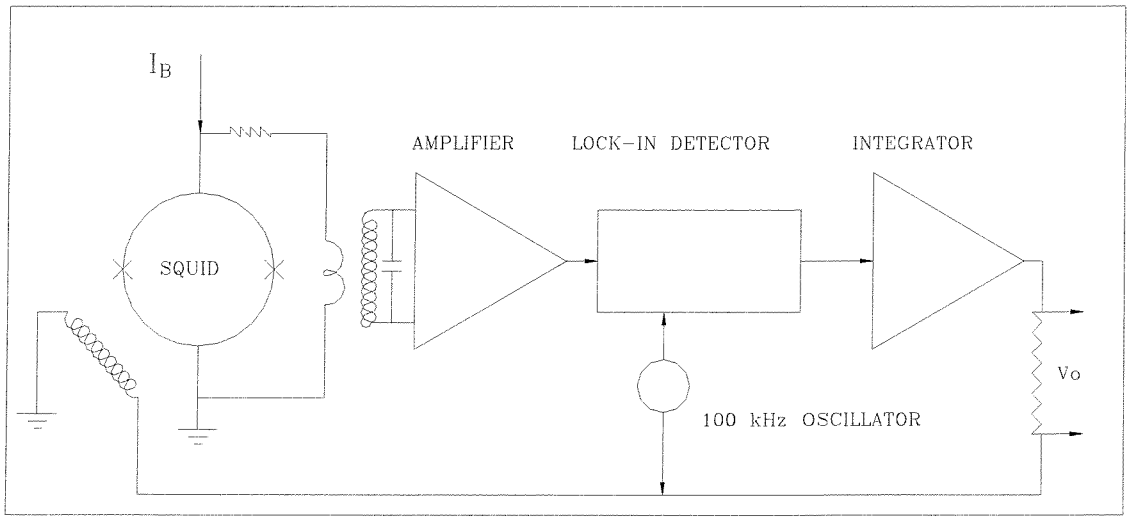

Figure 2.7. Flux locked loop schematic.

A modulated flux is applied to the SQUID with peak-to-peak amplitude of half a flux quantum and a frequency (f_m) of usually between 100 and 500 kHz. Figure 2.8 demonstrates the principle of operation of the FLL. If the averaged value of the flux in the SQUID is exactly $n\Phi_0$, then the resulting voltage is a rectified version of the input signal, i.e. it contains only the frequency $2f_m$ as shown in figure 2.8 (a). If this voltage is sent through a lock-in detector that has been referenced to the fundamental frequency f_m, the output voltage will equal zero. But if the averaged value of the flux equals $(n+1/4)\Phi_0$ then the voltage across the SQUID is at frequency f_m as in figure 2.8 (b) and the output from the lock-in will be a maximum. Hence, as the flux is increased from $n\Phi_0$ to $(n+1/4)\Phi_0$ the output from the lock-in will increase linearly in the positive direction. If the flux is decreased by the same amount, then the output from the lock-in decreases linearly as shown in figure 2.8 (c).

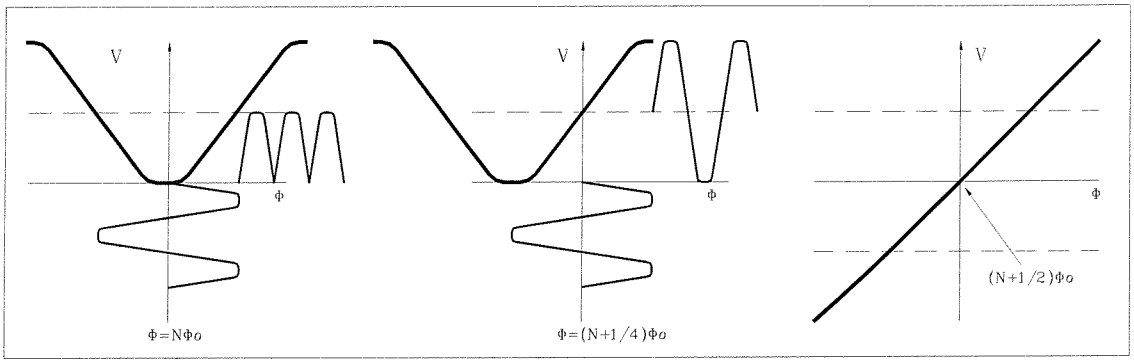

Figure 2.8. Non-linear input to a SQUID converted into a linear output.

The alternating voltage across the SQUID is coupled to a low-noise preamplifier, which is usually at room temperature, via a cooled transformer as in figure 2.7. An oscillator applies a modulating flux to the SQUID. After amplification, the signal from the SQUID is synchronously detected and sent through an integrating circuit. The smoothed output is connected to the modulation and feedback coil via a large series resistor R_f. Hence if the SQUID has an applied flux of $d\Phi$ the feedback circuit will generate a flux $-d\Phi$ which

opposes the original flux, and a voltage proportional to $d\Phi$ will appear across R_f. This technique enables the measurement of much less than one flux quantum to many flux quanta. It has been found that the use of a modulated flux greatly reduces 1/f noise and drift in the bias current and preamplifier.

2.4.2 FLUX-TRANSFORMER

Sometimes it is convenient to expose the SQUID directly to the magnetic field being measured, but more often the magnetic signal is conveyed to the SQUID by a flux transformer. The simplest type is the so-called directly-coupled magnetometer in which a pick-up loop, typically 10 mm across is directly coupled to the two arms extending from the body of the SQUID. The entire device is patterned from a single layer of YBCO and is shown in figure 2.9. The bi-crystal line is the region in which the orientation of the structure is broken to form the tunnelling junction of the SQUID.

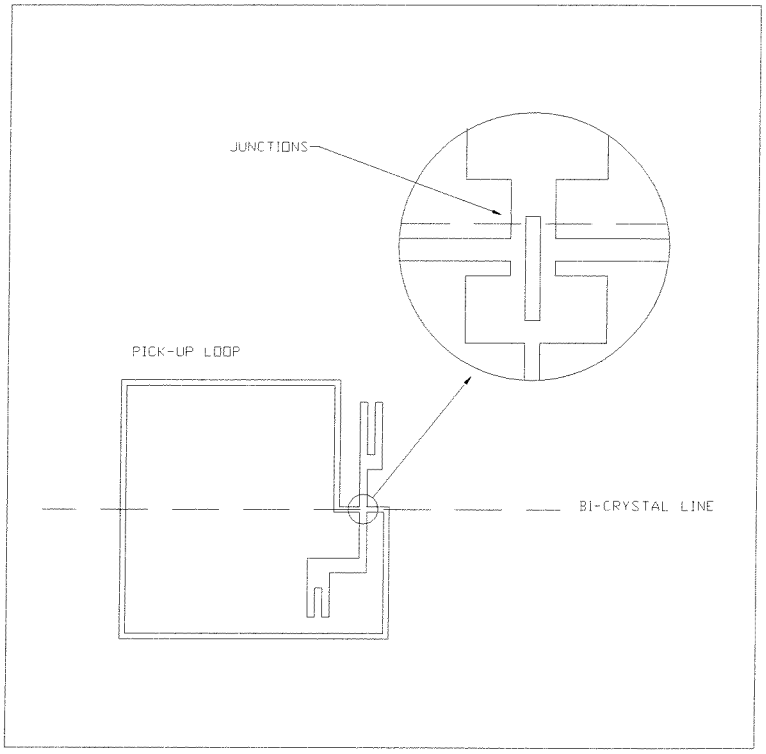

Figure 2.9. Directly coupled magnetometer.

The pick up loop will have a current induced when a change in magnetic field is incident upon it. The current is then transported across the junctions of the SQUID. The relatively large size of the pick up loop acts as an amplifier of the signal, thus increasing the sensitivity of the device.

Another more complicated type of flux transformer uses a three-layer make-up and consists of a closed superconducting loop incorporating two coils in series. One of the coils is termed the input coil, this is inductively coupled to the SQUID and is usually fabricated along with it. The other coil is called the pick-up coil and this is exposed to the field to be measured as represented in figure 2.10. The pick-up coil acts as a magnetic antenna that couples external signals into the SQUID. There is a basic principle in superconductivity that the flux inside a closed superconducting circuit cannot change. As a result of this fact, a change in field that causes the flux in the pick-up coil to change also causes a change in the flux in the input coil. This latter flux change being sensed by the SQUID itself. The area of the pick-up coil is usually much greater than the area of the SQUID. The primary function of the flux transformer is to convert the high magnetic flux sensitivity of the SQUID into a high magnetic field sensitivity.

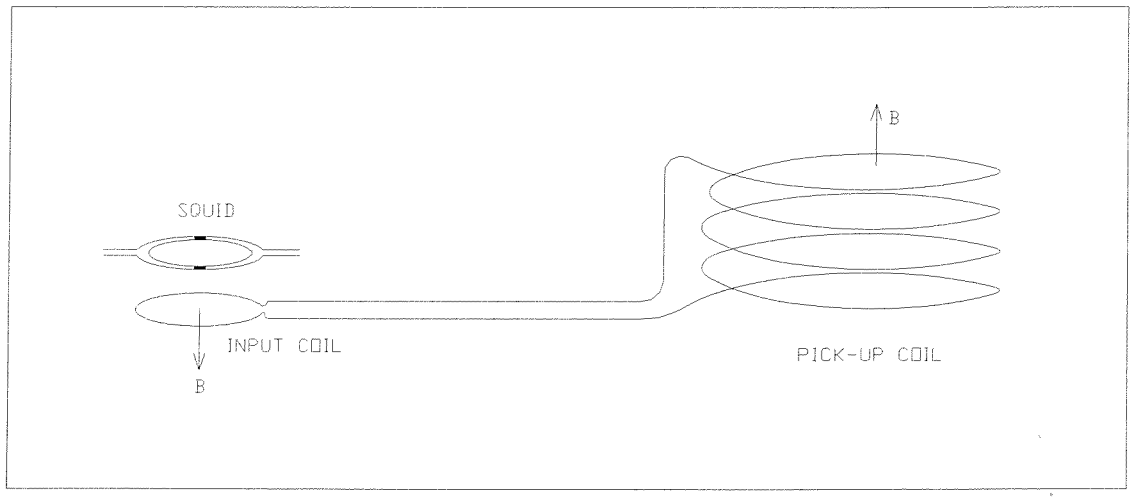

Figure 2.10. A multi-layer flux transformer.

2.5 MAGNETOMETER AND GRADIOMETER

As discussed in section 2.4.2 a flux transformer is useful to turn a SQUID from a sensor of magnetic flux into a sensor of magnetic field. This is how a SQUID magnetometer is constructed; it measures the change in magnetic field at the point in space in which the pick-up coil is located. For various different practical reasons it may be that a SQUID magnetometer is insufficient to perform the measurement required. There may be a lot of background interference that dominates the measurement. In this case using a gradiometer may be advantageous.

A gradiometer differs from a magnetometer because it has two coils on the pick-up coil end wound in series opposition. Figure 2.11 shows a magnetometer, a first order and a second order gradiometer. As the name implies the gradiometer measures the magnetic field gradient between the two input coils. If there is a uniform magnetic field surrounding the two gradiometer coils then the SQUID will not output any voltage, even if the magnetic field is oscillating but the field at both coils is the same, no signal is detected. Because the magnetic field gradient drops off quickly from its source a gradiometer is very useful at rejecting distant sources of magnetic field and only monitor those nearby. This can be especially useful when working in an environment where there are lots of external sources of noise and it is possible to get the gradiometer close to the source to be measured. Gradiometers have been used for conducting MCG measurements in an open hospital ward. A first order gradiometer can measure dB_z/dz as shown in figure 2.11; this is known as an axial gradiometer. A planar gradiometer will measure an off diagonal gradient, i.e. dB_z/dx. Many high T_c gradiometers are of the planar design, simply because a high T_c wire has not been invented yet that can be formed into a coil. The usual way to construct a high T_c axial gradiometer of sufficiently high quality for this purpose is to use two magnetometers, one above the other.

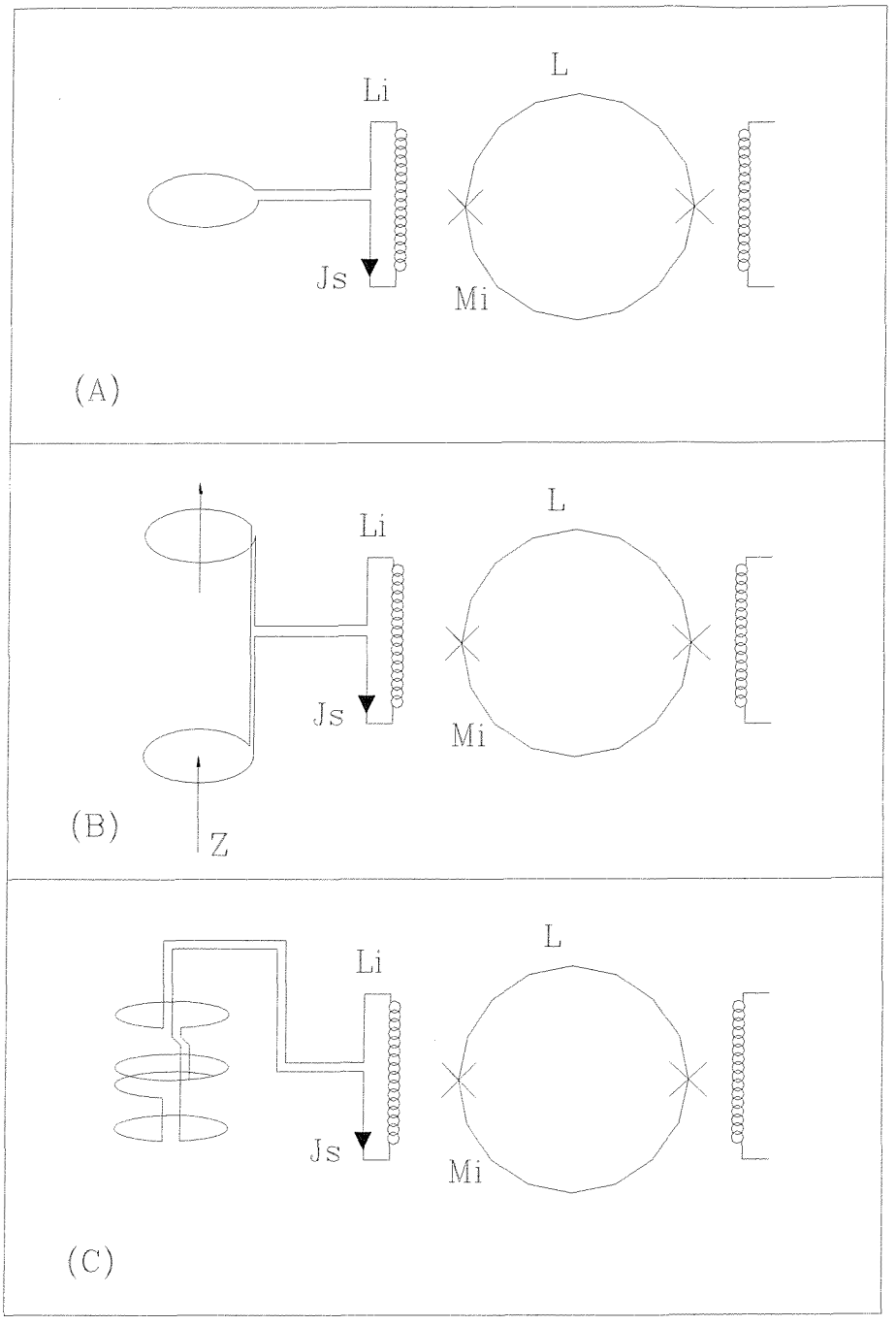

Figure 2.11. (A) Magnetometer.
(B) First order gradiometer.
(C) Second order gradiometer.

The second order gradiometer measures the change in the gradient over space. If magnetic field decreased linearly, then the second order gradiometer would not detect anything. It is the rate of change of field gradient that is measured in this case. An axial second order gradiometer, as shown in figure 2.11 (c) measures d^2B_z/dz^2, whereas the corresponding second order planar gradiometer will measure $d^2B_z/dxdy$.

2.6. SQUID FABRICATION

Since the advent of high T_c superconductors there has been a worldwide effort to develop SQUIDs and flux transformers operating at 77K. As a result there are a multitude of different techniques of Josephson junction manufacture. Some of which will be explained in this section. Many structures have been made and they can be divided into three main categories:

1 Grain boundary junctions
2 Barrier junctions
3 Weakened junctions

Grain boundary junctions can be further sub-divided into natural or engineered. Barrier junctions involve a barrier on non-superconducting material. Weakened junctions are formed by having the structure of the material weakened in a controlled way to form the junction. Figure 2.12 gives an overview of twelve types of Josephson junction construction.

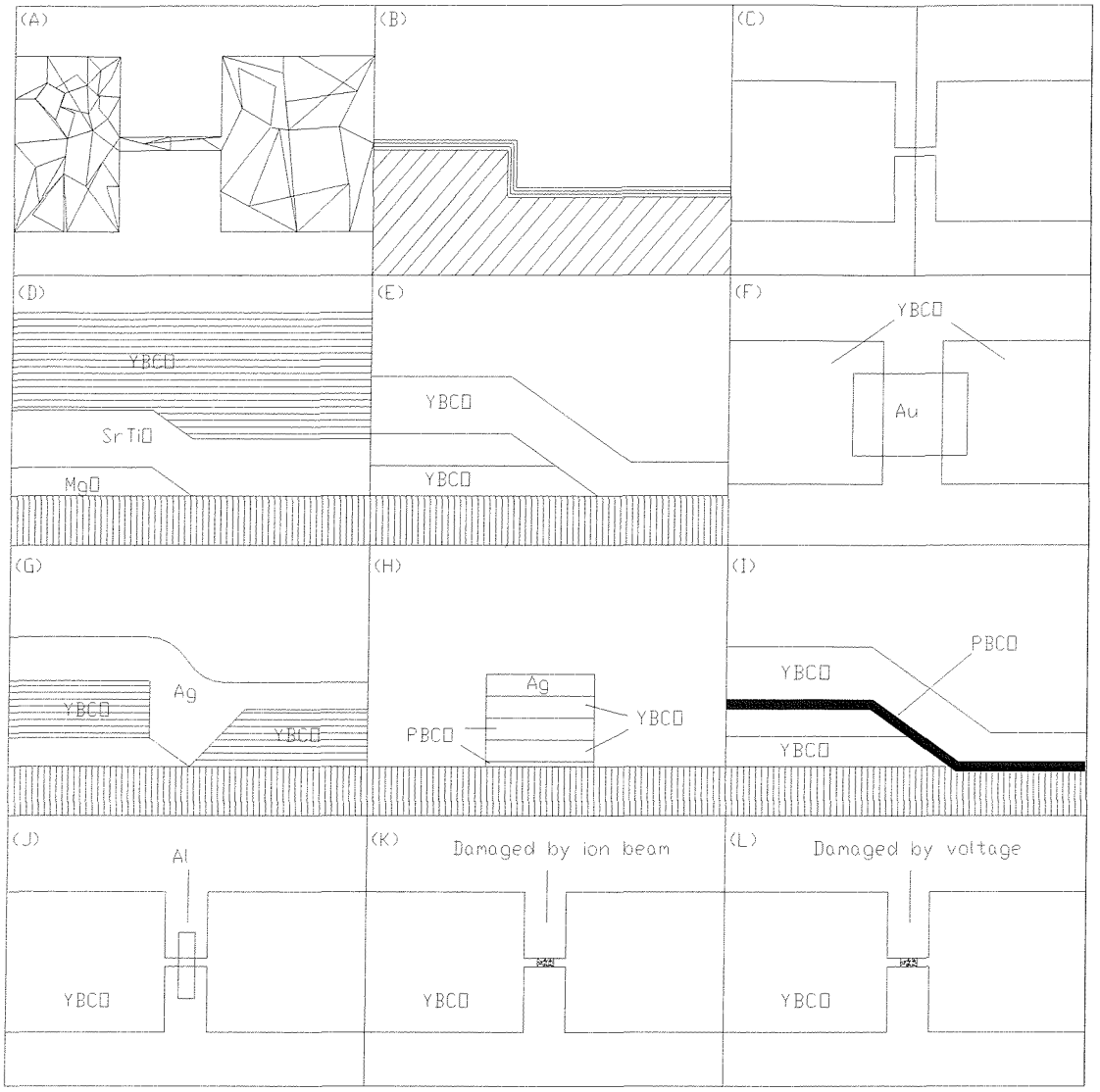

Figure 2.12. Twelve types of Josephson junction construction.

It is believed that the first high temperature thin film Josephson junction was made by Koch et al. [2.3]. They made polycrystalline films of $YBa_2Cu_3O_{7-x}$ containing randomly oriented grains as shown in figure 2.12 (A). Using a photo mask they ion implanted a region of the thin film to make it non-superconducting, leaving a microbridge of superconductor crossed by one or perhaps several grain boundaries that behaved as weak

links (Josephson junctions.) Since then many groups have made similar junctions, usually by removing regions of the film using acid etching or ion-beam milling, and extended the technique to other materials such as BiSrCaCuO [2.4] and TlBaCaCuO [2.5]. Grain boundary junctions with low critical current densities often exhibit almost ideal resistively shunted junction behaviour. Unfortunately they suffer from the drawback that one has little control of their properties and none on their location.

There are several techniques that have been devised to induce the growth of grain boundaries at a specific location. Simon et al. [2.6] deposited a film across a step etched in a substrate as in figure 2.12 (B). The film was then patterned to form a bridge across the step; provided the step edge is sharp enough, a grain boundary is formed at top and bottom. Subsequent transmission electron microscopy at Jülich [2.7] showed that if the step angle is steeper than 45 degrees then the film has an a-axis orientation on the step, thus forming a grain boundary with each of the c-axis films on either side.

Another technique that has been widely adopted involves bicrystal substrates [2.8], made by cutting a wedge from a crystal of (100) $SrTiO_3$ and fusing two pieces together to form a grain boundary between two regions with a known in plane misorientation, see figure 2.12 (C). When YBCO is deposited with an in situ-process, the a and b-axes mimic the orientation of the substrate, producing a grain boundary. Related to the bicrystal junction is the bi-epitaxial process [2.9], which can be viewed in figure 2.12 (D), in which an appropriate seed layer is deposited on the substrate and then selectively removed to leave edges in predetermined locations. $SrTiO_3$ is deposited as a buffer layer and then followed by a YBCO film which undergoes a 45 degree in-plane re-orientation wherever it crosses the edge of the seed layer. Again the microbridges are patterned across the 45 degree grain boundaries to form junctions.

This has dealt with the first group of junctions, now to deal with the second group, the barrier junctions. The first of which is the edge junction, see figure 2.12(E), by Laibowitz et al. [2.10]. Both junctions and SQUIDs have been made by this technique but the yield and reproducibility are poor. Schwartz et al. [2.11] fabricated a junction by patterning a narrow slit in a YBCO film using electron-beam lithography and depositing a gold film across the slit, see figure 2.12 (F). This junction only exhibited supercurrents up to temperatures of up to 16 K. Using a different configuration as in figure 2.12 (G),

Dilorio et al. [2.12] fabricated proximity effect junctions that exhibited Josephson effects to temperatures well over 77 K. Another class of proximity effect junctions, involving PrBaCuO (PBCO) as the barrier was pioneered by Rogers et al. [2.13]. Figure 2.12(H) shows how they grew a c-axis trilayer of YBCO-PBCO-YBCO, with a PBCO thickness of typically 50 nm, and patterned it to form junctions. An alternative configuration for a-axis junctions can be seen in figure 2.12 (I), which was adopted by Gao et al. [2.14] who fabricated edge junctions with PBCO barriers.

The third and final category contains the so-called weakened structures. Simon et al. [2.6] deposited a YBCO film across a thin aluminium strip which 'poisons' the superconductor locally thereby reducing its transition temperature, see figure 2.12 (J). In another method that is shown in figure 2.12 (K), one reduces the transition temperature of a narrow region by focusing high energy ions on to a microbridge [2.15]. Or by using a mask patterned with electron beam lithography [2.16] to define the area exposed to an ion beam. In a third technique [2.17], controlled electrical pulses were applied to microbridges at 77 K, again producing a weakened region as demonstrated in figure 2.12 (L). Although these weakening techniques are controllable at least to some degree, they usually lead to flux flow characteristics that are undesirable for most applications. However, if the region weakened could be reduced to a few tens of nanometres, these techniques might prove very useful.

To date, the best SQUIDs have been made from step edge grain boundary or bicrystal grain boundary junctions, see figure 2.12 (B) & (C). Although careful fabrication procedures have improved the yield of these junctions, particularly in the case of the bicrystal devices, the scatter in the critical current and resistance remains higher than one would like. There is ongoing work to improve the understanding and reproducibility of trilayer edge junctions with a variety of barrier materials, and it is hoped that there will be steady progress in the yield in this class of junction. The simplicity offered by the grain boundary junctions, which involve only a single YBCO layer makes them very appealing for practical applications.

CHAPTER 3.

3. UNSHIELDED APPLICATIONS

3.1 INTRODUCTION

The purpose of this chapter is to discuss the number of possible applications that have been considered during the course of this project. Each application is explained separately and the degree to which they may be applied with state of the art sensors is discussed. One potential application was evaluated in collaboration with the Southampton Oceanography Centre (SOC). Another application that is discussed is concerned with geophysical prospecting. Further areas for unshielded application that are described include non-destructive evaluation (NDE), magnetocardiography (MCG), magnetoencephalography (MEG), land mine detection and archaeological surveying.

3.2 DEEP SEA SURVEYING

The Challenger Division of the SOC were interested in mapping the magnetic profile of the deep ocean floor. They were interested in the geological features that existed on the seabed and below. Other potential applications that could result from the creation of such technology include the discovery of sunken wrecks, cables and unexploded bombs. Figure 3.1 shows how a potential set-up could look. Fluxgate magnetometers had been used in previous experiments [3.1], but it was decided that better resolution was required [3.2]. The main technical constraints of this proposal were:

1. Required sensitivity of magnetometer to be around 1 pT over measurement intervals of several thousands of seconds.
2. Compact size of system to fit into pressurised containers for the 5500 m depths of survey.

3. Ability of the sensor to operate without magnetic shielding whilst being trawled along at approximately 1 m s^{-1}.

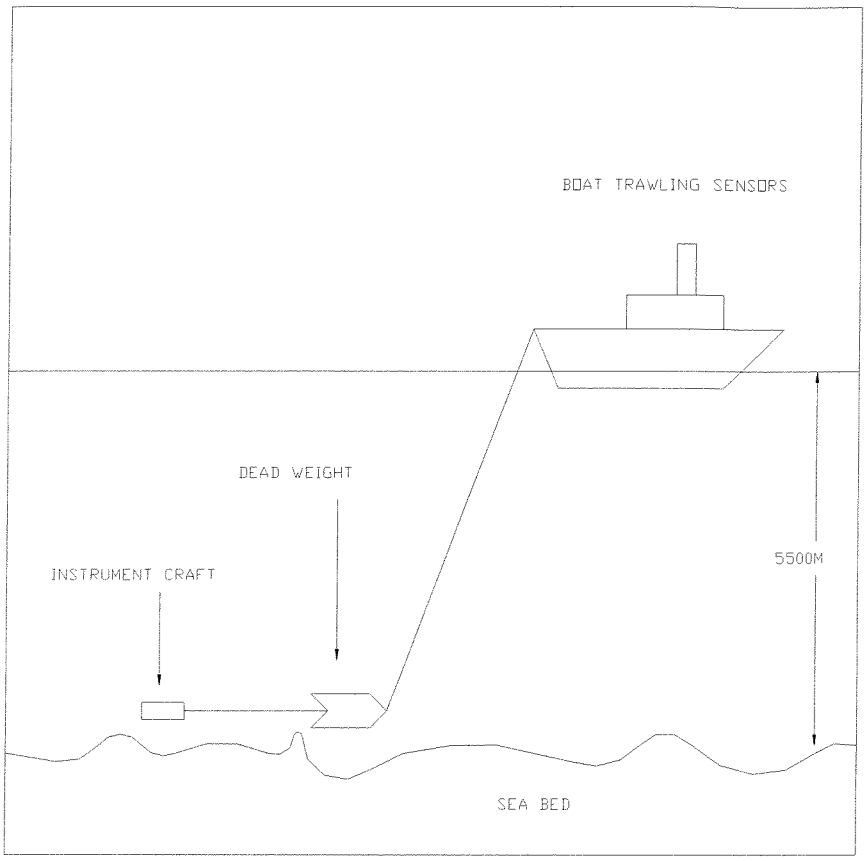

Figure 3.1. Potential set-up for deep sea SQUID surveying.

The ultimate sensitivity of a modern high T_c DC SQUID magnetometer was known to be as high as 10 fT $Hz^{-1/2}$ at measurement frequencies of around 100 Hz and above. At frequencies of measurement below 100 Hz, the so-called 1/f noise becomes a factor. This means that the stability of the instrument steadily decreases the longer one observes it. The result of this effect is that the 'DC' stability of the instrument requires investigation. The pressure that is experienced on the deep ocean floor is about double that used in industrial gas cylinders. At ocean floor depths of 5500 m the pressure due to the water is about 550 bar. It is therefore necessary for the system to be of compact size to fit into the pressure vessels that will protect it from the inhospitable conditions. The SOC required the system to be no more than 16 cm in diameter because it is very difficult and

prohibitively expensive to manufacture the pressure vessels with an internal diameter greater than 16 cm. This is one area where SQUIDs carry an advantage over much of their competition. A basic SQUID magnetometer sensor is only a few centimetres in length and less than two centimetres in diameter.

The fact that the system has to operate without magnetic shielding was not an insignificant matter. Almost all the applications of high T_c SQUIDs reported to date have been in magnetically shielded environments. There is very little documentation of unshielded applications outside the realm of non-destructive evaluation and magnetocardiography [3.3]. The unshielded performance of high T_c SQUIDs was very quickly identified to be the area of great interest and promise for new applications, due to the improved performance of modern high T_c sensors in such environments. The problems associated with high temperature SQUIDs being subject to the earth's magnetic field are two fold. First of all there is the dependence of the critical current of the Josephson junctions upon the magnetic flux penetrating the junction. Hence the geomagnetic field can adversely affect the performance of high T_c dc SQUIDs. The other problem associated with high T_c SQUIDs operating in magnetic fields is the fact that the intrinsic noise of the instrument is increased due to motion of the magnetic flux vortices that thread the Josephson junction. The flux vortices are loosely pinned to sites within the body of the superconductor. The effect of thermal energy given to the vortices causes them to jump from pinning site to pinning site. This causes the voltage output from the SQUID to increase in the form of intrinsic 1/f noise.

The problem with moving unshielded sensors in the earth's magnetic field only serves to increase the problem of noise intrinsic to the sensor. The motion of the SQUID in the earth's field increases the magnetic flux that moves through the body of the superconductor and hence the intrinsic noise will be increased. This increase in flux noise is unavoidable but needs to be taken into consideration. There are also a whole multitude of other aspects that need to be thought about when planning tests of SQUID performance whilst on a moving platform. If gradiometric measurements are to be made, (two sensors in series opposition) the amount of rotation of the sensors during measurement is crucial in determining their accuracy. The two sensors are immersed in the earth's magnetic field of approximately 50 μT, so even the slightest tilt in their

orientation causes a significant change in measured field. As SQUIDs are capable of measuring changes in magnetic field of the order of 50 fT, it is possible to see that a change in orientation in the earth's field of 1 part in 10^9 may be sensed by the system. Although it would not be possible to eliminate all twisting motion when trawling the SQUID in the sea it could be possible to subtract the effect if it is found to be cyclic.

To demonstrate just how technically challenging the SOC project was perceived to be, the different aspects and problems that required attention were listed. It was clear that there would be simpler applications to look at whilst still making progress towards the final SOC goals. Simpler applications would include unshielded measurements whilst keeping the system stationary. The intrinsic sensor noise sources in mobile gradiometer operations can be placed into four main categories as detailed below:

1. **STATIONARY SOURCES.**

- Johnson noise (white noise)
- Electromagnetic induction
- 1/f noise (flux motion and I_c variations)

2. **SOURCES FROM FIELD CHANGES.**

- Eddy currents
- Flux trapping
- Imbalance between sensors
- Magnetisation changes in normal metals

3. **ACCELERATION INDUCED SOURCES.**

- Motion of magnetic parts w.r.t. loops
- Cryogen slosh
- Changes in loop area and orientation

4. TEMPERATURE INDUCED SOURCES.

- Thermal expansion
- Critical current variations
- Changes in paramagnetic moment
- Penetration depth changes
- Thermal emfs

There are many issues outlined above and it was obvious that all could not be covered immediately. Hence stationary applications were considered and researched.

The subject of noise reduction whilst moving an unshielded SQUID in the earth's magnetic field is discussed in the papers by Keene [3.4] and Clem [3.5]. The two authors take a similar approach to minimising the effect of movement in magnetic fields. The paper by Keene explains the principle behind a prototype three-axis gradiometer system. In the paper the SQUID sensors are surrounded by a 'magnetic vacuum', this effect is achieved by surrounding the detecting sensors with three orthogonal Helmholtz coils. Each coil is linked to the two SQUIDs that comprise it's component of the gradiometer. The average field detected by the two SQUIDs is fed back to the Helmholtz coil, and an appropriate amount of current is supplied to the coils to cancel out the gross change in field, but leaving the gradient part intact. The effect of maintaining a constant magnetic field around the sensors is to reduce the noise induced due to magnetic flux moving through the superconducting material of the SQUID. Keene also goes on to discuss an adaptive signal-processing algorithm that compensates the incoming raw data allowing for small changes in the orientation of the sensors in the earth's magnetic field during the time they are in transit. This idea is a progression from the 1993 idea by Koch of a three SQUID gradiometer (TSG) in which a third SQUID was used to null out ambient field around two others that formed the gradiometer arrangement [3.6]. The only drawback of Koch's system was that a three-axis system would require nine SQUIDs, which in many applications could make a system prohibitively expensive, whereas the idea by Keene would only require six sensors for a three-axis gradiometer system. The Clem system was devised in collaboration with Koch and retains the three SQUID per axis requirement.

Both the systems noted in the last paragraph were still in development and had not actually reached the stage of a fully working prototype at time of writing. Initial reports by both parties have been encouraging and the promise of further results is awaited.

3.3 GEOPHYSICAL PROSPECTING.

Within the realm of geophysical prospecting there are a whole host of methods that have been employed in the search for natural resources. There are two methods that this project has been concerned with, magnetotellurics (MT) and time domain electromagnetic (TDEM) methods. Full details of the magnetotelluric method can be read in the book by Kaufman and Keller [3.7], with a fully detailed practical review given in the paper by Vozoff [3.8]. The book by Reedman [3.9] gives details on all the major techniques in geophysical prospecting including the time domain electromagnetic method. The magnetotelluric method is very similar to the time domain electromagnetic method and is concerned with measuring the resistance of the ground below the surface. The resistance of the ground down to many kilometres can be measured with this method. Because all materials have a representative resistance, knowledge of the resistance in the ground leads to knowledge of the material below. Hence a picture of the physical make up of the subsurface can be drawn up in layers to uncover any precious mineral reserves that may be present. The resistance is measured from looking at the magnetic and electric response of the ground to an induced electromagnetic wave that is injected into the ground. The crucial difference between MT and TDEM is the way in which the induced signal is created. MT uses the naturally created electromagnetic waves from such events as thunderstorms. These random events cause electromagnetic waves to permeate through the earth which are then reflected by conductive materials in the ground below. The reflected waves in TDEM are created by a source that is part of the experimental set up; this offers the advantage of allowing the timing and bandwidth of the signal to be optimised. In both methods sensitive magnetic detectors are required to measure extremely weak signals, often over large areas. It would appear that the TDEM method is desirable over MT because of the extra flexibility that it offers, enabling specific measurements to be made for particular materials at predefined depths. The

limitations of these methods lie in the bandwidth of measurement. The skin depth equation shows that the depth of penetration of electromagnetic wave is inversely proportional to the frequency of the wave. Hence the lower the frequency the greater the depth of penetration of the wave. Wave travel is also affected by the electrical conductivity of the ground that it must travel through. Highly conductive media limits the depth to which the electromagnetic waves penetrate. The depth of penetration in kilometres is given by [3.25]:

$$(1/2\pi)\sqrt{(10\rho T)}$$

Where T is the measurement period in seconds and ρ is the ground resistivity in ohm-metres. The reflected waves are collected and their frequency components analysed. Standard algorithms are used in the modelling of the underlying terrain. Both electric and magnetic measurements are taken; the electric measurements are made along a length of wire with two copper electrodes placed about 250-500m apart. Very large coils with high permeability cores often perform the magnetic measurements in this technique. Although very sensitive to changes in magnetic field, these induction coils can be relatively bulky, measuring over a metre in length. The measurements are also made in the field, often in awkward and inhospitable places. Ruggedness and portability are therefore important considerations. The construction of a 3-axis system could feasibly be made much more compact with the use of SQUID technology over a comparable coil system. It was therefore important to know the performance of the two systems relative to each other. If a SQUID system would perform at least as well as induction coils at the important frequencies, then the added advantage of their lightweight and compact size would give them an advantage for fieldwork, especially in more rugged environments.

The work by Chwala [3.10] documents the first tests carried out in the field performing transient electromagnetic (TDEM) measurements. In the study they compare the performance of a high T_c SQUID system with the more conventional induction coils. It is concluded that the SQUID system performed better than the coils in two areas. They found that greater depth information could be gained with a SQUID system because induction coils measure dB/dt, whereas SQUIDs measure the magnetic field with respect

to time. Their experiments showed depth information 2-3 times greater than that achieved by the induction coils. It was also found that a great saving in measurement time could be gained with SQUIDs, because coils required an increase in measurement time by a factor of between 25 and 100 to give the same quality of information.
The above work goes to prove that modern high T_c SQUIDs are on the verge of practical unshielded application, and that further investigation is very much warranted.

3.4 BIOMAGNETOMETRY.

Magnetocardiography (MCG), magnetoencephalography (MEG) and nerve tissue damage location are three of the leading potential applications in the medical world. MCG is concerned with the characteristics of the beating heart. A single beat of the human heart can be split into characteristic 'QRS' and 'T' wave components. Figure 3.2 shows how the human heartbeat should look in a healthy patient. The principle of operation is very simple. The electrical impulses that cause the heart to beat create a resultant magnetic field of the order of many hundreds of femto Tesla. A SQUID sensor placed close enough to the changing field will detect the action of the heart. The study of this activity can be useful for the diagnosis and prevention of a number of different conditions. A very comprehensive paper on the integration of MCG with high T_c SQUID sensors is given by Weidl [3.11]. This paper gives a description of how existing low T_c technology is being replaced by much less expensive high T_c technology. Because there is no longer any need for a magnetically shielded room it becomes much less expensive. This not only cuts the cost of the entire system down by orders of magnitude, but also gives the system the potential of being a portable one, allowing use within wards, so that the monitoring can be done at the bedside. A high T_c system offers the added advantages of being cheaper and easier to run because liquid nitrogen is cheaper and easier to handle.
A popular alternative to the MCG is the electrocardiogram (ECG), which operates on the principle of measuring the potential difference between two points on the surface of the skin. As the description insinuates this is a contact method, whereas MCG is not, in ECG, electrodes are taped across the area of interest and the changes in potential difference monitored. ECGs are a useful technique in their own right, but suffer from a

number of drawbacks. Being a contact method, any patient with a serious skin condition, such as a burn victim, would not be able to benefit from an ECG due to thecontact nature of its application.

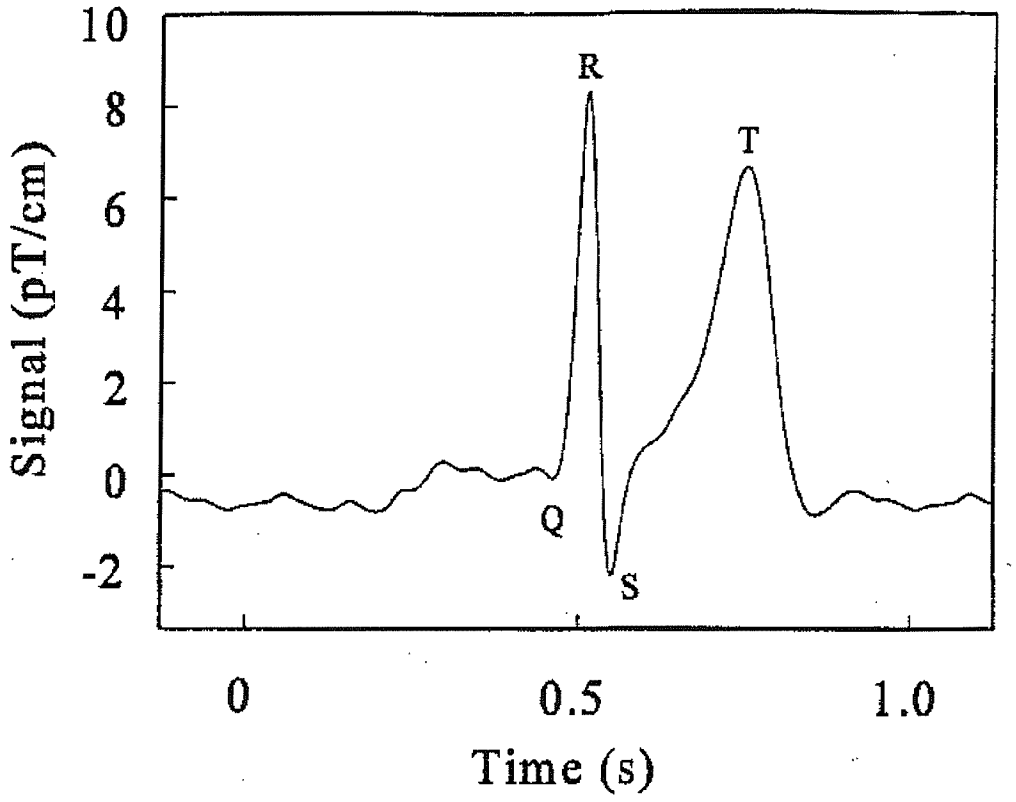

Figure 3.2. A healthy human heart beat.

Immediately after a suspected heart attack it is vital to learn whether the patient has damage to their heart, this is known as an infarction. It has been demonstrated that an ECG cannot detect the presence of damage or blockage of the blood vessel leading to the heart for around eight hours after an attack. It has been demonstrated however that an MCG has the ability to detect the infarction immediately by detecting the increase in amplitude of the 'T' wave. SQUID technology also offers the advantage of being able to locate the exact position of tissue damage, thus considerably speeding up operating time because the surgeon no longer needs to search such a wide area to identify exactly where the damage lies [3.12]. To put this idea into perspective, there are 100,000 people in

Germany alone who die of infarctions. Putting this into a global perspective the potential that a SQUID system has for saving lives is great.

Another promising application in this field comes from the detection of heart arrhythmia. This is a condition in which the patient's heart becomes unstable or stops beating. The clinician would look for fragmentation in the 'QRS' wave, where if an arrhythmia were present there would be extra frequencies contained. It is genuinely believed that the technology has been developed to conduct a mass screening exercise, they only wait on the necessary funding to prove their idea.

The practical application of a bedside foetal MCG system has already been demonstrated in an unshielded environment. Although this was with the use of low T_c SQUID sensors, with further development in the manufacturing of high T_c sensors it is only a matter of time before it is demonstrated with such technology.

Magnetoencephalography is concerned with looking at the electrical activity that occurs within the brain. An array of SQUID sensors are required to map the three dimensional electrical activity within the brain. A number of clinical applications have been identified for this technique, such as detection of certain types of epilepsy and other brain abnormalities. The reaction and processing of the brain to outside stimuli is an active area of current research as detailed in the paper by Laudahn [3.13]. The magnetic fields produced from electrical activity within the brain tend to be of the order of tens of femto Tesla. This tends to restrict usage to low temperature SQUIDs in magnetically shielded environments. High T_c SQUIDs do have the required sensitivity in the white noise of their spectrum, but to apply this to an unshielded environment is an application that will have to wait some time yet. Although one driving force that may provide enough momentum to apply high T_c to MEG is in screening for Parkinson's disease. This is a degenerative disease that becomes prevalent in older people generally. If a national screening program were to be introduced, it would not be practical to send everyone to a European facility where there was a magnetically shielded room, it would therefore be necessary for a portable system to operate with at least, very little shielding. Again reasons of practicality facilitate the possibility of application for high T_c SQUID technology.

3.5 NON-DESTRUCTIVE EVALUATION.

A recently established application for high T_c SQUIDs in an unshielded environment is the introduction of non-destructive evaluation (NDE). NDE is not a new technology; in fact the testing of items without breaking them has been in practice for many years. It is within the field of eddy current testing that SQUIDs have made the breakthrough. An excitation coil emits a magnetic field at a certain frequency, this emanates into the material being tested, and eddy currents are produced and detected by the magnetic sensors in use at that time. If there is a flaw somewhere in the material the shape of the resulting eddy current will be distorted. So, as the sensor is trawled over the surface of the material (or the material is moved under the sensor) any flaw in the material will be detected. Before SQUIDs were used the popular sensor technology was induction coils. The high temperature SQUID has now superseded the old induction coil in some applications because it has the ability to look deeper into materials and has greater spatial resolution due to its more compact nature [3.14]. There has been a large and successful collaboration with different groups and companies within Germany to facilitate the commercial testing of aeroplanes [3.15 – 3.19]. This technology is now in use in a busy airport in Germany where aircraft wheels are tested for cracks, the fuselage is tested for corrosion and the area around rivets are tested for cracking and splitting.

NDE is also proving useful in other areas outside of the aviation industry. It has been discovered that the low frequency noise of a SQUID magnetometer goes up when placed close enough to a material that is corroding [3.20]. This discovery could have far reaching effects on many structures that are known to deteriorate with time. None more so than large buildings and bridges. Being able to accurately assess whether a building or bridge is still safe for use could save many lives and a lot of money. Research continues in this field and looks set to open up into a successful and prosperous business.

3.6 OTHER APPLICATIONS.

In the previous sections, some of the more popular areas of research for applications of SQUIDs in an unshielded environment have been detailed. The purpose of this section is to mention some of the other work that has been conducted towards SQUID application. Another potential application of a portable high T_c SQUID gradiometer could be archaeological surveying. A highly sensitive magnetometer could be used to measure the varying susceptibility of the ground below as it is scanned across the surface of the earth. Because rocks and earth have slightly different susceptibility, a map of a field could be drawn up before any excavation took place on a site of potential interest for instance, where a Roman settlement may once have stood. A distinct pattern of the walls and buildings of the settlement can be drawn up, thus saving the archaeologist a lot of time and money on false digs.

A recent and potentially lucrative application is concerned with the testing of printed circuit boards (PCBs). It may be argued that this fits within the realm of NDE, but it relies on a different process to detect flaws in manufacture, and will become a subject all of its own if it becomes commercially successful. As everyone knows, the manufacture of PCBs is a massive global market with interests in all forms of manufacturing. SQUIDs can detect the failure of these PCBs because of the stray magnetic fields that are created when a short circuit or cross between conduction lines occurs. As PCB manufacturing tolerances become tighter and tighter the need for accurate and reliable testing mechanisms is self-evident.

An application that has raised some attention lately is that of land mine detection. Many types of land mines contain a small amount of ferrous metal, usually in the firing pin section. If SQUIDs could be developed to be an ultra sensitive 'metal detector' then they could be used to save many lives in the field of land mine detection. The present state of the art requires a human to lie down on the ground with a stick and prod it into the ground at a sharp angle until something solid is hit. Sometimes it's a stone sometimes it's a mine, but still a very slow, inefficient and dangerous process.

One relatively new application for high T_c SQUIDs that is showing a keen niche for itself is spectroscopy. Nuclear magnetic resonance (NMR) has been around for a long time,

but it appears that SQUIDs can help in this specialised form of spectroscopy [3.23]. Most NMR measurements are traditionally made at high magnetic fields because the signal is proportional to the product of sample magnetisation (M) and the Lamor frequency (ω). Since both magnetisation and precession frequency scale with magnetic field strength, the NMR signal is greatly enhanced as the magnetic field is increased. Unfortunately there is a problem with increasing the magnetic field when dealing with polycrystalline and amorphous materials due to the random nature of the orientation of the individual molecules with respect to the applied field. The result is local variations in the Lamor frequency, which deteriorates the quality of the spectrum. These high field problems can be substantially reduced by using low magnetic fields and a SQUID as detector. Conventional NMR pick-up coils measure the time derivative of a magnetic flux, the SQUID measures magnetic flux directly. Therefore the signal scales with ω, for this reason SQUIDs are much more sensitive than conventional detectors at low frequencies.

Another application to note is SQUID microscopy. Still in the developmental stage [3.21], this is a new and potentially exciting area for high T_c SQUIDs to move towards. Initial demonstrations showed a scan of a dollar bill on which a 'negative' of George Washington was seen due to the differing magnetic properties between the ink and the paper. These initial experiments were conducted with sample and SQUID both immersed in liquid nitrogen. Modern SQUID microscopes have become more refined and allow scanning of room temperature samples. It is possible to resolve magnetic particles with extremely small diameters that are very close together.

The use of SQUIDs as a highly accurate thermometer has been reported [3.22]. The principle of Josephson noise thermometry in the temperature range close to that of liquid helium is a well-established technique. This new research is attempting to increase the absolute temperature range of measurement to the 10-50 K range. A so called Resistive SQUID (or R-SQUID) is constructed, the noise from which is accurately used to measure the absolute temperature. It has been claimed that an uncertainty of 1 mK has been achieved at a temperature of 50 K.

There is work being conducted towards sending SQUIDs into space to be used as part of a gravity probe relativity gyroscope mission [3.23]. There are a huge number of practical

aspects that have to be looked at that can be of use to researchers looking at more earthly applications. Aspects such as thermal stability, electromagnetic radiation, changing of earth's magnetic field, energetic charged particles and launch vibrations are all issues that if resolved could assist work ongoing in other areas.

This chapter has highlighted at least a dozen real and potential applications for high temperature SQUIDs for the market place. The number of applications is in a very large part due to the huge progress made by the different SQUID manufacturing and development groups over the world. Since the discovery of high T_c in 1986 and the subsequent construction of the first high T_c SQUIDs there has been rapid and remarkable progress in the development of these devices. Initial high T_c SQUIDs were many orders of magnitude noisier and less sensitive than their low temperature counterparts. The noise levels of many modern high T_c SQUIDs are now within a single order of magnitude of their low temperature contemporaries. With progress being made all the time, money spinning applications appear increasingly likely.

CHAPTER 4.

4. TYPES OF MAGNETOMETER

4.1 INTRODUCTION

This chapter describes various types of magnetometer that are commercially available. A brief description of each type of magnetometer will be given, along with their respective applications, advantages and disadvantages. There are many criteria on which magnetometers can be compared, such as cost, noise, sensitivity, portability and ease of operation.

4.2 HIGH T_C SQUID

The operation of a high-T_c SQUID has already been discussed in chapter 2 and therefore does not need to be mentioned here. The over-riding advantage of a SQUID is the sensitivity of such an instrument, with quoted figures of around 10 fT/√Hz at 1 Hz within a well-shielded environment [4.1]. A major concern of this project however is to investigate the behaviour of a SQUID in less well-shielded environments. The main perceived disadvantage of using a SQUID system is the requirement of cryogenic cooling. This is often an unfounded concern because a modern nitrogen cryostat can be left for many days without the need of attention, thus allowing unskilled operators to use the system for prolonged periods. For portable applications, a high T_c SQUID can be very desirable because a system can be made that is very small and relatively lightweight. Hand held portable systems weighing just a few kilograms have been reported. These types of systems are ideal for unshielded applications such as non-destructive evaluation, ward magnetocardiography and geophysical prospecting. Most commercially available systems are very user friendly, with just a push of a button required to operate the electronics, with all the tuning and running functions being completed automatically.

The cost of commercially available SQUID systems is relatively large at around £10,000 per channel. It is well understood though that the prices would fall considerably if the annual sales of SQUID systems increased significantly after a major application is discovered and exploited.

4.3 LOW T_C SQUID

It is believed that low temperature SQUIDs can obtain an order of magnitude improvement in performance over their high temperature counterparts, due to their lower operating temperature. Figures of around 1 fT/√Hz have been recorded, again within a magnetically shielded environment [3.24]. Hence ultimate resolution in a very well shielded environment is obtained by a low temperature SQUID. In a less hospitable environment other considerations are required, such as portability ruggedness and user friendliness. Aspects in which the high T_c SQUID can have an advantage. The low T_c SQUID uses liquid helium as coolant, which is less efficient than liquid nitrogen, with a boil off rate approximately ten times higher compared to nitrogen. This can have far reaching effects on the design of a portable system, because it has to be small enough to be portable, but contain enough helium to last a sufficiently large period of time. Low temperature systems also tend to be less robust because of the intricacy involved in the construction of a liquid helium cryostat. It is likely that a portable low T_c SQUID system would require topping up with helium on a daily basis, this is a skilled operation and therefore decreases its user friendliness. The initial purchase costs are similar to that of a high T_c system, but the running costs are a lot higher because liquid nitrogen is very cheap, of the order of 30p a litre where as helium is very expensive at several pounds per litre. This is of budgetary importance when one realises that not only is helium more expensive but it is likely that ten times as much will be consumed compared to a nitrogen system. Current applications of low T_c SQUIDs are in areas where their ultimate resolution is required. A prime example of such an application is in the detection of brain activity. The electrical signals within the brain produce tiny magnetic fields, of the order of 10 fT. Magnetoencephalography (MEG) can therefore only be successfully accomplished with the aid of low temperature SQUIDs, at this time.

4.4 FLUXGATE MAGNETOMETER

The fluxgate magnetometer was one of the first modern high sensitivity magnetometers to achieve widespread use. Its popularity is due to its relatively good sensitivity combined with ease of operation and portability. The device was originally developed during world war two as a submarine detector. Several designs have been used for recording diurnal variations in the earth's field, for airborne geomagnetics and as portable ground magnetometers.

The most common design of fluxgate consists of two cores of high permeability at low magnetic fields. Common core materials include mu-metal, permalloy and ferrite. Each core is wound with primary and secondary coils, the two assemblies being as close as possible identical and mounted parallel so that the windings are in opposition. The two primary windings are connected in series and energised by a low (50-1000 Hz) frequency current. The maximum current of which is sufficient to magnetise the cores to saturation, in opposite polarity, twice each cycle. The secondary coils, which consist of many turns of fine wire, are connected to a differential amplifier, whose output is proportional to the difference between the two input signals.

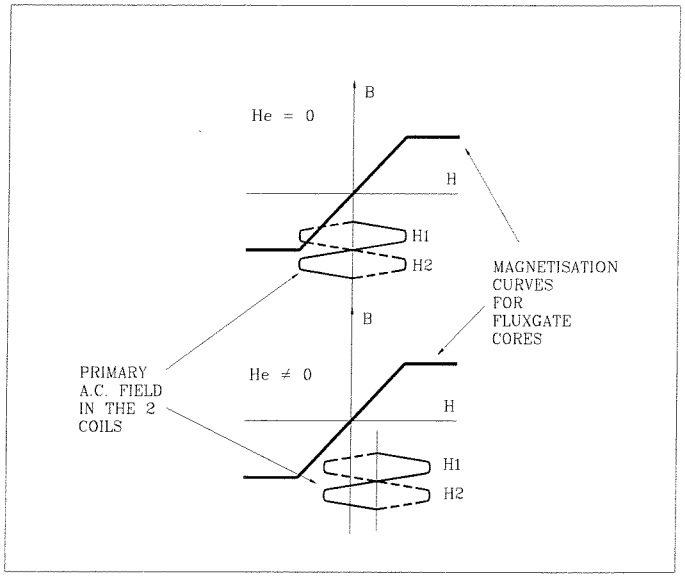

Figure 4.1. Fluxgate core magnetisation.

Figure 4.1 shows the magnetisation characteristics of the core in relation to the current through the primary windings. In the absence of an external magnetic field the saturation of the cores is symmetrical and of opposite sign, near the peak of each half cycle so that the outputs from the two secondary windings cancel. The presence of an external field component parallel to the cores causes saturation to occur earlier for one half cycle than the other, producing an imbalance. The difference between the output voltages from the secondary windings is a series of voltage pulses which are fed into the amplifier, as shown in figure 4.2. the pulse height is proportional to the amplitude of the biasing field of the earth. Any component can be measured by suitable orientation of the cores.

Much of the noise in a fluxgate can be attributed to the hysteresis of the core, as better materials have been developed noise has decreased in these magnetometers. Another source of noise comes from eddy currents that are produced in the cores; this is minimised by making them as long and thin as possible. There are several other fundamental sources of error in the fluxgate instrument. These include imbalance between the two cores, thermal noise in the cores, drift in the biasing circuits and a temperature sensitivity of around 1 nT/degree centigrade or less. These disadvantages are relatively minor however, when compared to the advantages, which include direct readout, no azimuth orientation, lightweight (2-3 kg) and small size. It is an advantage that any component of a magnetic field can be measured, and done relatively quickly, in about 15 seconds. The best fluxgates claim sensitivities of around $10\,pT/\sqrt{Hz}$ at 1 Hz in a magnetically shielded environment [4.2 – 4.4]

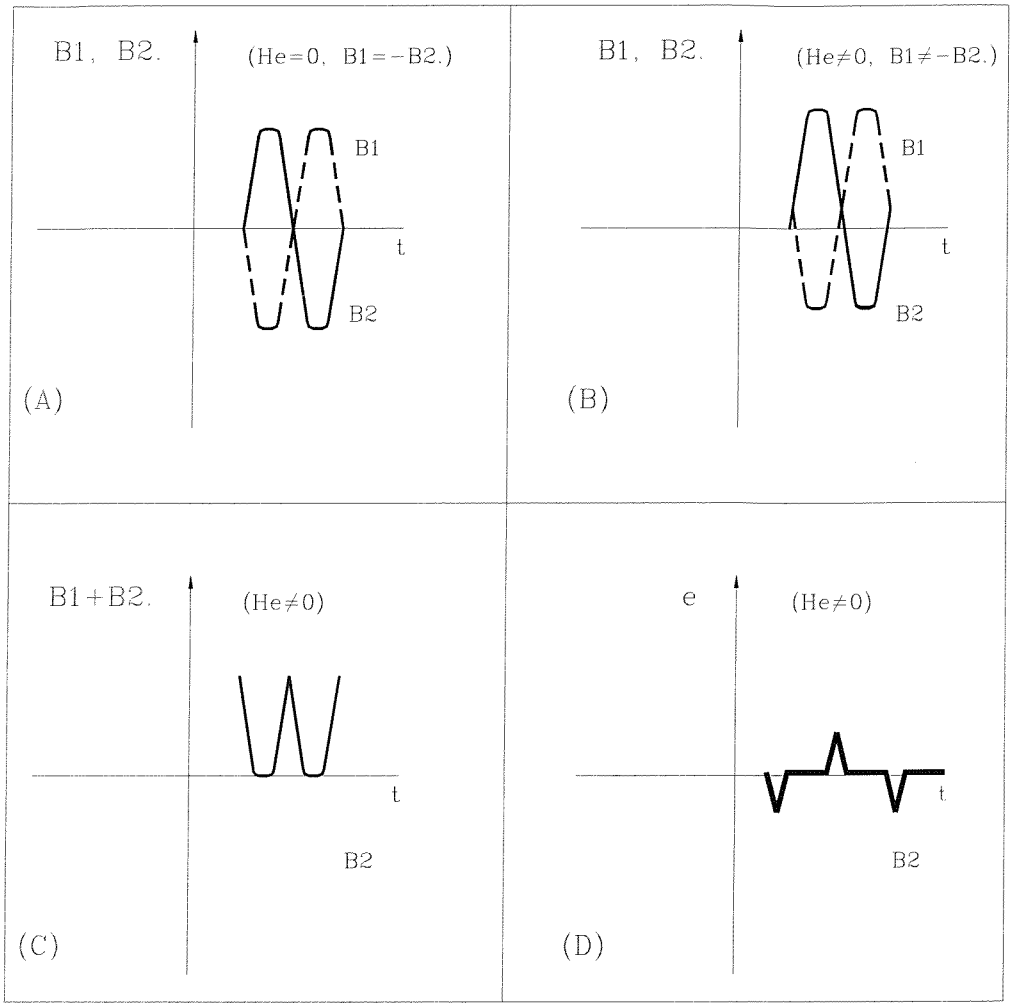

Figure 4.2. Characteristics of the fluxgate magnetometer.

4.5 PROTON PRECESSION MAGNETOMETER

The proton precession magnetometer grew out of the discovery of nuclear magnetic resonance. Some nuclei have a net magnetic moment that, coupled with their spin, causes them to precess about an axial magnetic field. The proton precession magnetometer depends on the measurement of the free precession frequency of protons that have been polarised in a direction approximately normal to the direction of the field to be measured. When the polarising field is suddenly removed, the protons precess

about the earth's field in a manner analogous to that of a spinning top precessing under the influence of gravity. The protons precess at an angular velocity ω, known as the Lamor precession frequency, which is proportional to the magnetic field B, so that,

$$\omega = \gamma_p B$$

The constant γ_p is called the gyromagnetic ratio of the proton. It is the ratio of its magnetic moment to its spin angular momentum, the value of which is known to an accuracy of 0.001%. Because frequency measurements can be made quite precisely, the magnetic field can be determined equally as accurately. The magnetic moment from the moving proton induces a voltage that varies with the precession frequency ν, in a coil that surrounds the sample. It is therefore possible to determine the magnetic field from,

$$B = 2\pi\nu / \gamma_p,$$

where the factor $2\pi / \gamma_p$ = 23.487 +/- 0.002 nT / Hz. It is the magnitude but not the direction of the total field that can be obtained. The accuracy of measurement of magnetic field is determined in part by the accuracy of measurement of frequency. To realise the full potential of the method, the frequency needs to be measured to an accuracy of 0.001%. Although this is not particularly difficult to realise in a static installation, it can be problematic to achieve in portable equipment. The proton precession magnetometers sensitivity is quoted to be around 1 nT whilst immersed in the earth's magnetic field [4.5]. One advantage of the system comes from the fact that it requires no orientation or levelling, which is good for marine and airborne operation. One down side being its rather low resolution compared to SQUIDs. Proton precession magnetometers are only able to measure the total field and at intervals between measurement of a second or more which can be disadvantageous in some applications.

4.6 OPTICALLY PUMPED ATOM MAGNETOMETER

The optically pumped magnetometer was born from the technology gained around the time of the first lasers. The technique was developed by using the energy in transferring atomic electrons from one energy level to another. The principle of operation may be understood by looking at figure 4.3, which shows three possible energy levels, A_1, A_2 and B for a hypothetical atom. Under normal conditions of temperature and pressure, the atoms occupy the ground state levels A_1 and A_2. The energy difference between A_1 and A_2 being minute, representing the fine Zeeman splitting structure difference of opposing spin electrons in the local magnetic field, with energy in the region of 10^{-8} eV. Because thermal energies are much larger than this, at around 10^{-2} eV, the likelihood of the electrons being in state A_1 or A_2 are equally probable. The energy level at point B represents a much larger jump in energy compared to that from A_1 to A_2. The transition from A_1 or A_2 to B corresponds to infrared or visible spectral lines. The electrons are forced into the A_2 energy state by irradiation of the atom with a photon beam, where the energy corresponding to the difference between A_2 and B has been removed. This has the effect of lifting all the electrons in the A_1 energy state up to the B energy state. When the excited atoms fall back into the ground state, they will fall back into either A_1 or A_2 with equal probability. But the electrons in the A_1 state will be re-excited back up to the B state, whereas the ones that fell down to the A_2 state will remain there because the photon beam does not contain the correct energy to excite them out of that state. The net effect of this is to excite all the atoms from the A_1 to the A_2 state and is known as optical pumping. If a RF signal corresponding to the energy difference between levels A_1 and A_2 is now applied the pumping effect is nullified. The proper frequency for this signal being given by $\nu = E / h$, where E is the energy difference and h is Planck's constant (6.62×10^{-34} Js.)

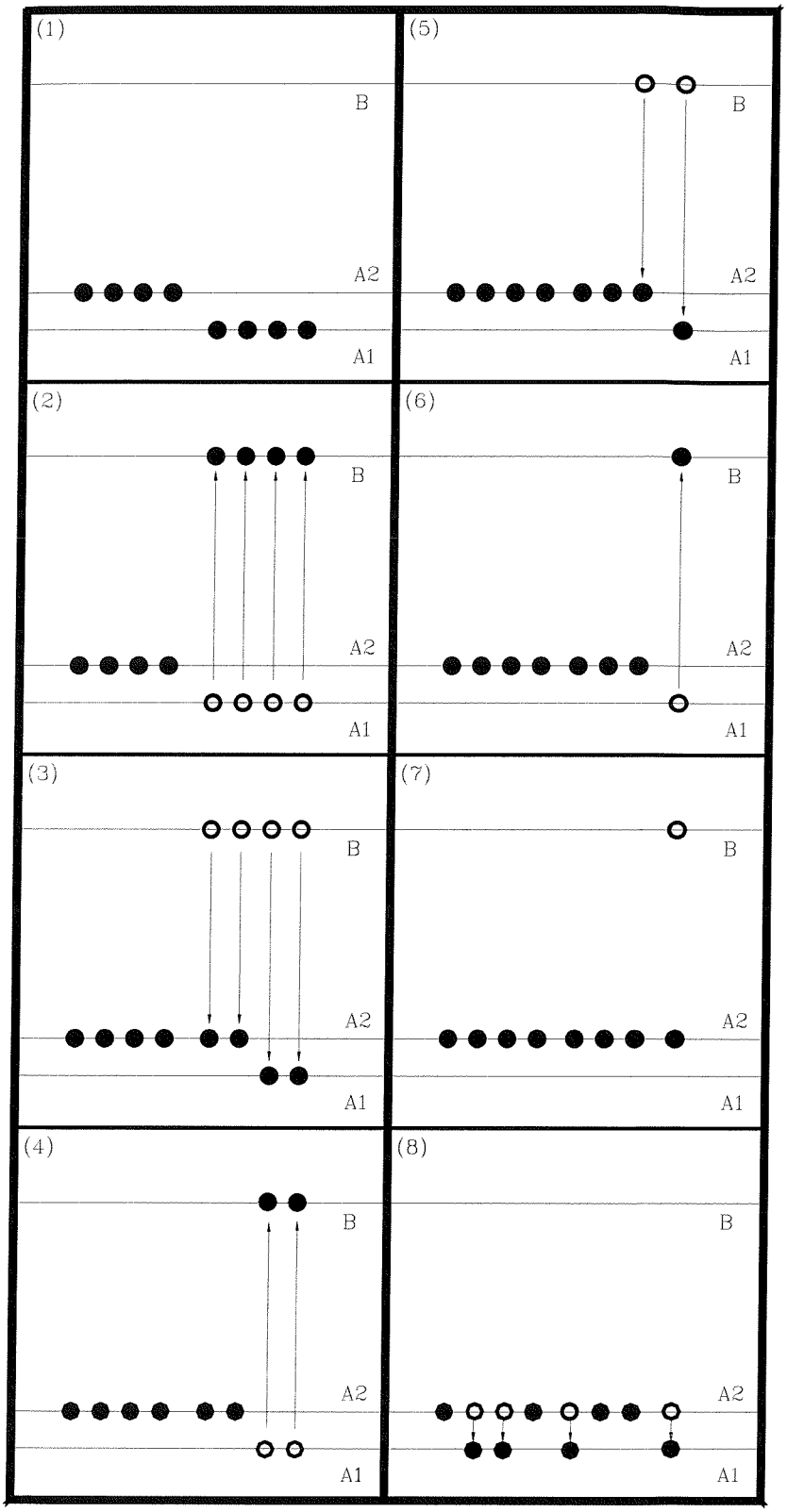

Figure 4.3. Optically pumped magnetometer.

To turn this idea into a working magnetometer it is necessary to select atoms that have magnetic energy sub-levels that are suitably spaced to give a measure of very weak magnetic fields. Elements that have been used for this purpose include caesium, rubidium, sodium and helium. In a rubidium-vapour magnetometer light from the rubidium lamp is circularly polarised to illuminate the rubidium vapour cell, after which it is refocused on to a photocell. The axis of this beam is inclined at approximately 45 degrees to the earth's field, which causes the electrons to precess about the axis of the field at the Lamor frequency. At one point in the precession cycle the atoms will be nearly parallel to the light beam direction and one-half cycle later they will be anti-parallel. In the first position, more light is transmitted than in the second. Thus the precession frequency produces a variable light intensity that flickers at the Lamor frequency. If the signal is received on a photocell, amplified and fed back to a coil wound on the cell, the coil-amplifier system becomes an oscillator whose frequency, ν, is given by:

$$B = 2\pi\nu / \gamma_e$$

Where γ_e is the gyromagnetic ratio of the electron. For rubidium the value of $\gamma_e / 2\pi$ is approximately 4.67 Hz / nT, whereas the corresponding frequency for the earth's field of approximately 50 μT is 233 kHz. Because γ_e for the electron is known to a precision of about 1 part in 10^7, and because of the relatively high frequencies involved, it is easily possible to measure magnetic field variations of around 10 pT. Indeed there are claims that these types of magnetometer can reach a resolution of 3 pT [4.6]. Since 1965, optically pumped caesium and rubidium-vapour magnetometers have been increasingly employed in airborne gradiometers [4.7].

4.7 INDUCTION COILS

Induction coil magnetometers represent one of the closest rivals to SQUID magnetometers in the area of geophysical prospecting. They are relatively cheap,

lightweight, fairly portable, with low power consumption and can have great accuracy. The principle of operation follows the law of induction, where a coil of wire with a high permeability core is energised by a changing magnetic field. The sensitivity of an induction coil is directly proportional to the number of turns of wire it contains (hence its size) and to the frequency of the magnetisation signal. To obtain sensitivities around the 20 fT mark, induction coils need to be over a metre in length. This length requirement can inhibit the practicality of fieldwork, especially if a three-axis magnetometer is deployed. Induction coils have a good frequency range in which they can operate for applications in geophysical prospecting [4.8]. It has been quoted that the best induction coils can measure to an accuracy of less than 100 fT from 1 Hz to over 1 kHz. They are at a disadvantage when compared to SQUIDs in two major ways, one of which being the portability aspect of a three-axis system. The other being that an induction coil takes longer to make a measurement than a corresponding SQUID system [4.9]. The SQUID has a faster measurement rate because of it's lower self inductance due to it's smaller size and the lower signal to noise ratio compared to induction coils. This means that greater depth penetration could be obtained with the use of a SQUID than with the induction coil as discussed in chapter 3. It is clear however that one of the greatest competitors in geophysical measuring instrument technology is that of the induction coil.

4.8 HALL PROBE

Hall sensors are sometimes used in non-destructive evaluation because of their good spatial resolution and relatively low cost. The main reason they are not very widespread is due to their relatively low signal sensitivity [4.10]. With a measurement range from slightly less than 100 μT to many Tesla, they are not really likely to pose any direct competition to the SQUID.

5. NOISE

5.1 INTRODUCTION

In this chapter the distinction between desired signal and unwanted noise is discussed. The essence of this entire project is concerned with the measurement and reduction of noise to allow the measurement of signals. Any SQUID output voltage will be composed of three main elements, signal, intrinsic noise and external noise, and it is the experimental goal to measure the magnitude of the signal as accurately as possible. The sensitivity of dc SQUIDs made from a high T_c superconductor is always limited by noise and comes in the two forms stated above, intrinsic and external. Intrinsic noise usually consists of white noise and 1/f noise. The white noise voltage is proportional to the operating temperature, due to the distribution of electron energies that cause this noise. The 1/f noise results from a large number of different physical sources and will be discussed below. The external noise comes from sources outside the measurement system, such as electromagnetic interference and changing magnetic fields. Different sources of error can also creep into measurements due to the inability to set up the apparatus perfectly. This form of noise can often be unavoidable but still needs to be addressed. This section will also discuss the ways in which intrusive noise is minimised, both in experimental set-up and in SQUID design and fabrication.

5.2 INTRINSIC NOISE

There are many papers that report on the general sources of noise within a SQUID [5.1-5.4] and some that just concentrate on particular aspects. The term 1/f noise was created from the observation that at a certain frequency the noise increased in proportion with the reciprocal of the frequency. It is now commonly agreed that the two main sources of this noise come from critical current fluctuations in the Josephson junctions and thermally assisted flux flow of vortices in the main body of the SQUID ring [5.5-5.8]. For SQUIDs to be useful in many applications they often require frequencies of less than 1 Hz. The

1/f noise becomes a significant factor at frequencies below 1 Hz, hence a huge amount of research effort has been dedicated towards reducing the frequency at which the on-set of this noise occurs [5.9-5.11].

The two main sources of 1/f noise will be described here, but these are not necessarily the only sources of intrinsic 1/f noise. The first one mentioned here arises due to the fluctuations in the critical current of the Josephson junctions, and the mechanism for this process is quite well understood. In the process of tunnelling through the barrier, an electron becomes trapped on a defect in the barrier and is then subsequently released. While the electron is in the trap there is a change in the height of the tunnel barrier and hence a change in the critical current density of that region. As a result of this, the presence of a single trap causes the critical current of the junction to switch randomly back and forth between two values, producing a random telegraph signal. If the mean time between pulses is τ, the spectral density of this process is a Lorentzian,

$$S(f) \propto \tau/(1+(2\pi f\tau)^2),$$

hence it is white at low frequencies and falling off as $1/f^2$ at frequencies above $1/2\pi\tau$. In many cases, the trapping process is thermally activated, and τ is of the form

$$\tau = \tau_0 \exp (E/k_BT),$$

where τ_0 is a constant and E is the barrier height.

In general, there may be several traps in the junction, each with it's own characteristic time τ_i. One can superimpose the trapping processes, assuming them to be statistically independent, to obtain the spectral density,

$$S(f) \propto \int dE\ D(E)\ [\ \tau_0 \exp(E/k_BT)/(1+(2\pi f\tau_0)^2 \exp(2E/k_BT)],$$

where D(E) is the distribution of activation energies. The term in square brackets is a strongly peaked function of E, centred at $E=k_BT\ln(1/2\pi f\tau_0)$, with a width of approximately k_BT. Thus at a given temperature, only traps with energies within a range

k_BT of E_{av} contribute significantly to the noise. If one now assumes D(E) is broad with respect to k_BT, one can take $D(E_{av})$ outside the integral, and carry out the integral to obtain

$$S(f,T) \propto (k_BT/f)\, D(E_{av}).$$

In fact one obtains a 1/f like spectrum from just a few traps. The magnitude of the 1/f noise in the critical current depends strongly on the quality of the junction as measured by the current leakage at voltages below $(\Delta_1 + \Delta_2)/e$, where Δ_1 and Δ_2 are the energy gaps of the two superconductors. Traps in the barrier enable electrons to tunnel in this voltage range, a process producing both leakage current and 1/f noise. Thus, for a given technology, junctions with low subgap leakage currents will have low 1/f noise.

The second source of 1/f noise in SQUIDs arises from the motion of flux lines trapped in the body of the SQUID. This noise has the same qualities as a simple flux noise i.e. it behaves as if an external flux noise were applied to the SQUID. This means that the spectral density of the 1/f flux noise scales with the square of the flux velocity, V_Φ^2 , and vanishes when $\Phi=(n +/- ½)\Phi_0$ where $V_\Phi=0$. In contrast, there is still critical current noise when $V_\Phi=0$, although the magnitude depends on the applied flux. The origin of the noise can be physically described in terms of the motion of flux quanta in the superconducting film. Each vortex hops independently between two pinning sites under thermal activation, a process that produces a random telegraph signal with a Lorentzian power spectrum of the form $\tau/(1+\omega^2\tau^2)$, where $\tau=\tau_0 \exp [-U(T)/k_BT]$ is a characteristic time, τ_0 is an attempt frequency and U(T) is the height of the energy barrier separating the wells. One computes the spectral density of an ensemble of such independent processes by adding the individual Lorentzians; if the distribution of activation energies is broad on the scale of k_BT, the result is a 1/f power spectrum. The spectral density of the noise can increase approximately linearly with the magnetic field in which the SQUID is cooled. This highlights the need for research in this area for applications such as geophysics because cooling and operation in the earth's magnetic field is crucial. It was found that the 1/f noise in multilayer structures were higher than in single layer films, due to the difficulty in maintaining sufficiently high quality microstructure through several growth

processes. Considerable progress has been made in this area however, with multilayer structures often outperforming their single layer counterparts.

The white noise level of a dc SQUID comes from the finite temperature at which it is operated. In a classical analysis the dominant sources of this noise come from Nyquist voltage and current fluctuations associated with the normal state junction resistance. For a ring with inductance L and two symmetrical junctions with critical currents i_c and resistances R, the spectral density of the noise voltage appearing across the junction is

$$S(V) = 4k_BTR/2$$

In addition to this voltage noise there will also be current fluctuations in the ring, with a spectral density,

$$S(i) = 8k_BT/R.$$

The simplest assumption is that these two noise sources are uncorrelated. Although this is not the case in general, because circulating noise currents will influence the voltages appearing across the junctions and vice versa. But to gain an approximation of the noise it is convenient to ignore any extra contribution from these cross-correlations. The flux spectral noise density $S(\Phi)$ is simply related to both minimum detectable energy in unit bandwidth δE and to S(V) and S(i):

$$\delta E = S(\Phi)/2L = [S(V)/(dV/d\Phi)^2 + S(i)/(di/d\Phi)^2] /2L.$$

The non-linearity of a SQUIDs response means that to evaluate the derivatives in the above expression requires numerical solution of differential equations. Tesche and Clarke [5.12] have given such an analysis. For the purposes of an approximate solution, it is possible to find solutions that yield results that are correct to within a small numerical factor. It is known that the maximum change in critical current that can be produced by an external flux is $\Phi_0/2L$ and this requires a change of applied flux of $\Phi_0/2$. Thus $di/d\Phi \sim 1/L$. Similarly

$$dV/d\Phi \sim (dV/di)\,(di/d\Phi) = R/2L.$$

Substituting these approximate values back into the previous equation yields the minimum detectable energy δE, set by thermal fluctuations in the SQUID ring:

$$\delta E \sim 8k_B TL/R.$$

This has the simple physical basis that a SQUID possesses two degrees of freedom (voltage and current) each of which is associated with $k_B T/2$ of thermal noise. This is distributed as white noise throughout a bandwidth of approximately $R/2\pi L$. However, it is the minimum theoretically achievable noise level possible in a SQUID, and the goal that is chased in all SQUID design and manufacture.

It is often convenient to eliminate R from the last equation, this can be done using the McCumber β parameter as follows:

$$\beta_c = 2\,\pi\, I_0\, R^2\, C\,/\,\Phi_0$$

The McCumber β parameter, β_c, is used in the design and characterisation of SQUIDs. It is used to minimise the hysteresis in the current-voltage characteristic and determine the maximum resistance that can be tolerated for a given capacitance. Hence:

$$\delta E \sim 16k_B T(LC/\beta_c)^{1/2}.\ (\beta_c \leq 1)$$

This equation gives a clear indication of how to improve the resolution of a SQUID by reducing T, L and C. A large number of SQUIDs with a wide range of parameters have been tested and found to have white noise energies generally in good agreement with the predicted values.

There have been reports of rf SQUIDs competing with dc SQUIDs due to their lower 1/f corner [5.13]. Although rf SQUIDs can have a higher white noise compared to their dc counterparts, they can have a lower frequency of onset of the 1/f knee. This means that

in applications where measurements down to low frequencies are required, but the absolute accuracy of a dc SQUID is not required, a rf SQUID could be a useful option for use in these applications [5.29].

5.3 EXTERNAL NOISE

The type and level of external noise that a SQUID will encounter is dependent upon the application. But it is the object of this section to highlight some of the more general sources of external noise and then refine the discussion towards specific applications relevant to this project. The general specification of modern high T_c SQUIDs is of the order of a few tens of femto Tesla; this is much less than the background noise signals generated in an ordinary laboratory environment. Figure 5.1 shows a schematic representation of the external noise signals in an ordinary laboratory or medical clinical environment. It is composed of a continuous background noise in the form of the hatched area and certain peaks at discrete frequencies. It is clear to see that over the whole frequency spectrum the external noise level is orders of magnitude larger than the field resolution of SQUID devices. The background signals are more or less uniform fields with the peaks being associated with relatively large non-uniform components induced by conductors and magnetic materials in the direct surrounding of the sensor. The peak amplitude of these signals can change very rapidly by the starting up or shutting down of electrical machines.

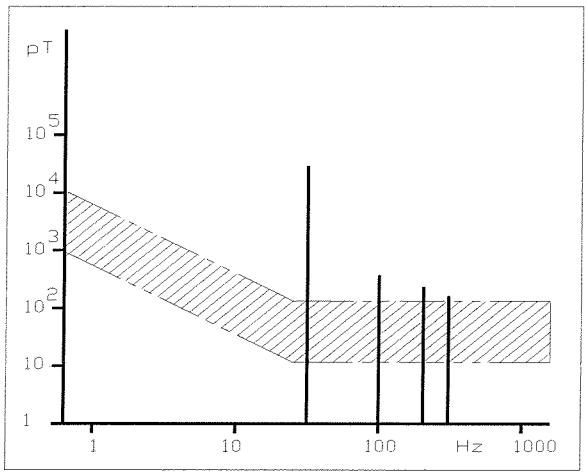

Figure 5.1. Typical noise spectrum of a laboratory.

5.3.1 ELECTROMAGNETIC INTERFERENCE.

It has been known for a long time that SQUIDs are very sensitive to electromagnetic interference (EMI). Especially in the vicinity of urban centres, EMI can seriously affect the operation of a SQUID. EMI can be suppressed by the introduction of magnetically shielded rooms, but these are very complicated and expensive to construct. In many applications such as geomagnetics it is not feasible to construct shielded rooms. Normal conducting shields placed around each individual SQUID can substantially reduce EMI, unfortunately this is done at the expense of an increased thermal magnetic noise, a reduced bandwidth and a frequency dependent phase shift due to eddy currents in the shield. There have been investigations into the effects of EMI on dc SQUIDs [5.14]. It has been found that EMI of sufficient intensity can reduce the modulation depth of dc SQUIDs as well as induce a low frequency excess noise, especially if the EMI has an amplitude-modulated part. Special readout techniques such as bias reversal can reduce this excess low frequency noise, as discussed later in this chapter.

The physical dimension of a SQUID is small in general when compared to the wavelength of EMI. EMI radiation incident upon the SQUID can then be considered to be a pure r.f. flux bias, hence the SQUID senses only the magnetic component of the electromagnetic field. For this reason it is appropriate to mainly consider the effects of an EMI flux (Φ_{EMI}) on SQUID operation. For simplicity it is assumed that only the bias current, the a.c. modulation flux ($\Phi_{a.c.}$) used for a flux locked loop and an EMI flux of single frequency are present. The r.f. flux induced by an EMI generates an additional screening current in the SQUID loop, which adds to the bias current. The SQUID modulation voltage will then be the result of a superposition of the SQUID response to $\Phi_{a.c.}$ and the interference flux. EMI of low frequency up to the order of several hundred kHz will probably be sensed by the flux locked loop and will therefore be present at the loop output. Higher frequencies will not appear at the amplifier output because the bandwidth of the readout electronics limits the frequency response of the system to less than a few MHz. Regardless of this fact the SQUID itself will respond to much faster flux changes, because its response time is given only by the switching time of it's Josephson junctions and the L/R time constant of the SQUID ring, which for

conventional thin film SQUIDs can be of the order of 50 ps. For EMI above a few MHz the amplified SQUID modulation voltage (V_m) will not contain components of the EMI signal, but only show its average value. No EMI is thus directly detectable at the output of the electronics assuming that the EMI is not amplitude modulated.

Due to the periodic nature of the SQUID transfer function, the r.f. flux generated by EMI will lead to a 'washing out' of the transfer function if the Φ_{EMI} is large enough. Even larger Φ_{EMI} can completely suppress flux modulation of the SQUID.

5.3.2. THERMAL FLUCTUATIONS

Temperature fluctuations within the SQUID system can have far reaching effects on the noise performance of such a system. They can influence both the stability and sensitivity of a high temperature dc SQUID. Temperature fluctuations as small as a few mK can have considerable influence on the sensitivity of a SQUID.

An example where temperature fluctuations are inevitable is a HTS SQUID cooled by a cryocooler. A pulse-tube refrigerator (PTR) is a type of cryocooler that operates by pulsing helium gas through a cold head at a frequency of around 2 Hz. In an experiment with a SQUID in two layers of mu metal and the PTR being made solely from non-magnetic materials [5.15], it was found that there was a 2 Hz period in the sensed magnetic field, even though there was no external signal applied. The periodic change in the flux signal had an amplitude of several $m\Phi_0$. With a measured temperature dependence of the SQUID ($d\Phi/dT$) of 1 Φ_0/K and an estimated temperature change of the cold stage in the PTR of 6 mK lead to the observed flux signal of some $m\Phi_0$. The temperature fluctuations of a cold head on a cryocooler can be reduced by the use of thermal low pass filters, but due to the periodic nature of the temperature variation, even small temperature fluctuations can give rise to a noticeable flux signal.

Depending on the type of SQUID used there can be up to four different mechanisms that contribute to the instability and increased noise of SQUIDs, due to temperature variation [5.16]. An initial mechanism to consider is the London penetration depth (λ_L), which has a temperature dependence of $\lambda_L = \lambda_L(0) / \sqrt{[1- (T/T_C)^4]}$. Temperature variations will therefore lead to changes in the London penetration depth, which in turn will lead to a

variation of the effective area of the SQUID, and hence it's field-to-flux transfer coefficient $b_\Phi = dB/d\Phi$. This will have a more serious effect on SQUIDs with smaller loop areas. It will also have greater effect close to T_c because the London penetration depth is proportional to $1/\sqrt{[1-(T/T_C)^4]}$. For a 20 pH HTS SQUID operated at 77 K, $B(\Phi)$ will change by nearly 1% for a $\Delta T = 1$ K. In an applied field of 50 μT, such as the earth's field, the $dB(\Phi)/dT$ dependence results in a $d\Phi/dT$ of about 5 Φ_0/K for a typical HTS SQUID with L = 20 pH and $B(\Phi) = 100$ nT/Φ_0. Whereas a typical low temperature SQUID would have a value several orders of magnitude lower of 5 mΦ_0/K.

A second mechanism, which has greater influence on noise, is thermally activated motion of flux in the SQUID body. During cool down in an ambient magnetic field, vortices can be trapped in the body of the SQUID, as mentioned earlier in the slightly different context of 1/f noise. The vortices that thread the superconductor are usually pinned at impurities or thickness variations of the superconducting ring. Thermal fluctuations can change the pinning energy and thus allow for the escape of vortices, which will move across the ring and thus change the flux in the SQUID. This effect is irreproducible in nature since the number of trapped vortices and their position in the SQUID is likely to vary with time.

The use of dc SQUIDs introduce two additional effects that can be compensated for with the use of appropriate readout schemes. Temperature fluctuations lead to a 1/f voltage noise across the weak links, which in turn leads to a 1/f component in the noise spectrum. This effect, which has already been discussed earlier in this chapter, is greatly reduced by the operation of a flux locked loop. The second effect springs from asymmetry in the critical currents in the junctions. This leads to a temperature dependent difference in current flow through the individual weak links. This results in a variation of the flux through the SQUID. If the critical currents of the two Josephson junctions (I_{C1} and I_{C2}) are not identical, the bias current (I_0) in the dc SQUID will be split up asymmetrically between I_{C1} and I_{C2} into the two branches of the SQUID ring, generating a net flux through the dc SQUID. As an example, consider an asymmetry in I_C of $I_{C1} = 2I_{C2}$. For a typical SQUID inductance of L = 100 pH and an $I_{C1} = 5$ μA, a $|d\Phi/dT| = 0.035\ \Phi_0$/K is expected. Reversing the bias current changes the sign of the temperature dependence

caused by this effect. It is therefore possible to reduce a temperature drift in the flux signal by using one of several bias reversal schemes.

As a consequence of these results, a cryocooler system used for cooling SQUIDs should be designed to have a temperature stability that is given by the acceptable influence of temperature changes on the flux signal. For random temperature fluctuations generated by boiling liquid cryogen for example, the fluctuation amplitude must not exceed 1 mK in order to observe the intrinsic noise of the SQUID, if it is assumed that the fluctuations are indeed white in a bandwidth of 100 Hz. Strong demands are made upon the periodic temperature stability of cryocoolers such as the PTR. For a $d\Phi/dT$ of 1 Φ_0/K (HTS SQUID in 50 μT field) and an intrinsic SQUID noise of 10^{-5} $\Phi_0/\sqrt{Hz}$, the periodic temperature fluctuations due to the cryocooler should not exceed a few μK.

5.3.3. OTHER EXTERNAL SOURCES

It is important to mention some of the other sources of noise that can compromise the measurement of magnetic signals. The production of eddy currents can seriously hamper the performance of a SQUID system. Any moving conductor that is immersed in a magnetic field can induce eddy currents that result in a varying magnetic field at the sensor. In a similar way, if there are magnetisation changes in a material for any reason it can affect the signal detected by the magnetometer. Some materials magnetic properties are dependent upon temperature, hence slight changes in temperature can vary their magnetisation and hence the amount of field incident upon the sensor. Because liquid nitrogen is slightly paramagnetic, the slosh of the nitrogen as it circulates around the cryostat can set up stray fields. In fact any magnetic material that is moving in a magnetic field will cause noise. Thermal emfs can be created if magnetic materials have temperature differences whilst moving around the sensor.

We will estimate the effect of sea water circulating around a SQUID sensor. This calculation has relevance to deep sea magnetometry, and demonstrates just how critical certain factors are. In this project the SQUID will be towed in a pressurised container at approximately 1 ms^{-1} through the water. When a conductor moves with velocity ($\underline{v}$)

through a magnetic field ($\underline{B}$) there is a field ($\underline{E} = \underline{v} \times \underline{B}$) generated at every point. The current density produced at any point will be:

$$\underline{J} = \sigma\underline{E} = \sigma(\underline{v} \times \underline{B})$$

Where σ is the conductivity of the medium. Assuming that $\underline{v}$ and $\underline{B}$ are perpendicular and with the knowledge that J is simply the current (I) divided by the area (A), we get:

$$I = \sigma \, v \, B \, A$$

Using the values for B = earth's field ~ 50 μT,
v = velocity of circulating water ~ 0.1 ms^{-1},
σ = conductivity of seawater ~ 5 $\Omega^{-1}m^{-1}$,
A = area of 0.5 m whirlpool = $\pi R^2 = \pi/8$.

Hence the current produced by this flow of water is:

$I = 5 \times 0.1 \times 50x10^{-6} \times \pi/8$
$I = 9.8x10^{-6}$ A.

If this circulating current of approximately 10 μA is now calculated as a magnetic field at a distance (r) of 1 m, the magnetic field will approximately be:

$$B = \mu_0 \, I / 2 \, \pi \, r$$

With $\mu_0 = 1.26x10^{-6}$ H m^{-1}, we get a value for the magnetic field sensed at a distance of one metre being approximately 2 pT. Hence the total field produced by a circulating current of sea water around the SQUID sensor could exceed one picotesla. This would not be a problem if the field produced was constant, but of course, due to the nature of water flow and water currents, field would vary. It is likely that there would be a random

fluctuation in the field produced, hence creating another source of external noise. A similar estimation was made by Clarke [5.17], in a paper written regarding geophysical applications of SQUIDs.

5.3.4 GRADIOMETER NOISE AND MEASUREMENT ERRORS

It is often convenient to use magnetic sensors in a gradiometer arrangement. As already discussed in chapter 2, this can be done in two ways, either with a gradiometric pick up coil or with two magnetometers in series opposition. High T_c SQUID gradiometers of sufficient quality can only be manufactured in the form of a thin film. These gradiometers are planar in design, generally with a separation between coils of 1-2 cm. To create an axial gradiometer from high T_c SQUIDs, it is necessary to use two magnetometers that are set a certain distance apart and configured to measure magnetic field in the opposite sense. The great advantage of a gradiometer is that it will largely reject distant sources of magnetic noise. This is so because of the $1/r^3$ attenuation of magnetic dipole field with distance meaning that the gradient of a distant magnetic field will have greatly attenuated by the time it reaches a gradiometer. There are several technical difficulties involved in using two magnetometers to create a gradiometer. It is crucial that the sensors are similar in performance, accurately aligned and held rigid.

To give an insight into the degree of accuracy in aligning the sensors, it is possible to perform the following calculation. If we assume that it is possible to achieve an accuracy of 500 fT with each individual magnetometer and the earth's magnetic field is approximately 50 μT. A gradiometer operated in the earth's field will need a sensitivity of 500×10^{-15} parts in a background of 50×10^{-6}. This difference equates to a sensing criteria of 1 part in 10^8. From a practical point of view, this means that the two individual magnetometers must remain aligned at an angle of within 1 part in 10^8 to maintain maximum sensitivity.

There are many other sources of error associated with the use of two magnetometers configured as an electronic gradiometer. Although most of these errors will only cause a small error they are still worth considering. The consideration of a deep sea

magnetometry project highlighted many of these potential sources of error. When two magnetometers are set one metre apart, any expansion or contraction of the material that the sensors are mounted on will introduce errors. When being towed under water there will be a certain amount of tipping as the craft under goes yaw and tow movements. As the originally vertical sensors are tipped at an angle the effective vertical distance between the sensors is reduced, thus introducing more error. If the two sensors are not mounted with the pick-up coils in exactly the same plane, their calibrations will therefore not be accurate because both sensors will trap different degrees of the vertical component of the earth's field.

The common mode rejection of an analogue to digital converter (ADC) can be another important area to avoid errors. In the electronic gradiometer arrangement where two magnetometers are arranged in series opposition the output of each SQUID is fed to an ADC. The common mode rejection of an ADC is dependent upon the number of 'bits' that the converter has. Because the analogue signal is placed into a digital value, the more bits the ADC has the more values the analogue signal can take. Going back to the 500 fT sensitivity in the earth's field of 50 μT requiring rejection of 1 part in 10^8 means that the ADC will ideally have a common mode rejection value at least as high as this. The digital value of each sample is stored in an array of binary units. To achieve a resolution of 10^8 would require an ADC with around 27 bits, which is impossible with present technology. Fortunately the variation of the earth's field over a period of a few minutes is a lot less. Diurnal fluctuations in the earth's magnetic field are generally of the order of a few nanotesla. This results in a required common mode rejection value of 500 fT in 5 nT, which equates to 1 part in 10,000. An ADC with 14 bits has sufficient resolution to fulfil this requirement and are readily available. There are many papers that discuss this issue, some of which will be discussed in the forthcoming section.

Continuing with a focus on the SOC project, the craft that was envisaged to tow the SQUID magnetometer array along the deep sea would also contain other measurement instruments. It would have been very important to assess any magnetic signal that emanated from other instruments and measure their effect on the gradiometer. It may then be possible to filter out the noise if it is found to be cyclic.

5.4 NOISE REDUCTION TECHNIQUES

5.4.1 SENSOR DESIGN

One of the major criteria of SQUID sensor design is to make a low noise instrument that can be successfully operated in the earth's magnetic field and preferably whilst in motion. Since the advent of high T_c materials the noise of SQUIDs has decreased by around eight orders of magnitude [5.18]. A recent discovery that was made by Dantsker et al demonstrated that the addition of slots and holes within the body of the SQUID could help reduce the low frequency noise, especially when the sensor is subject to the earth's field [5.19]. The reduction in noise was believed to be due to a reduction of flux motion by thermal activation within the superconductor. It was also found that by reducing the linewidth of the SQUID body it was possible to largely reduce noise. It was predicted that magnetic fields would be excluded from the body of the superconductor, below some threshold field, so long as the line width was below a certain value:

$$B_T = \pi\Phi_0/4w^2.$$

Where B_T is the threshold field and w is the linewidth of the superconductor. Experiments showed that there was very little increase in the low frequency noise for fields below the threshold value B_T, and a rapid increase with field at higher values as flux entered the superconductor. Fields of up to 100 μT were used in experiments and showed no degradation in the performance of some SQUIDs with sufficient slots. This was in marked contrast to non-machined SQUIDs that showed a great increase in their 1/f noise when immersed in these fields. It was calculated that a linewidth of 4 μm should return a threshold field of just under 100 μT. The motivation for reducing the linewidth is a reduction in the vortices that thread the superconductor. It is the thermally assisted flux flow within the superconductor body that causes 1/f noise as reported in section 5.2. This 1/f noise is increased when immersed in the earth's field because more flux vortices thread the superconductor creating more movement of these vortices to create extra noise. It has been demonstrated that it is energetically favourable for flux vortices to exist

outside the superconductor when linewidths of 4 μm or less are used. This effect was demonstrated up to the predicted field of 100 μT.

In a paper by Selders et al [5.20], a different approach was taken to the same problem. The introduction of antidots was used to introduce extra pinning sites within the superconductor body. Artificial pinning sites were created by the preparation of networks of sub micrometer holes. These defects were placed arbitrarily over the superconductor, where a periodic array of antidots with a radius much smaller than the distance between them was created. YBCO films were used and there was no deterioration of the superconducting properties caused by the introduction of holes. The antidots, sometimes referred to as sputter holes, were created by a high pressure on-axis magnetron-sputter technique on CeO_2 buffered sapphire and $LaAlO_3$. The experiment proved that there was a large dependence on the 1/f noise with the arrangement of antidots. Depending on geometrical arrangement the 1/f noise could either go up or down.

An alternative approach is the addition of a flux dam in the pick-up loop which has been demonstrated to reduce the amount of low frequency noise in a SQUID magnetometer when operated in the earth's magnetic field. The work by Koch et al [5.21] and [5.22] put a weak link or Josephson junction into the superconducting pick-up coil to create the flux dam. It is believed that a flux dam can prevent flux lines from being pinned to sites within the superconductor by providing an easy route for flux lines to enter and exit from the SQUID. Tests with commercial high T_c SQUIDs showed a marked increase in the low frequency noise when sensors were immersed in fields of 1 μT, whereas the flux dam sensors could withstand ambient magnetic fields up to 34 μT, which is at the lower end of the earth's magnetic field. Work carried out by Leslie et al [5.23] on rf SQUIDs operated in magnetic fields of 50 μT found no conclusive evidence of flux dams being an effective way to reduce excess noise. This may be an indication that the benefits from flux dams are rather marginal, but further investigation is required before definite conclusions can be drawn.

The reduction of low frequency excess noise and temperature drift of SQUIDs by 'degaussing' using high frequency magnetic fields has been reported by Muck et al [5.24]. The principle behind this scheme involves removing the vortices from the

SQUID body to reduce the 1/f noise generated by the thermally assisted flux hopping, or at least moving the vortices to pinning sites with high pinning energy. The demagnetisation is achieved by using a high frequency magnetic field of several hundred MHz and a maximum power of 10 mW. It was found that a demagnetising frequency of 200 MHz and above gave nearly two orders of magnitude improvement to the flux noise.

5.4.2 BIAS REVERSAL

The term bias reversal has been mentioned already, but is worth mentioning in some more detail due to its success and application. Most modern high T_c SQUID electronics operate bias reversal schemes to reduce the lower frequency noise. Instead of running the SQUID with a constant bias current, it is rapidly modulated from positive to negative maxima. Bias reversal does not affect the thermally assisted flux hopping noise aspect, but it reduces the contribution attributed to the critical current fluctuations within the junction.

The standard flux modulation schemes with a static bias current I_b through the SQUID eliminates the influence of in-phase fluctuations of critical current and shunt resistance of the two Josephson junctions. The in-phase fluctuations occur when each of the two junctions produce fluctuations of the same polarity. Out of phase fluctuations, which occur when the oscillations are of opposite polarity, appear as corresponding fluctuations of the magnetic flux in the SQUID and may deteriorate the low frequency noise performance. However, flux changes caused by these out of phase fluctuations are inverted if the bias current is reversed, and the resulting V-Φ characteristic is shifted along the flux axis. Therefore the influence of out of phase fluctuations can be eliminated by bias reversal schemes where the bias current is periodically switched. The 1/f voltage noise across the SQUID can be written in the following approximate form,

$$S_V(f) \approx \tfrac{1}{2} \left[(dV/dI_0)^2 + L^2 V_\Phi^2 \right] S_{I_0}(f)$$

The first term on the right hand side in the equation relates to the in phase mode which is eliminated by flux modulation. The second term relates to the out of phase fluctuations,

which can be reduced by bias reversal techniques as detailed in [5.25-5.27]. The effect of ac bias can be seen in figure 5.2, there is a much lower level of noise at lower frequencies as compared to the spectrum with dc bias. The line in figure 5.2 labelled BMSR results from a run taken in the Berlin magnetically shielded room. This room was constructed from different materials to minimise magnetic interference incident upon this space to create a bench mark for comparison. At very low frequencies below about 1 Hz, the ac biased spectrum follows very closely to the background noise in the magnetically shielded room that the measurements were taken.

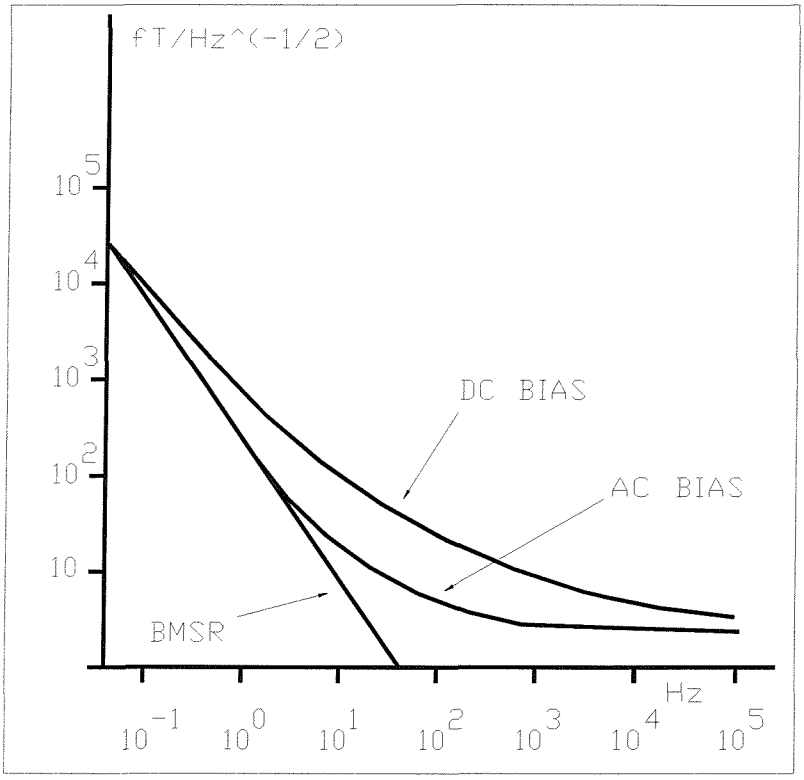

Figure 5.2. Reduction of low frequency noise by a.c. bias.

5.4.3 THREE SQUID GRADIOMETER

A method of noise reduction that was pioneered by Koch et al [5.28] is the three SQUID gradiometer (TSG). It has been the subject of much interest and refinement by several groups around the world. The basic principle takes advantage of a magnetometer to feed back magnetic field information to a coil that compensates for changes in the ambient magnetic field. The net effect being that the SQUID sensors that do the measurements are maintained within a low field environment.

A diagram of the circuit to make one of the axial components of the three SQUID gradiometer is shown in figure 5.3. It is important to note that this system requires nine SQUIDs to produce a three-axis TSG system. Within an axis of the system one of the SQUIDs is designated as the reference SQUID. The reference SQUID measures the changes in magnetic field that occur, in the normal way, except for the fact that the output is fed back to all three SQUIDs through identical coils that surround each SQUID. The two remaining SQUIDs are called the sensor SQUIDs, and their feedback loops measure the difference in magnetic field between reference SQUID and sensor SQUIDs. A calculation summing the two differences and dividing by the baseline (distance between sensor SQUIDs) results in the average magnetic field gradient in that area. It was found that the TSG had excellent linearity and common mode rejection ratio, because the uniform field subtraction is done magnetically. The subtraction to form the gradient is done electronically, which can reduce the linearity and common mode rejection in some circumstances. But because in most applications that the TSG would be used for, the magnetic gradient times the baseline is far less than the uniform applied field, the error introduced by the electronics is negligible. Since all the superconducting parts of the TSG operate in a constant magnetic field, the detrimental effects of magnetic hysteresis in the SQUID I-V characteristic are eliminated.

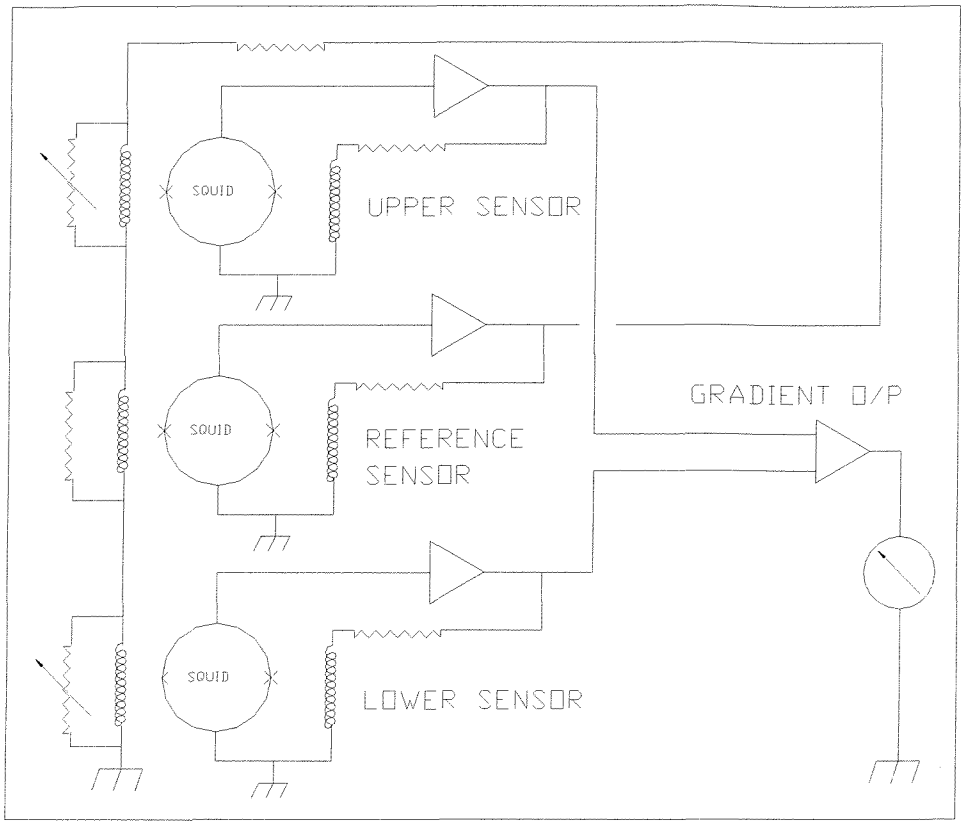

Figure 5.3. Idealised schematic of 3-SQUID gradiometer circuit.

5.4.4 SHIELDING (MAGNETIC AND EMI)

Two types of shielding will be discussed in this section because they are most widely used in SQUID applications. The point of shielding a SQUID is to protect it from the external environment, hence allowing it to make measurements without certain forms of interference. The two types of shielding most commonly employed are magnetic and electromagnetic interference (EMI) protection. Magnetic shielding can take the form of either a mu metal shield or a superconducting shield. Radio frequency interference (RFI), which is a sub-group of EMI, shielding is usually achieved with the aid of a thin sheet of conducting material such as copper or aluminium.

Mu metal shields attenuate the magnitude of magnetic field that is incident upon the SQUID. This is achieved because mu metal is a material of very high magnetic permeability, thus acting as a type of magnetic 'sponge', soaking up the magnetic field in

the area surrounding it. Mu metal is a generic name for the alloy containing approximately 77% nickel, 14% Iron, 5% copper and 4% molybdenum with a permeability of several thousand Henries per metre depending on frequency and ambient field. If mu metal surrounds the SQUID sensor then less of the earth's field, for example, will be incident upon the sensor, hence allowing it to work at a lower noise level. The level of attenuation of magnetic field from one side of the wall of an infinitely long mu metal cylinder to the other can be calculated with the following relation,

$$g = (\mu/4)\,(1 - (a^2 / b^2)),$$

where g is the ratio of magnetic field strength on one side of the shield wall to the other. μ is the permeability in Henries per metre, with a and b being the inner and outer radii of the shield respectively. Low frequency magnetic shield effectiveness is directly proportional to shield thickness because the shield's reluctance to magnetic flux is inversely proportional to its thickness. The above calculation was for an infinite cylinder. When the cylinder length is finite the effectiveness is reduced.

Electromagnetic noise can cause a real obstacle to achieving optimal performance within a SQUID. The associated rapidly oscillating magnetic fields can hinder the V-Φ performance of the SQUID. RFI and EMI typically enter the system through the various interconnecting conductors, which act as antennae. These antennae take the form of power supply and signal leads and data lines. RFI spanning across the electromagnetic spectrum from about 100 kHz to 100 GHz is the most common form of EMI found on earth, especially in industrialised nations. These noise sources include everything from broadcast radio stations to satellite uplinks to military and civilian radar. Ensuring that the SQUID is well shielded can eliminate the majority of RFI noise problems. Using thin layers of copper or aluminium in a complete grounded circuit around the sensors and all accompanying circuitry minimises the effect caused by RFI. It is extremely difficult to shield equipment from low frequency electromagnetic fields, because these fields all permeate non-magnetic conductors such as copper and aluminium.

CHAPTER 6.

6. APPARATUS DEVELOPMENT

6.1 INTRODUCTION

The purpose of this chapter is to explain the work that contributed towards the experimental aspect of this project. Because the project is of an experimental nature, there has been considerable work carried out in creating systems to collect and process data, to provide greater understanding of the usefulness of high temperature SQUIDs. The mechanical elements such as the cryostat and SQUID holder are discussed, with attention given to aspects such as circuitry and electronics.

6.2 CRYOSTAT

6.2.1 CRITERIA FOR CRYOSTAT DESIGN.

There are several important aspects to consider when designing a cryostat to house a SQUID. One such consideration is the minimisation of magnetic field production by the cryostat If the cryostat produces changing magnetic fields that the SQUIDs can detect, this will take the form of noise, which is undesirable. To minimise noise generated by the cryostat, it is important to minimise the ferrous and metallic components used. It is usually possible to eliminate all ferrous metals from the design of the cryostat. The reason ferrous metals are so detrimental to the operation of a SQUID is the fact that they are easily magnetised by movement in the earth's magnetic field, which in a portable system could swamp the actual signal that is being measured. All metallic objects near to

the SQUID will create eddy currents if there is a sufficiently strong changing electromagnetic field present. But the design is a compromise, because a complete radio frequency interference (RFI) shield is required to protect the SQUID from the potentially harmful electromagnetic interference. The RFI shield consists of a complete thin conducting layer around the SQUID to earth. This shielding often takes the form of a thin aluminium casing around the sensor which is in electrical contact with the shielding around the wires, which is also earthed to ensure all EMI goes straight to earth.

Other design considerations should include, materials used in construction to be poor thermal conductors, they must also be strong and rigid enough to support the stresses of acute temperature change, mass of liquid and transportation forces. Because high temperature SQUIDs need liquid nitrogen for them to operate, it is important to keep the temperature and pressure in which they operate as constant as possible to maintain consistent performance from the SQUID. The main material used must also be strong enough to withstand the forces involved in creating a vacuum within the main body of the cryostat. The reason for a vacuum is to reduce the thermal conductivity from the liquid nitrogen at 77 K and room temperature of 300 K; this will in turn reduce the rate at which the liquid nitrogen boils off into the atmosphere. The longer the cryostat can go between refills provides the opportunity for longer experimentation runs hence less disruption to the SQUID.

A very popular material as a result of all these considerations is fibreglass, which is not only a very poor, non-magnetic, thermal conductor, but has the mechanical strength to withstand the forces imposed by transportation and vacuum.

Figure 6.0 shows the arrangement used in the single, double and triple shielded experiments in the laboratory.

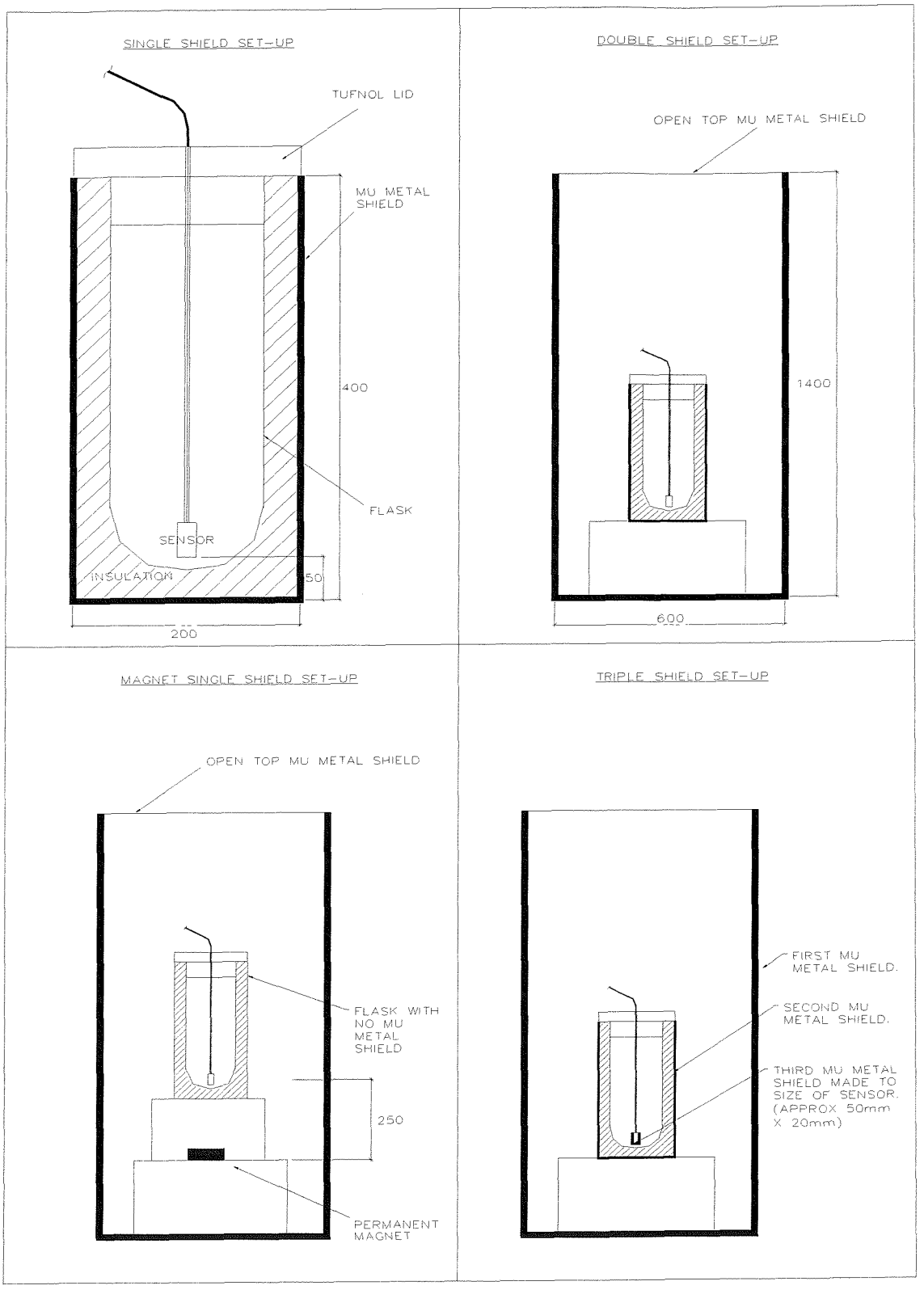

Figure 6.0. The four types of set-up used in the laboratory experiments.

6.2.2 GLASS FIBRE CRYOSTAT.

A fibreglass cryostat in the laboratory was identified that would be suitable for the testing of the high temperature SQUIDs. The general design and construction of the cryostat can be seen in figure 6.1. This cryostat was used for almost all of the laboratory tests and the early field tests on Southampton common.

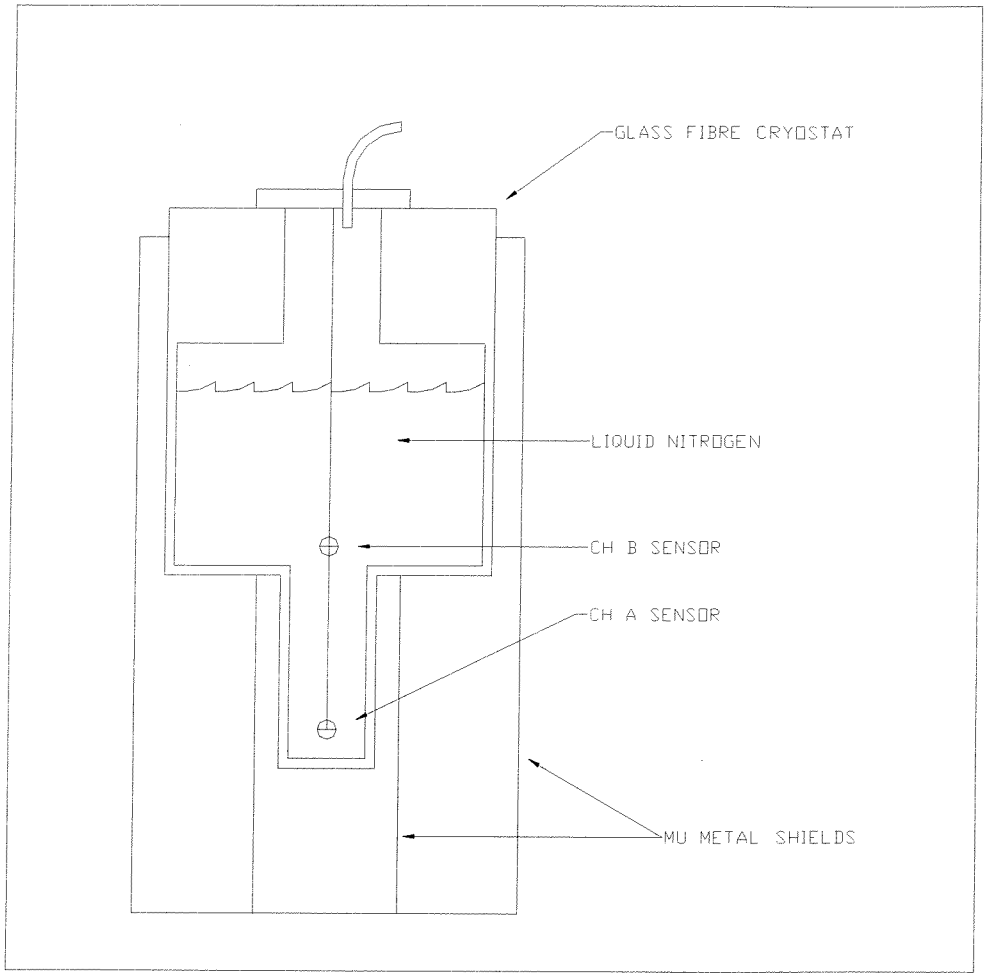

Figure 6.1. Glass-fibre cryostat.

The calculated volume of liquid nitrogen that this cryostat held was approximately 12 litres of liquid, it had an average boil off rate of less than 2 litres of gas per minute. When nitrogen liquid evaporates into a gas it expands to approximately 700 times it's volume, this meant that the cryostat had a time between fills of up to 3 to 4 days. For applications of prospecting in remote places, a hold time of this length is an obvious advantage. The cryostat had no metallic parts other than the thin aluminised-mylar insulation outside the nitrogen can and the non-ferrous metallic valve and screws on top of the cryostat. All other joints were made with epoxy-resin, 'o' rings and rubber matt, all of which is non-magnetic. It was found that the noise of comparable cryostats was less than 10 $fT/Hz^{1/2}$ at 1 Hz [6.1], which is far below the level of noise that is of most interest by nearly two orders of magnitude.

6.2.3 TRISTAN CRYOSTAT.

With the HTM1 sensors came a small cryostat from Tristan technologies. This cryostat was also made from fibreglass but was much smaller in scale, and could therefore only hold one sensor. This would mean that a gradiometer system would not only require two sensors, but also two cryostats. This would have made the capital cost of a three-axis gradiometer system very expensive, although it would give the flexibility of a huge baseline, because the sensors no longer need to be constrained within the same cryostat. The longer the baseline of a gradiometer the better the resolution of the system as a whole. In practice, due to the small size of the cryostat, it only held nitrogen for a matter of a few hours, due also because the valve on the cryostat was faulty and let air into the vacuum space. Even with this problem it was encouraging to see that the SQUID could still detect land mines, see figure 6.1A and chapter 7. A perfectly working cryostat of this type has a quoted hold time of the order of a day, which is quite acceptable for field use just as long as there is access to further supplies of liquid nitrogen.

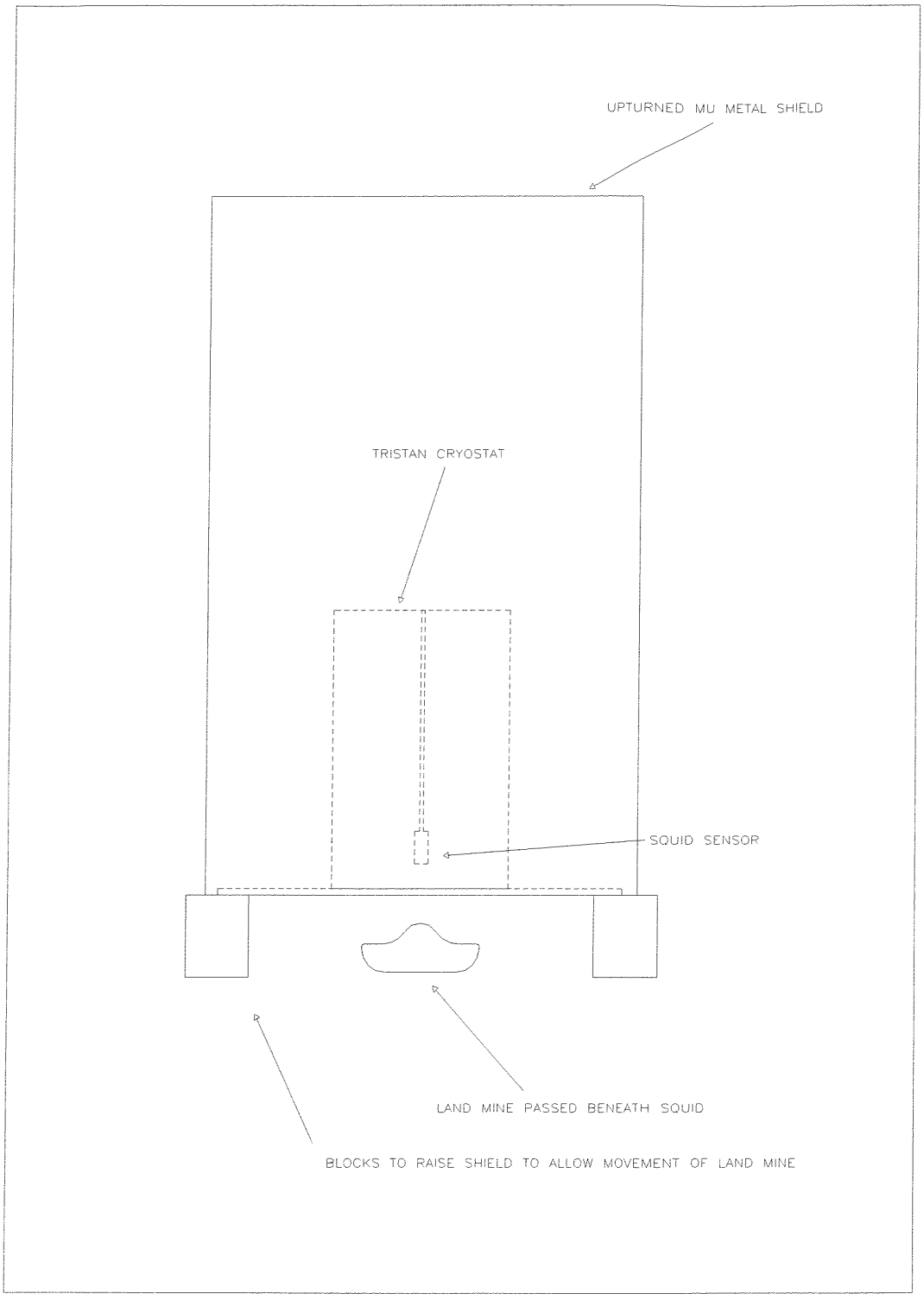

Figure 6.1A. Set-up for land mine detection.

6.2.4 GLASS FLASK.

One of the simplest forms of cryostat to operate a SQUID is the glass flask. This is simply a vacuum insulated glass container with a lid and insulation, as shown below in figure 6.2. The set-up shown below was used in the early stages of the project and was designed to incorporate a Helmholtz coil set to emulate the earth's magnetic field.

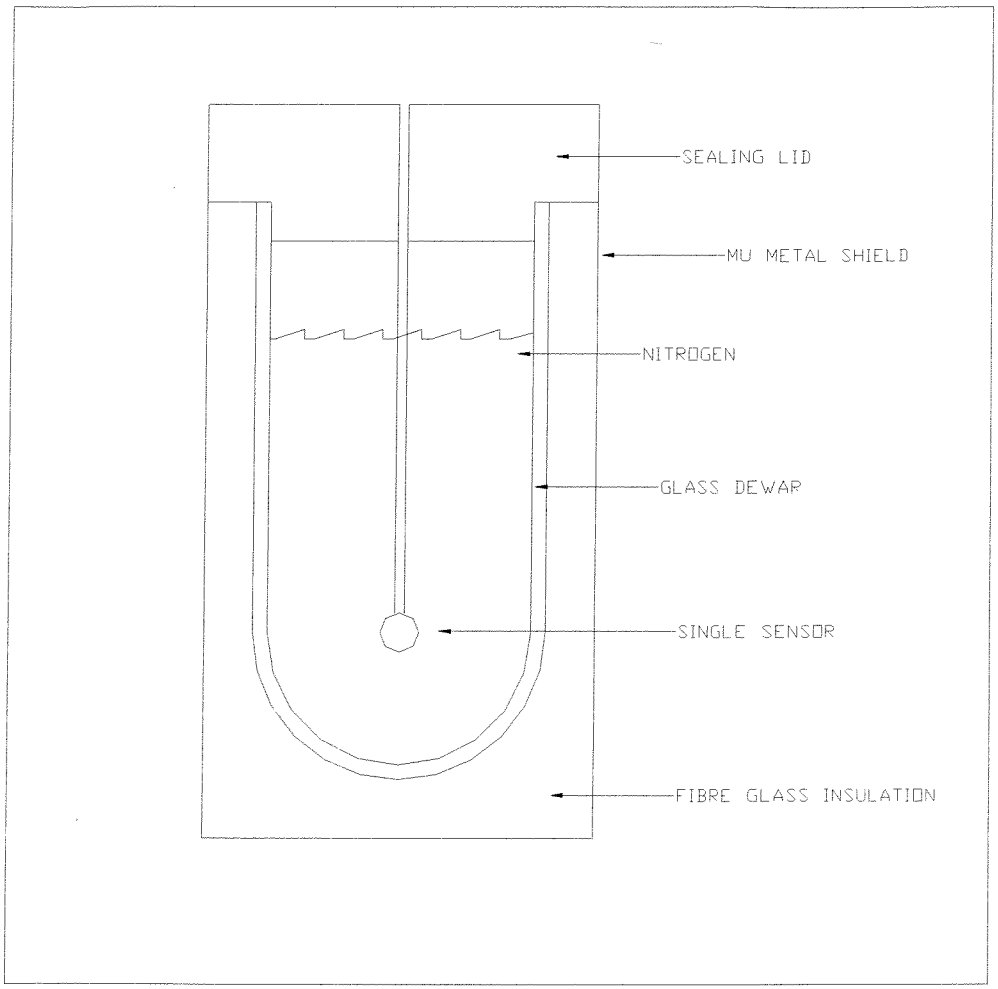

Figure 6.2. Glass-flask cryostat.

The set-up was later adapted for use in the field, as shown in figure 6.3. The glass flask provided a good non-magnetic container for the SQUIDs, whilst the large bucket full of sand provided a sturdy base for the arrangement. The importance of a vibration free platform from which to take measurements is immense, because the sensors are

completely unshielded in the field, hence they are fully responsive to the relatively large magnetic field of the earth. It does not therefore take much movement, such as that caused by a gust of wind, before it can be measured by the SQUIDs, thus introducing more noise into the system.

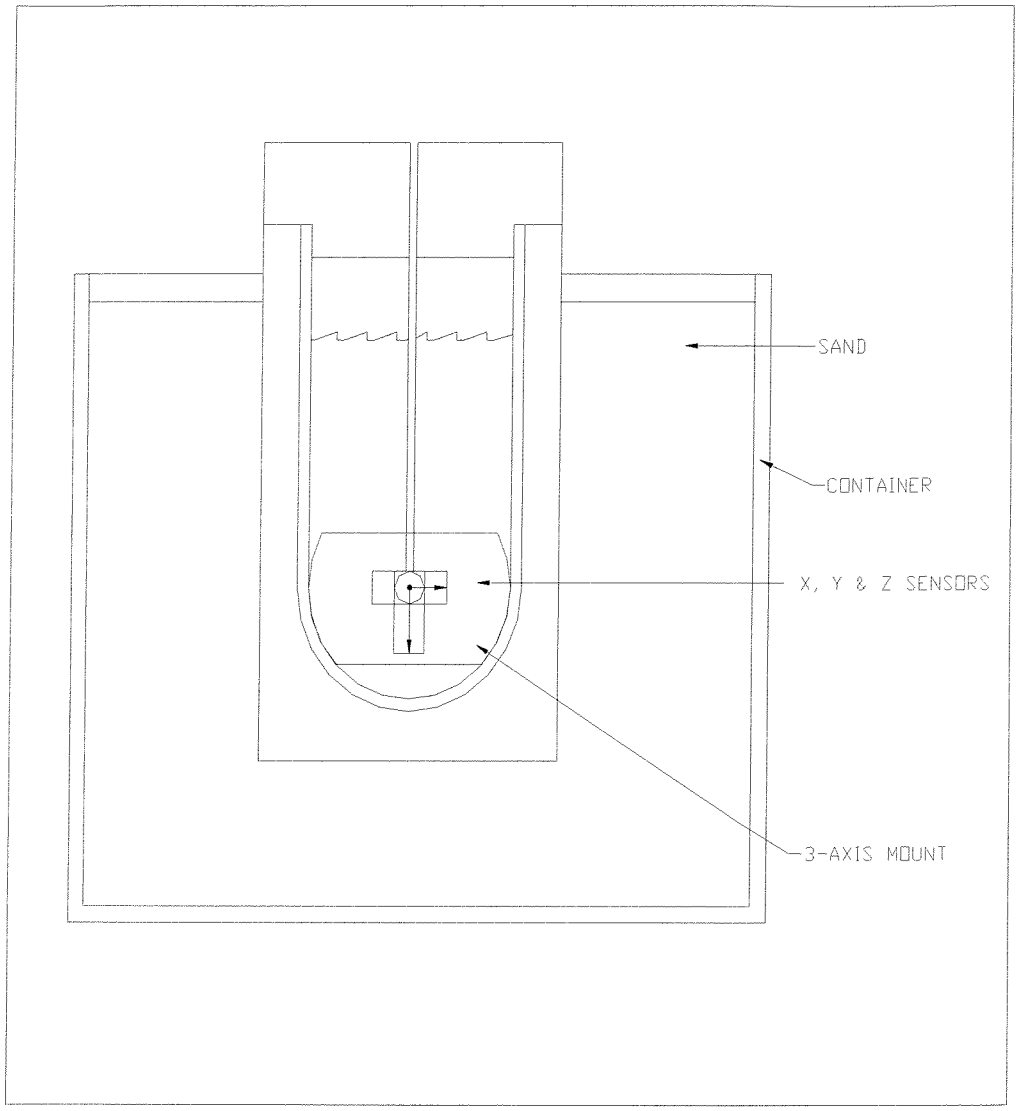

Figure 6.3. Glass-flask cryostat for field use.

6.3 SQUID SELECTION AND SPECIFICATION

There were a number of different SQUID companies contacted about the purchase of a high temperature SQUID system. There were only two companies found that marketed high temperature SQUIDs of sufficient quality that were able to lend a system for evaluation. The following sections discuss their design, construction and integration.

6.3.1 OXFORD INSTRUMENTS GRADIOMETER.

The system supplied by Oxford Instruments was a single chip gradiometer system. The gradiometer had a quoted baseline of better than 1900 fT / $Hz^{1/2}$ / cm at 1 kHz.
The system was collected from the company after a demonstration of its operation. When the system was set-up in the laboratory, satisfactory operation was never achieved, until complete failure occurred and the system was returned. Although a complete calibrated run was never achieved, it was during this time that the basics of operation of the SQUID were learnt. It was also possible to undertake some qualitative experiments with the system whilst it was still operating.
Oxford Instruments were unable to provide a satisfactory and fault free system that was reliable enough for evaluation. This fact ended the testing of this system, however it was concluded that the system as a whole was complicated and slow to control.

6.3.2 TRISTAN TECHNOLOGIES MAGNETOMETERS.

Tristan Technologies is a company that was formed from the break up of Conductus Incorporated, a large American company specialising in superconductor technology. The first system that we received and tested was called the HTM1. This name is derived from the fact that the HTM1 sensors were designed for optimised operation in magnetic fields up to 1 μT. The second type of system received was called the HTM100, which was designed for optimum performance in ambient fields of up to 100 μT. The SQUID controller was common for both the HTM1 and HTM100 systems, and came from the

original Conductus low temperature SQUID system that had been marketed for many years.

6.3.2.1 HTM1 MAGNETOMETER.

The first system type received from Tristan was the HTM1, so-called because it was designed for operation in small ambient magnetic fields below 1 μT.
During the testing period with these sensors, which lasted for nearly a year and used three different HTM1 sensors, the entire system operated faultlessly and with ease. The control box had an automatic start up routine, which put the sensors straight into test mode automatically. This is an advantage for field operation because any untrained non-specialist could operate the SQUID without any prior knowledge of SQUID systems.

6.3.2.2 HTM100 MAGNETOMETER.

Two high field HTM100 magnetometers were delivered as soon as they became available. They were called high field sensors because they were the first commercially available high temperature sensors on the market designed for operation in magnetic fields as high as the earth's. This was an advantage when searching for unshielded applications of high temperature SQUIDs. Where the HTM1 sensors were manufactured by Conductus, the HTM100 sensors were made by the Jülich group in Germany [6.2].
The circuit design used to collect and process data was identical to that described for the HTM1 in section 6.3.2.1 and 6.9.2.

6.4 SENSOR HOLDER

There were a number of sensor holders designed and constructed for this project. The first was the small tufnol holder with Helmholtz coil for the glass flask. The second was the larger tufnol holder for the fibreglass cryostat. The third and final sensor holder of

note was the holder for the field set-up that went into the bigger glass flask to allow all three-axis components of measurement.

6.4.1 HELMHOLTZ COIL SENSOR HOLDER

This sensor holder was designed when there was only one sensor available for testing; hence it accommodates one sensor. This holder was designed to incorporate an integral Helmholtz coil set. It was planned to run the SQUID within the magnetic shielding to create a zero magnetic field environment for the SQUID. The Helmholtz coils would then be connected to a constant current source to produce a constant field of around 50 μT. The theory therefore was to immerse the SQUID in a constant magnetic field similar to that of the earth's, because the mu metal would cut out most of the interference from the external environment and the Helmholtz coil would create a steady magnetic field. The results from this run could then be compared to runs with the Helmholtz coils switched off. This would give a direct comparison of performance of the high T_c SQUID in a near zero magnetic field and that of the earth's. The design and integration of this system can be seen in figure 6.4.

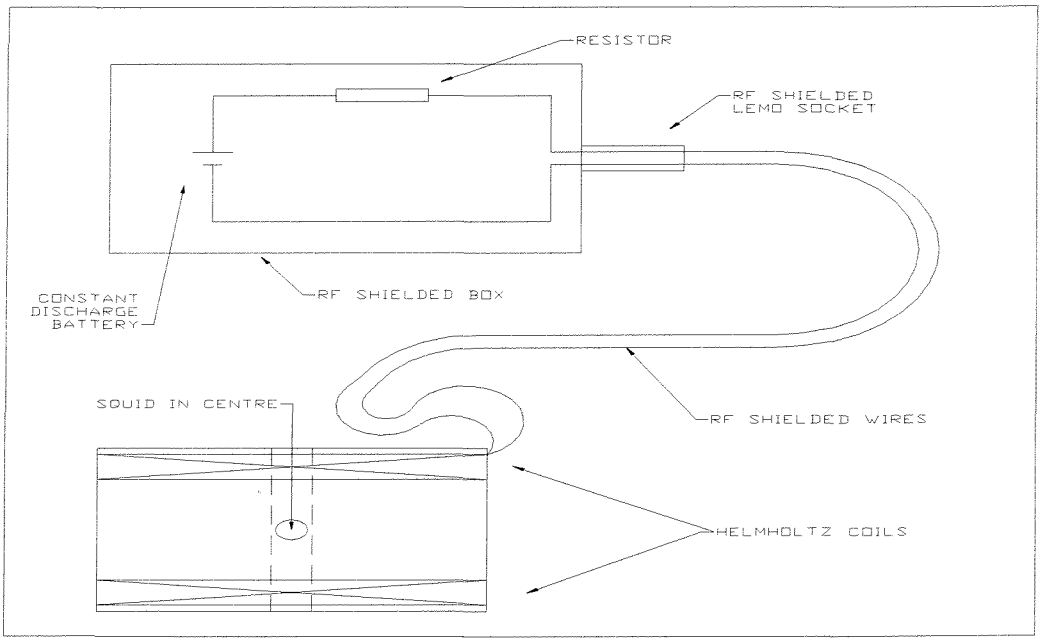

Figure 6.4. Helmholtz coil-sensor holder.

6.4.2 LARGE TUFNOL HOLDER

This sensor holder was the most complicated and intricate holder to design and construct. Figure 6.5 shows a simplified schematic of the sensor holder, it is a two sensor holder which meant it was capable of enabling gradiometric measurements for the first time. The two sensors were held rigid with respect to each other to minimise errors. As the sensor holder was such a tight fit in the cryostat, it ensured that there was no movement or vibration of the two sensors between sensor holder and cryostat. There were tracks put into the sensor holder for the wires to lie in. The size of the tracks were designed specifically to make the wires lie tightly in the tracks to ensure there was no movement between wires and sensors, hence ensuring that no magnetic fields would be produced by these wires moving with respect to the sensors.

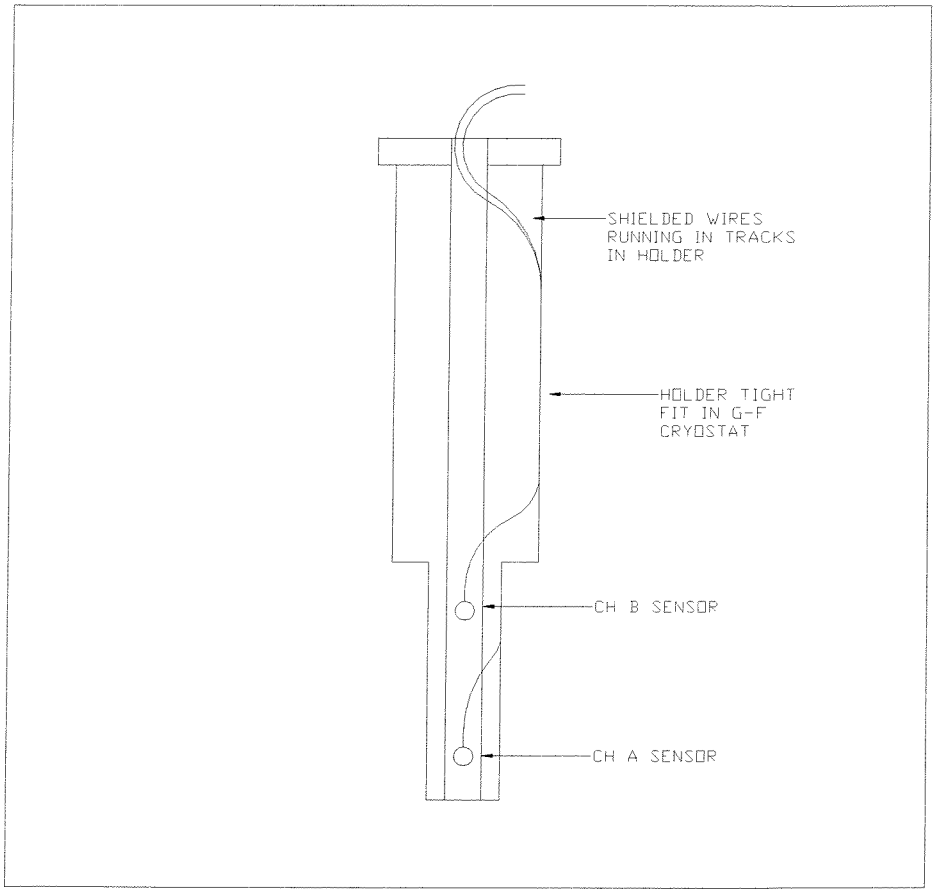

Figure 6.5. Two SQUID gradiometer set-up.

6.4.3 THREE-AXIS SENSOR HOLDER.

This sensor holder was the only one designed and built that was capable of measuring all three axes at once. The collaboration with the Swansea group allowed the use of another sensor to make a three-axis magnetometer system, capable of undertaking magnetotelluric measurements in the field. Figure 6.6 shows the design and construction of the three-axis set-up. Again the set-up was designed to make everything sturdy and vibration resistant. In the field tests, the large bucket full of damp sand that surrounded the sensors was protected from the wind by a large windbreak that was situated up-wind from the SQUID and control electronics. As far as was practicably possible in a portable system, it was vibration resistant.

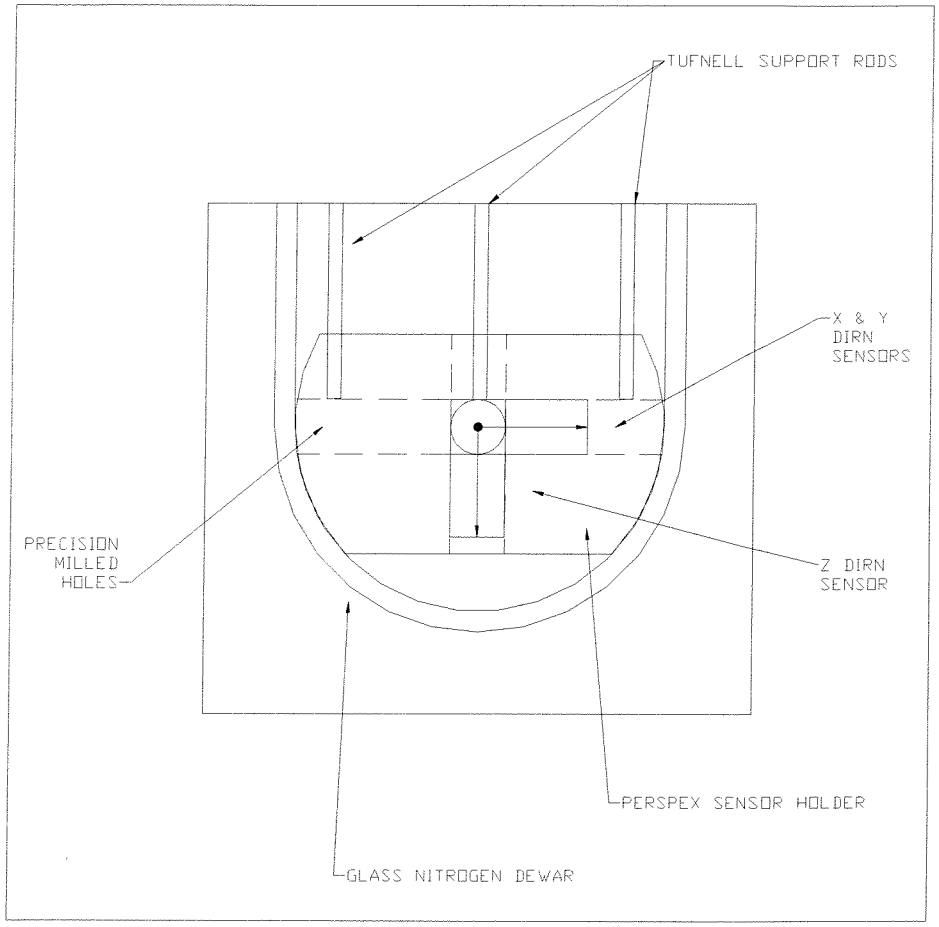

Figure 6.6. Three axis magnetometer set-up.

6.5 SQUID CONTROLLER

Tristan Technologies supplied a fully automatic SQUID controller, which operated both the HTM1 and HTM100 sensors. All aspects of control were possible, from fully automatic set-up to manual control. A full explanation is not necessary here; full details can be found in the Tristan Technologies HTS SQUID controller manuals.

6.6 DATA COLLECTION

6.6.1 ADC100

The ADC100 analogue to digital converter (ADC) measures voltages at pre-set intervals and stores those values in the form of columns of data in the computer. Accuracy relies on the precision of the ADC to measure minute changes in voltages. The ADC100 is a two-channel analogue to digital converter externally mounted to the computer and is powered and operated from the printer port on the computer. The maximum sampling rate was 1 kHz or 1000 samples per second. The sensitivity of the ADC100 was determined by the scale that it was set on when sampling a voltage. The converter was 12-bit, which meant that it had 2^{12} 'bins' in which it can convert the analogue data into digital data. The 4096 bins when used on their finest scale of +/- 50 mV on the ADC100 resulted in a digitisation sensitivity of 0.025 mV per bin. The manufacturers quoted accuracy was 1% typical error, which converts to an accuracy at best of around 10 fT +/- 0.1 fT when set on the finest scale of 50 mV. When the ADC100 was set to allow full scale deflection of the SQUID of +/- 5 V the sensitivity and error for a typical sensor works out to be around 1 pT +/- 10 fT. It was obvious from this result that careful attention had to be paid to the scale on which the converter was set before starting any run. If a power spectrum were required with a sensitivity of 10 fT, then the +/- 50 mV range would have to be used. On the other hand, if a longer run was required to study the stability of the SQUIDs then a greater dynamic range was required to suit the dynamic range of the SQUID output.

6.6.2 FIELD DATA COLLECTION ADC.

Because the ADC100 was a two-channel device and the fieldwork required a three-channel system and greater accuracy, an eight channel 16-bit analogue to digital converter was acquired for the project. With the ADC being 16-bit, it gave much greater sensitivity over a greater range of voltages. This gave the capability of 65,536 bins to be spread over a dynamic range of +/- 5 V. The result of this improved performance gave a typical sensitivity of 0.15 mV with a 1% error. SQUID performance could then be measured to an accuracy of typically 60 fT +/- 0.6 fT, which is an accuracy that can be improved upon by reducing the dynamic range if necessary. With a three times over-sampling method the accuracy was brought down to less than 20 fT +/- 0.2 fT. Over-sampling involves taking multiple samples and averaging them. Hence three times over-sampling involved averaging every three samples taken. This gave the advantage of greater accuracy but with reduced effective sampling frequency to one third of the actual sampling frequency.

6.7 DATA PROCESSING

It is important to explain the manner in which the data was collected, processed and presented. The 12-bit ADC100 and the 16-bit 8-channel analogue to digital converters both collected a data column for each channel being measured, with an additional column for the time data. All data was saved as a text file to allow maximum flexibility of transportation to graphical packages. All graphs were ultimately plotted in Microcal Origin graphical package, although the more complicated calculations were performed in Matlab.

The processing of the raw data went as follows; three columns of data were imported into Origin as an ASCII text file. The three columns consisted of time data, and data from the two channels (assuming two channels were in use.) The voltage data from both channels was corrected so that the first element in both columns was zero. This is justified by the fact that the SQUID is a 'null' detector, and therefore does not measure absolute values

of magnetic field (just changes), hence the zero point is arbitrary and was taken as the first point of both channels. This time versus voltage data could therefore be plotted and is referred to as the 'voltage drift' of the two channels. It was found that if the voltages were not set to zero, and their start points were several volts apart, with their respective drifts only a few parts of a volt, there was insufficient resolution to obtain any kind of impression of the SQUID performance.

The second graph that was plotted from the data was the 'field drift'. The voltage data was calibrated from the conversion in the specification of the sensors. This graph gave a more accurate view of exactly what magnetic field the sensors were recording during a run.

The final graph that could be produced from any run was the 'field difference' graph. As the title suggests, the two columns of data representing the actual field change of each individual sensor were subtracted from each other. This subtraction produced one column of data: the field difference, which is directly analogous to the gradient in an application environment.

The field difference graph could be used to find some very important information. It was possible to work out the common mode rejection of the system within the correct experimental constraints. If both sensors are placed in an identical environment, and they both have the same levels of intrinsic noise then the field gradient should be equal to zero at all times. It is impossible to place both sensors in exactly the same piece of space and time, hence there may be slight differences in the magnetic fields that both sensors experience. Because the intrinsic noise of SQUIDs has a random component, the intrinsic noise between two SQUIDs is unlikely to be fully correlated. Hence, in reality the measure of common mode rejection between the two channels of data becomes a measure of the intrinsic gradiometric noise of the system, if it is assumed that the sensors are placed in as far is possible, the same environment.

Before a run was undertaken to obtain a power spectrum it was important to realise the time constraints involved. Because the power spectrum involves the Fourier transform of the data, the time domain is converted into the reciprocal of the time domain, the frequency domain. The area of greatest interest for a power spectrum for SQUID application lies between 0.001 Hz and 1000 Hz. Because the frequency is the reciprocal

of the time domain, to achieve definition of spectrum down to 0.001 Hz, sampling must run for at least 1000 seconds. But to achieve a resolution of 1000Hz, it is necessary to sample 2000 times a second. One thousand times a second being 1000 Hz, but due to the Nyquist law it is necessary to sample at least twice this rate. Hence to achieve a spectrum that runs from 0.001 Hz to 1000 Hz it is necessary to sample 2000 times a second for 1000 seconds. This would produce a data file of two million rows per channel. Thetime taken to process this data becomes difficult to justify for the gain that is achieved. For this reason a compromise is made over the frequency range required. It was found that a power spectrum from 0.1 to 500 Hz was acceptable. This therefore required a sampling rate of 1000 per second for 10 seconds at a time.

To maintain consistency, the data that formed the Matlab power spectra was converted into ASCII text format and imported into Origin where it was graphed. Hence, all data that was collected in this project was presented by the Origin package. All graphs that were gathered from other sources, such as the calibration were left in their original format.

As a final note to this section, it is worth explaining how the spectra were gathered in the laboratory and in the field. Because the SQUIDs in the laboratory were well shielded and the two channels run simultaneously were not correlated, it was assumed that it was safe to do a straight transform on each channel separately. This would result in two individual power spectra per run. When such runs were performed in the field, the situation was very different. Because the earth's magnetic field is constantly changing by the order of many hundreds of picotesla per minute, any spectra of any individual channel could be dominated by such noise. It was therefore decided that open field spectra data would be obtained from the subtracted field data. The resulting spectra would therefore represent a kind of average of the noise of the two channels. In fact, statistically the power spectra obtained in the field from two SQUIDs would represent $\sqrt{2}$ times the actual intrinsic noise of each individual SQUID.

6.8 FILTERING.

There were two forms of filtering used to minimise the amount of unwanted noise that was detected by the SQUIDs. The first form of filter used was electronic. The filter integral to the SQUID controller was electronic and trimmed off the high and low frequency signals. Later there was time spent on manufacturing electronic notch filters to reduce the huge 50 Hz noise that is ever present in all apart from in the most remote regions. The other form of filtering was by software, in which a Matlab program was written to remove certain unwanted frequencies from the data.

6.8.1 ELECTRONIC FILTERING.

The electronic filtering provided by the SQUID electronics was highly controllable and versatile depending on application. There was a variable high pass and low pass filter available on the control panel. The high pass filter could be set to DC which is effectively doing no filtering at all, or 0.5 Hz and 5 Hz, in which all frequencies above 0.5 and 5 Hz are passed through the electronics and collected as data. A high pass filter could be useful in circumstances where a long run were to be taken, but the low frequency drift of the SQUID caused it to go past full scale deflection. The high pass filter ensures that the output of the SQUID will remain within the limits of the electronics output unless a high frequency spike occurs, causing the SQUID to reset. The low pass filter would allow all frequencies below the pre-set value to pass through the electronics. The pre-set values on the SQUID electronics were 500 and 5000 Hz.

The only feature that the SQUID electronics lacked was a 50 Hz notch filter, which operates in a manner to remove a particular narrow frequency band, in this case 50 Hz. There were many potential designs of notch filter investigated, with their effectiveness increasing with cost. It was decided to start with a simple and economic design of filter to gain experience in filter design and construction.

One of the main drawbacks of electronic filters is the fact that they do not stop filtering at precisely the desired frequency – there is a degree of roll-off. For example, a 50 Hz notch filter will not only remove signals at 50 Hz, it will also remove some at 49 and

51 Hz. The amount of extra frequencies taken or desired frequency let through all depend upon, type, design, specification and cost of components and circuit.

6.8.2 SOFTWARE.

Noise of a periodic nature can be eliminated by using software filtering. The 50 Hz signal that comes from mains electricity can be filtered this way. The frequency at which mains electricity is generated can vary with time, but is generally around 50 Hz. Software methods allow very accurate filtering over a definite range of frequencies. Software filtering was used in the field runs to attenuate the effect of mains electricity.

6.9 POWER.

The purpose of this section is to explain how the system was powered during the respective modes of testing. When field tests were conducted, it was obvious that mains power was not going to be available, but in the laboratory it was not convenient to use batteries because they need constant recharging or replacing which is inconvenient and expensive. For these reasons there were two different power set-ups, one for the laboratory and one for the field.

6.9.1 LABORATORY POWER

The SQUID control unit from Tristan Technologies was converted by Tristan Technologies from its normal 240 V a.c. mains power supply to allow d.c. battery power to be used. This meant that the controller came with a power lead that consisted of three live wires and one neutral. The live wires required 12 V, and plus andminus 24 V. The simplest way to achieve this to allow integration with a single power source of battery or main origin was to use a single 12 V power source with two 12 to 24 V DC to DC converters. This allowed the use of a single 12 V power supply to run the entire SQUID system.

6.9.2 FIELD POWER.

The only power source suitable for portable application in this project was battery power. It was part of the design to allow the straightforward removal of the power supply unit and the replacement of a 12 V battery to allow portable use. The SQUID controller, laptop computer, DC to DC converters and rechargeable 12 V battery were all placed in a portable racking system for convenient portability. The use of battery power was thought to provide a cleaner source of power for the experimental set-up. Where the mains supply suffers from drops in voltage and the ever present 50 Hz hum, battery power is DC and therefore more constant and less susceptible to fluctuations. It is logical to reason that battery power can only help to lower the noise captured by the data collection system. The wiring arrangement and the power consumed can be seen in figure 6.7.

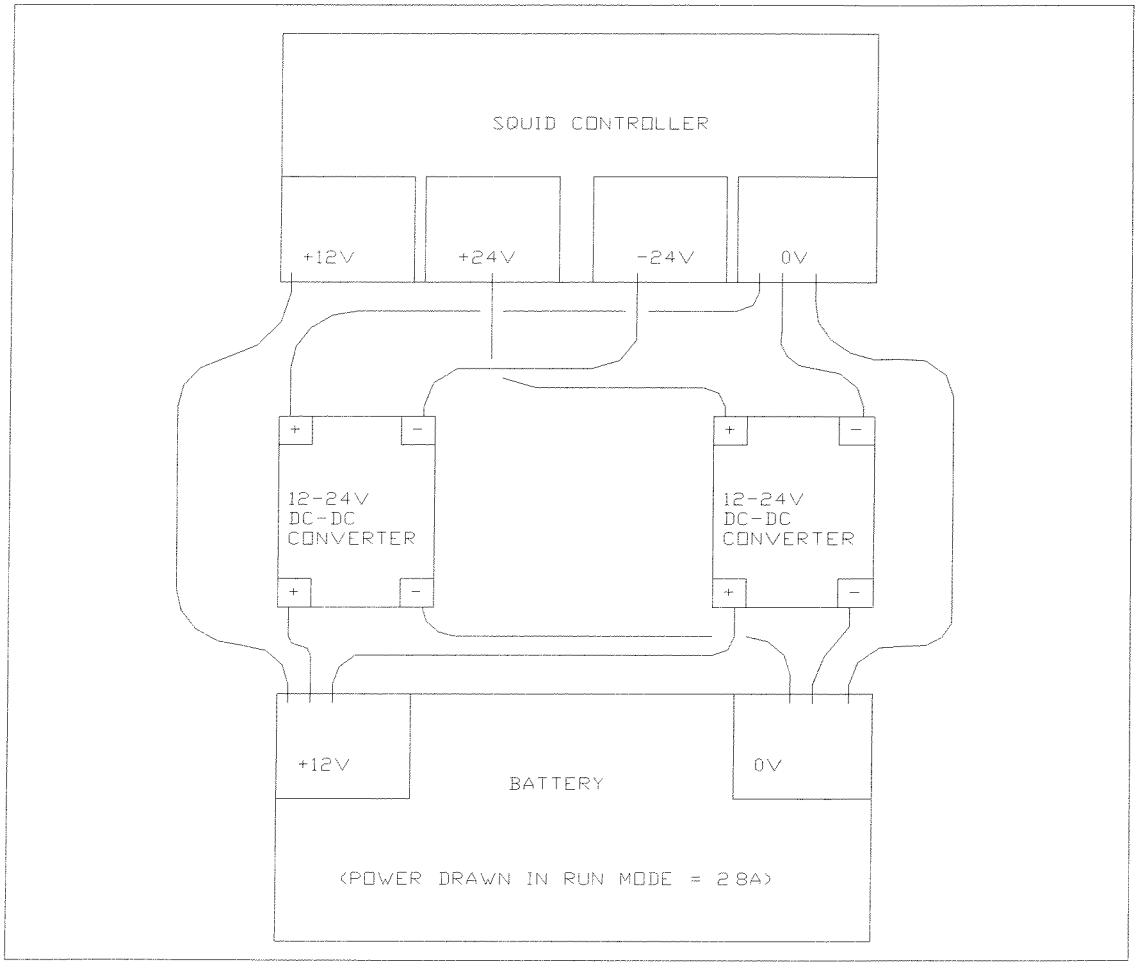

Figure 6.7. Schematic set-up for HTM1 and 100 SQUIDs.

CHAPTER 7

7. TESTS AND RESULTS.

7.1 INTRODUCTION

The motivation behind the early tests was two fold, it was important to get a feel of how to operate a high temperature SQUID and it's limitations. Part of this project was in collaboration with the Southampton Oceanography Centre, which was very interested to learn about SQUID operation in the earth's magnetic field for deep sea surveying applications. As a result, two SQUID magnetometers were required to allow gradiometric measurements to be undertaken. Several commercial SQUID manufacturers were approached with the aim of evaluating the performance of systems before a final decision was made on purchasing. Two companies agreed on a loan period to evaluate their systems before any commitment was made. It was decided that tests would initially not be conducted in the field because the system would need modified to allow portability in an open field environment. It was important however to try to re-create the environment in which the manufacturer's sensor specification were created, so that they could be checked. As a first step towards the full characterisation of a system, tests were undertaken in the laboratory. Due to the high levels of noise present within the laboratory, it was necessary to shield the SQUIDs from external noise sources. Magnetic shielding was achieved with the aid of mu metal, and rf shielding via screened cables and aluminised mylar around the sensors to form a complete conducting shield from low frequency electromagnetic interference.

It was planned for tests in the laboratory to start with the sensor in maximum shielding to give a good approximation of the sensors ultimate performance. The number of shields could then be reduced to zero. Once all the levels of performance within the laboratory environment were complete, the opportunity to test the system in a magnetically remote environment was planned.

7.2 OXFORD INSTRUMENTS SYSTEM.

The first company to supply a SQUID system was Oxford Instruments (O.I.), who supplied a YBCO bicrystal junction single sensor gradiometer system. The white noise performance quoted by O.I. was under 1900 fT / cm $Hz^{-1/2}$, with the sensor operated in a laboratory environment with a superconducting shield to protect from magnetic interference.

Unfortunately the system never operated completely reliably during the loan period, but it was possible however to demonstrate the power of SQUIDs in a non-quantitative manner by measuring the signals from an analogue wristwatch. The SQUID was operated in an unshielded laboratory environment and an ordinary wristwatch was placed as close as possible to the SQUID whilst avoiding the liquid nitrogen, and the magnetic signal was measured, the result of which is shown in graph 7.1. It was also possible to measure the effect of rotating a metal-framed chair within the same laboratory environment. Although these results do not contribute directly towards the greater understanding of science, they are a clear and direct demonstration of the power of a high temperature SQUID. It also demonstrates the clear practical advantage a high temperature SQUID has over its low temperature counterpart. It would be unthinkable to casually operate a low T_c SQUID from an open container because the liquid helium required for operation would vaporise immediately, thus ceasing operation of the device.

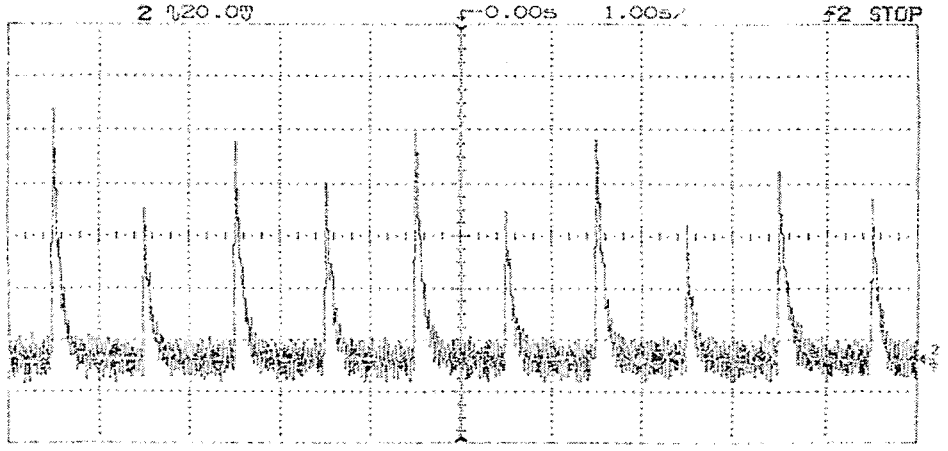

Graph 7.1 – Detection of the magnetic signal from a wristwatch using a high T_c SQUID.

7.3 TRISTAN TECHNOLOGIES SYSTEMS.

7.3.1 TRISTAN HTM1 MAGNETOMETER.

The so-called HTM1 magnetometer derives its name from the fact that it is a high temperature magnetometer suitable for use in magnetic fields up to 1 μT. As will be seen later the HTM100 is specifically designed to be a similar magnetometer, but with the extra advantage of operation in magnetic fields of up to 100 μT (i.e. the earth's magnetic field.) The first shipment of HTM1 sensors consisted of a single magnetometer with control electronics. The sensor came with a specification curve as shown in graph 7.2, where a white noise level of less than 60 fT $Hz^{-1/2}$ was guaranteed. The ultimate aim of the loan period was to confirm the specification in the laboratory and quantify the performance in a magnetic field equal to that of the earth. To become familiar with the system, many runs were undertaken in various different conditions. At this point of development there was access to only one mu metal shield, so this was the maximum shielding possible at this stage.

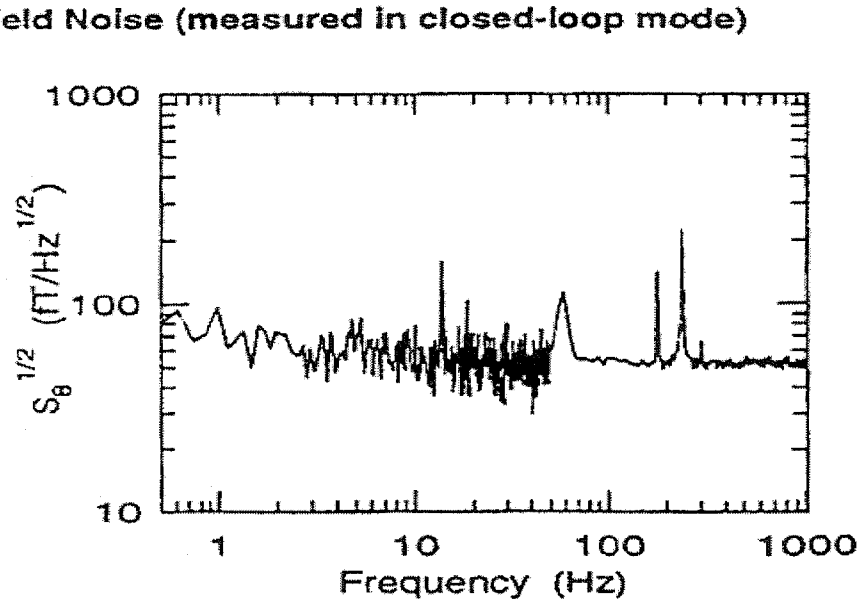

Graph 7.2- Noise curve of HTM1 sensor.

To gauge the interaction between the shielding and the laboratory environment three short runs of 60 seconds were completed. Graph 7.3 shows the sensor output with the SQUID completely unshielded, resulting in a peak to peak voltage of around 5V over the sixty seconds. This voltage swing equates to around 15 nT, which is far more than the intrinsic noise expected from the SQUID, but is understandable due to the fact that the SQUID is completely unshielded in a noisy laboratory. The next stage was to place the sensor in a single mu metal shield, graph 7.4 shows the effect of this operation. There is a massive attenuation in the peak to peak noise measured at this level of just over 0.2V, which equates to around 700 pT. 700 pT is still far higher than the values quoted for the intrinsic noise of the SQUID, hence further shielding was required to give the ability to view the intrinsic noise of the sensor. Whilst the SQUID was in the single shield, a permanent magnet was placed near to the sensor in order to create a steady 100μT ambient field. Graph 7.5 displays the resultant trace from this environment, where the voltage drift over the minute was around 2.5 V or 7.5 nT. Although the drift in voltage of graph 7.5 is similar to that in graph 7.3 it is worth noting that the amplitude of the noise observed when the SQUID was unshielded was much higher, probably due to the high levels of interference from sources in the laboratory. Whereas the single shield 100μT run has a high drift, but relatively low amplitude of signal, which could be due to the presence of the magnet.

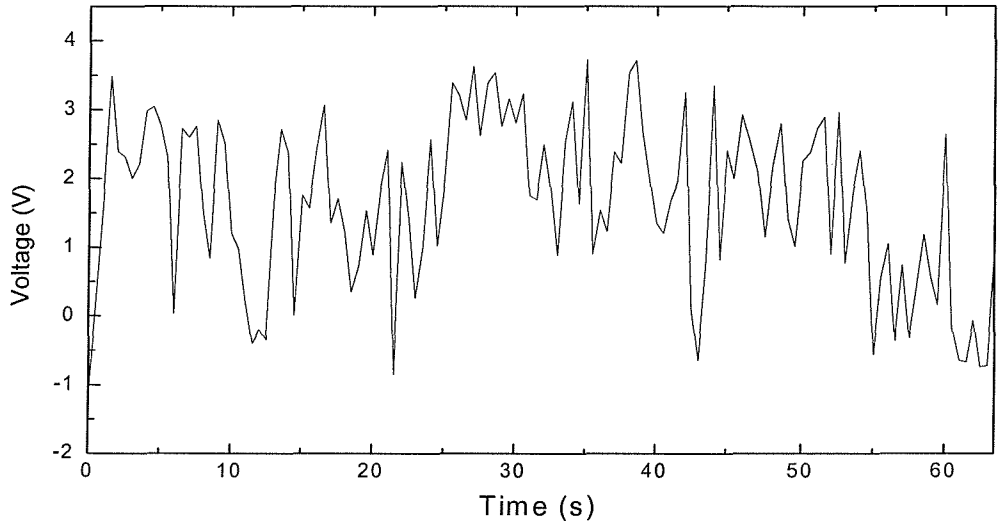

Graph 7.3- HTM1 unshielded in laboratory.

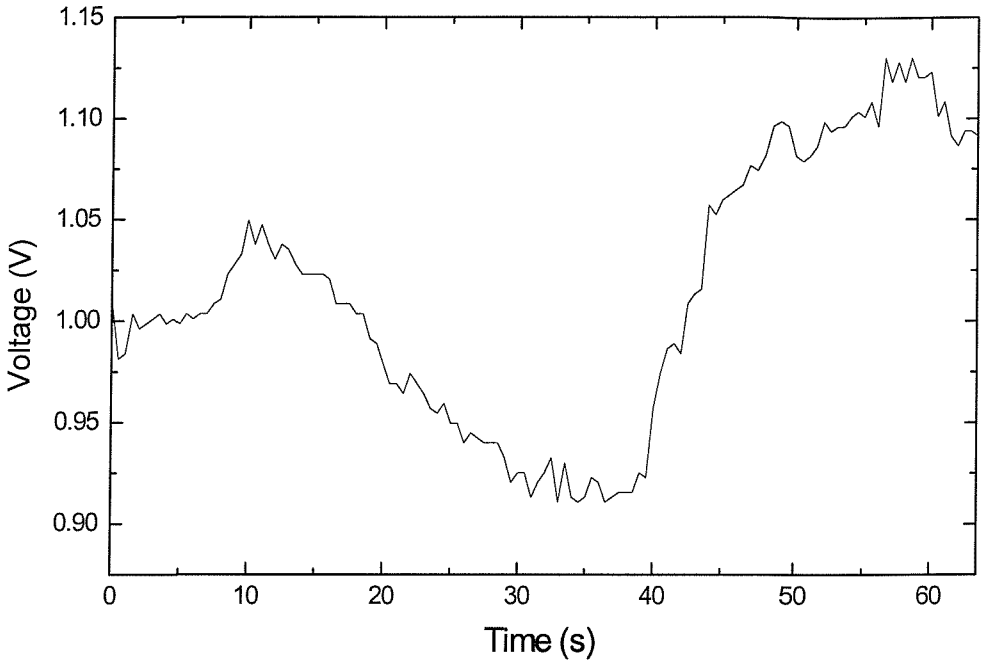

Graph 7.4- HTM1 in one mu metal shield in laboratory.

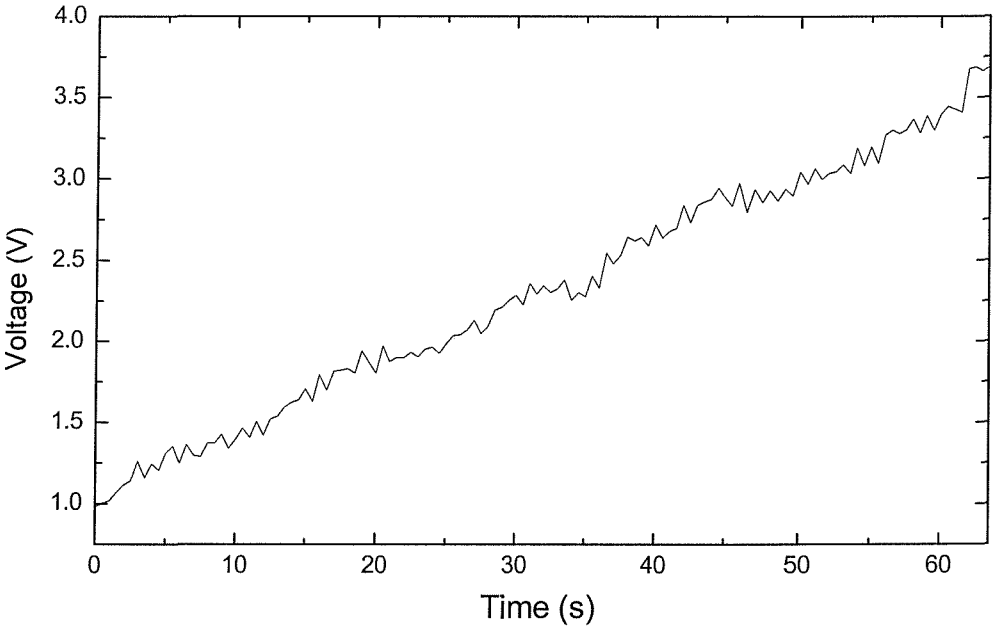

Graph 7.5- HTM1 in one mu metal shield with permanent magnet creating steady field.

The magnet used to create the 100 μT field had dimensions of 90 mm in diameter and 25 mm deep. The magnetic field from the magnet was measured by a fluxgate magnetometer, the results of which are shown in graph 7.6. It is clear to see that at a distance of 250 mm, a field of around 100 μT is produced by the magnet. The distance at which the magnet was placed was not critical because the object was to create a steady magnetic field equal in magnitude to that of the earth, which varies depending on latitude within the region of 30 – 70 μT. It was therefore acceptable to place the magnet anywhere between 25 and 30 cm from the SQUID to create a steady field of over 50 μT.

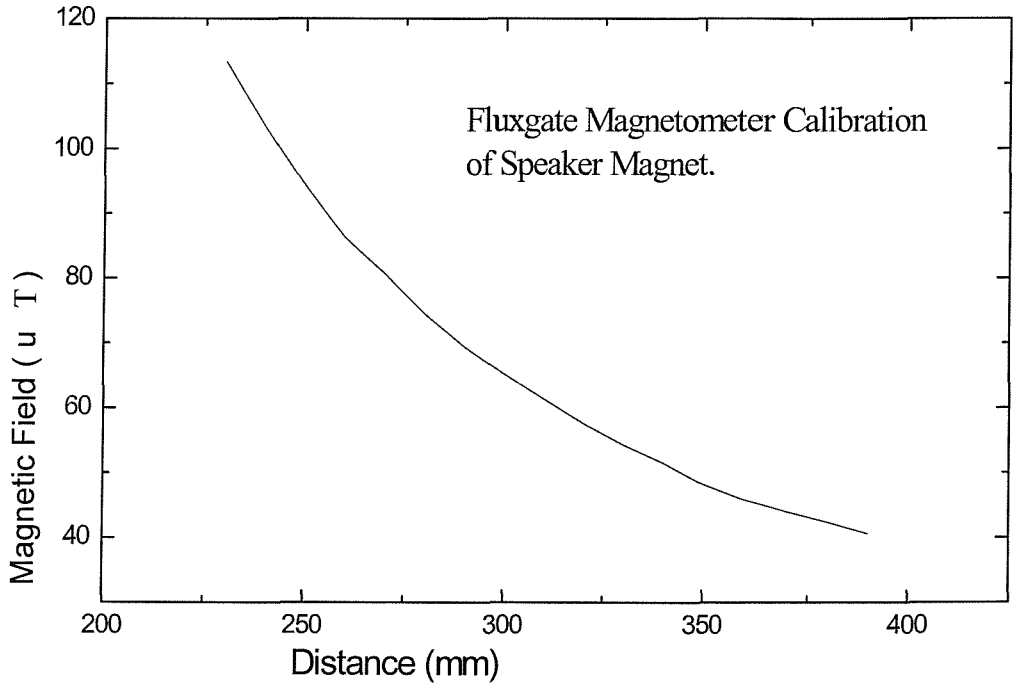

Graph 7.6- Calibration curve of permanent magnet.

Further investigation was conducted into the effect of a 'high' ambient magnetic field on the output drift of the HTM1 SQUID. Graph 7.7 is indicative of many 2000 second runs conducted in a 100 μT steady field with the SQUID having a single shield of protection from external interference. It was apparent that the magnet had the effect of causing the sensor output to oscillate over a time period of many hundreds of seconds with an amplitude of oscillation over 10 nT. The origin of this fluctuation is not clear, although may have a connection with the movement of flux lines within the magnetically saturated SQUID body.

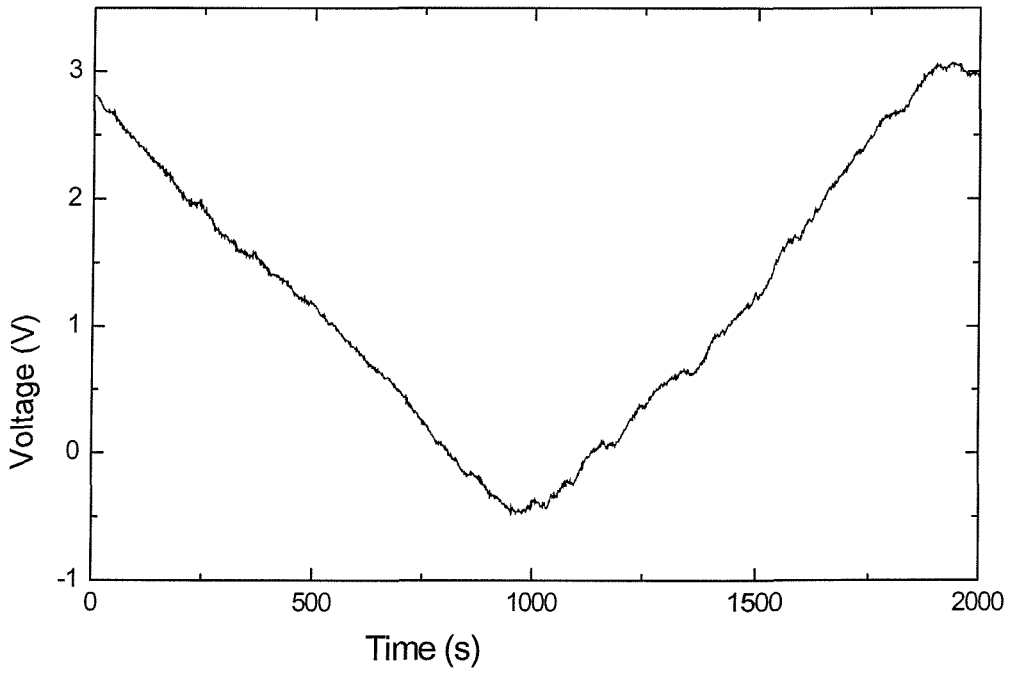

Graph 7.7- 2000 second run with sensor in steady 100 μT field.

A second mu metal shield was obtained, as shown in figure 6.0, which allowed a set of three repeated tests to be conducted with the sensors in two shields, one shield and then one shield with the permanent magnet creating a steady 100 μT field. A typical two shield run is shown in graph 7.8 where the peak to peak noise over 2000 seconds was

1.74 nT. This is in contrast to the single shield figure of graph 7.9 of 4.2nT. The apparent effect of a high magnetic field is evident in graph 7.10, in which the single shield magnet run results in a drift of over 30 nT. The effect of the 100 μT field on the SQUID appeared to cause a periodic output from the sensor.

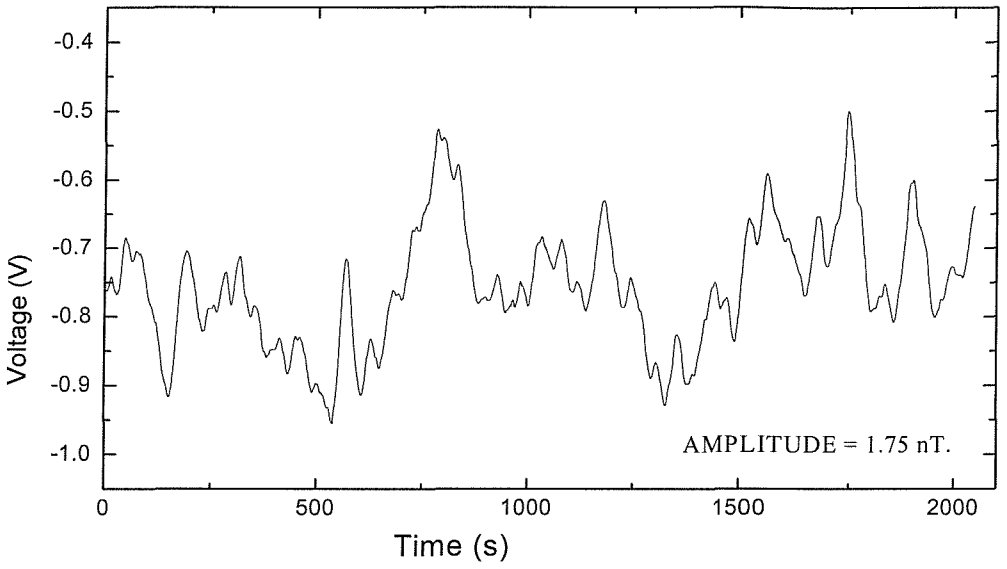

Graph 7.8- Average of five runs with two mu metal shields.

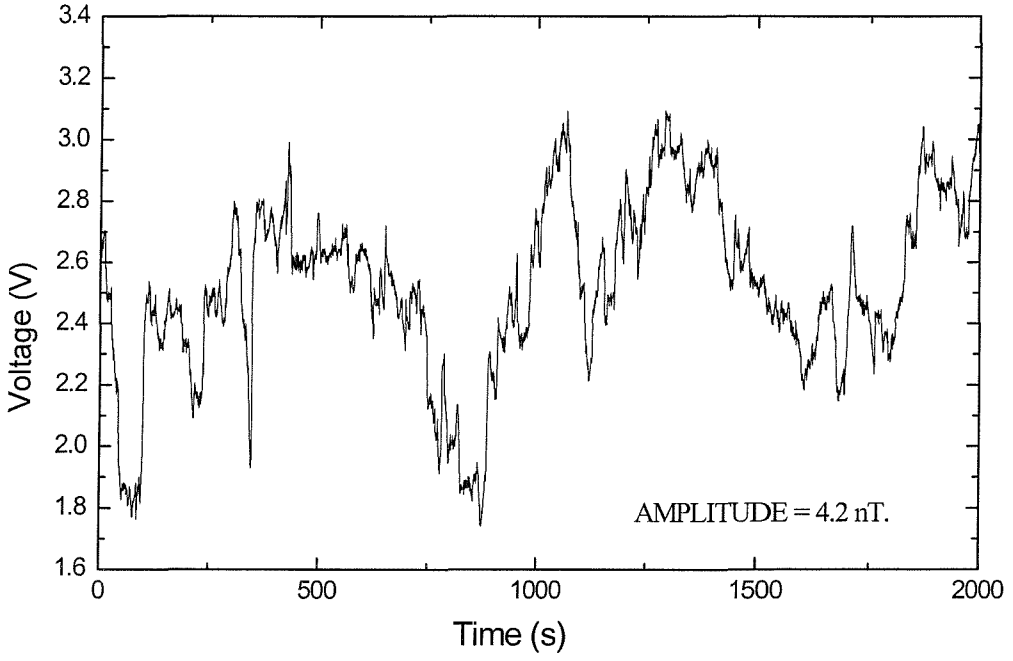

Graph 7.9- Average of five runs with one mu metal shield.

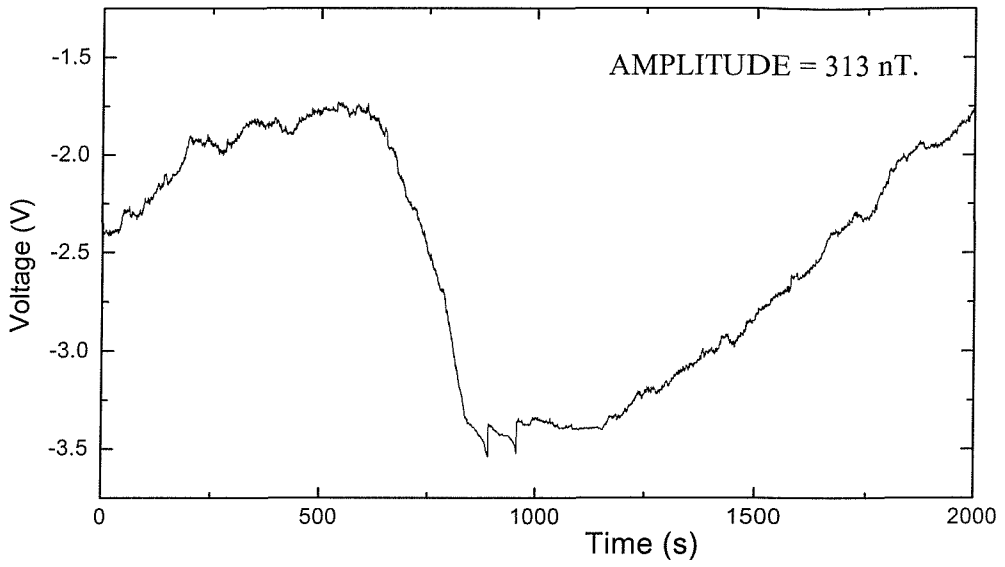

Graph 7.10- Average of five runs with one mu metal shield and 100 μT magnet.

To research this matter further, the SQUID remained within the high field environment and several long runs were undertaken. Again the periodic effect was very noticeable; graph 7.11(a) shows a run of around six hours in which the period of oscillation varied. The large oscillations had a period of order of several hours, whereas the smaller oscillations as detailed in graph 7.11(b) were around 200 seconds in period.

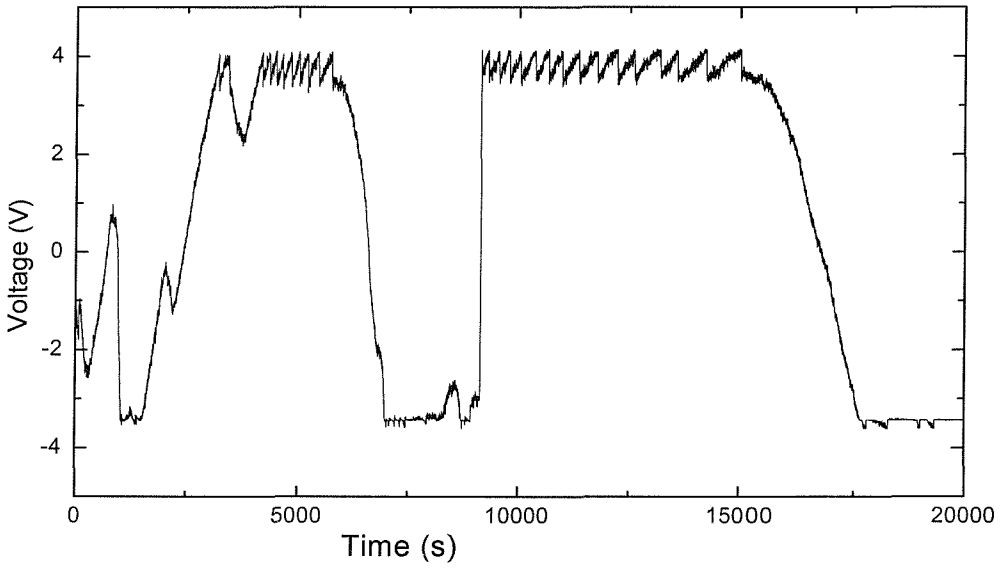

Graph 7.11a- Investigation into apparent sinusoidal effect of high magnetic fields on sensor output, ran over 12 hours.

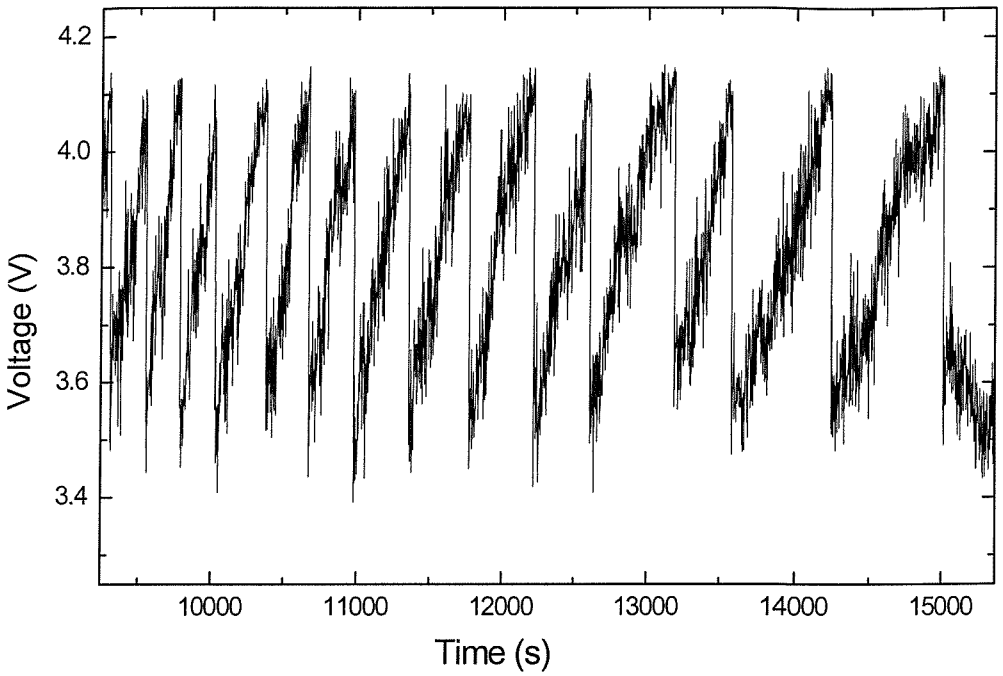

Graph 7.11b- Zoomed in view of periodic behaviour.

After some debate with the manufacturers over the cause of this apparent field induced oscillation, it was suggested that atmospheric pressure fluctuations might be the cause. It was suggested that it could just have been coincidental that the magnet was present when the output oscillations from the SQUID were observed. It was proposed that the natural changes in atmospheric pressure could have caused the temperature of the nitrogen to vary. To investigate the validity of this claim some kind of pressure tests were essential. In the absence of accurate barometric pressure measuring equipment a simpler test was devised. By placing a rubber bladder over the exhaust port of the cryostat the temperature of the nitrogen would gradually increase with the increasing pressure. This would cause the SQUID to warm up and in theory cause the noise from the SQUID to increase. The experiment was conducted successfully, with the bladder being left over the exhaust port for 75 minutes, in which time it ballooned to a diameter of nearly 50 cm. Graph 7.12 shows the entire run where the bladder is in place for the first 4000 seconds of the 9000 second run. The general level of noise remains unaffected for the entire run

at less than 500 pT per thousand seconds. Again the graph demonstrates the SQUID changing output in large jumps. There is no ready explanation for these flux jumps, but may be caused by sudden movement of flux in the SQUID washer, possibly caused by movement of the cryostat.

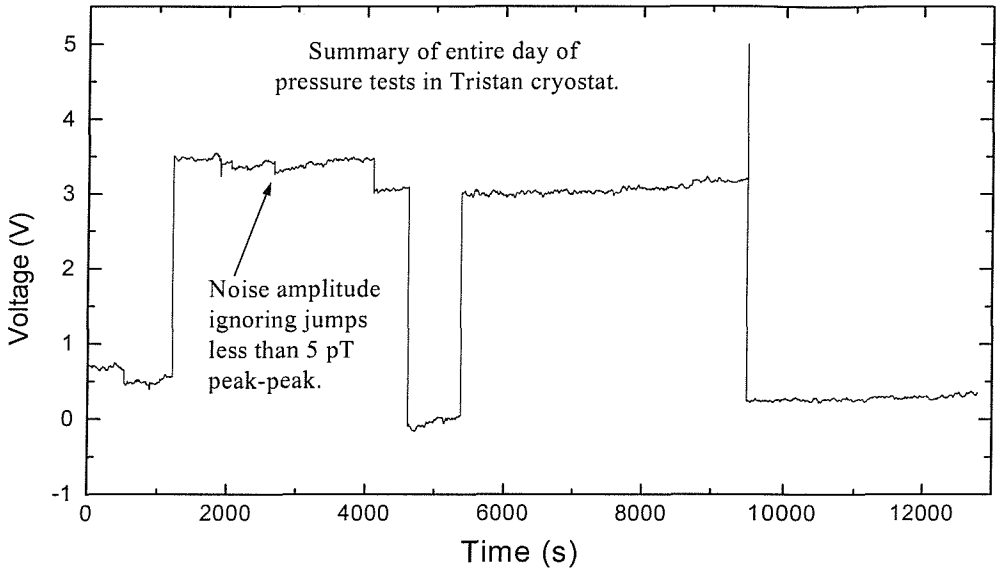

Graph 7.12- Investigation of the effect of ambient air pressure on SQUID output.

To investigate the performance of a well established competitor to the SQUID magnetometer, we conducted several runs with a modern fluxgate magnetometer. Tests were conducted of fluxgate performance in single and double shielding and with the 100 μT field. The fluxgate magnetometer was borrowed from the SOC and had a quoted noise level of <10 pT white noise, although it was not possible to confirm this. It was also believed that a fluxgate should be unaffected by the ambient magnetic field that surrounds it. Graph 7.13 shows the output from the fluxgate when inside two mu metal shields, giving a peak to peak noise of over 1 nT. Graph 7.13 is very coarse because the scale selection of the device was limited, but it does provide a guide to the noise, so that a comparison with the high T_c SQUID can be made. When the fluxgate was in a single shield the noise level increased by over an order of magnitude to around 15 nT, as demonstrated by graph 7.14. There is an increase in noise due to the presence of the magnet in graph 7.15 to around 80 nT. Evidence to suggest that a fluxgate magnetometer may be affected by magnetic fields.

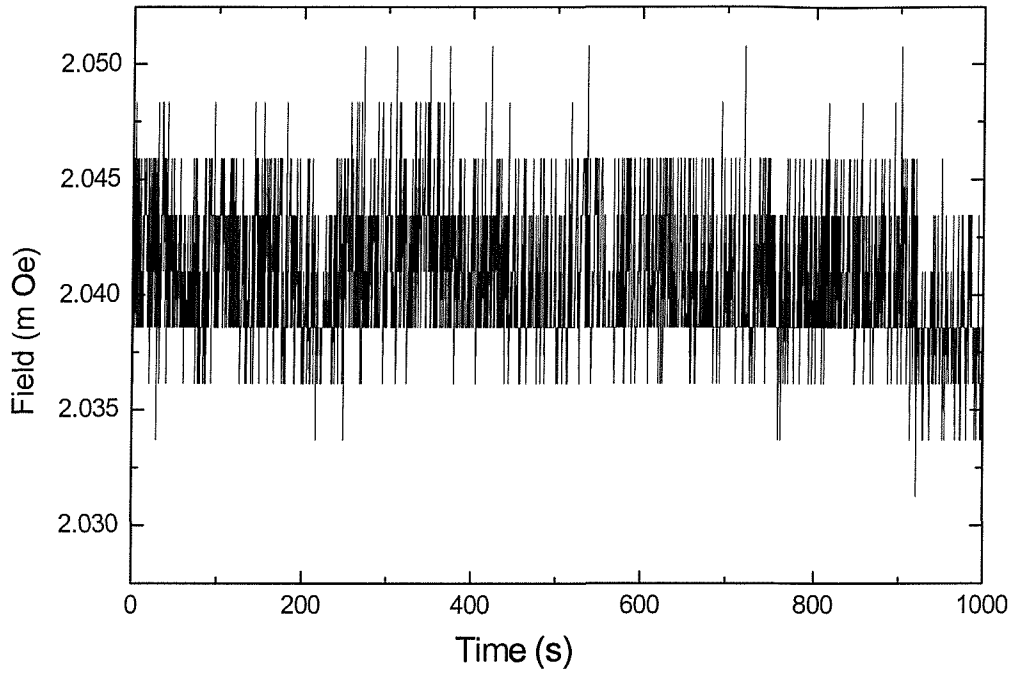

Graph 7.13- Fluxgate magnetometer with two mu metal shields.

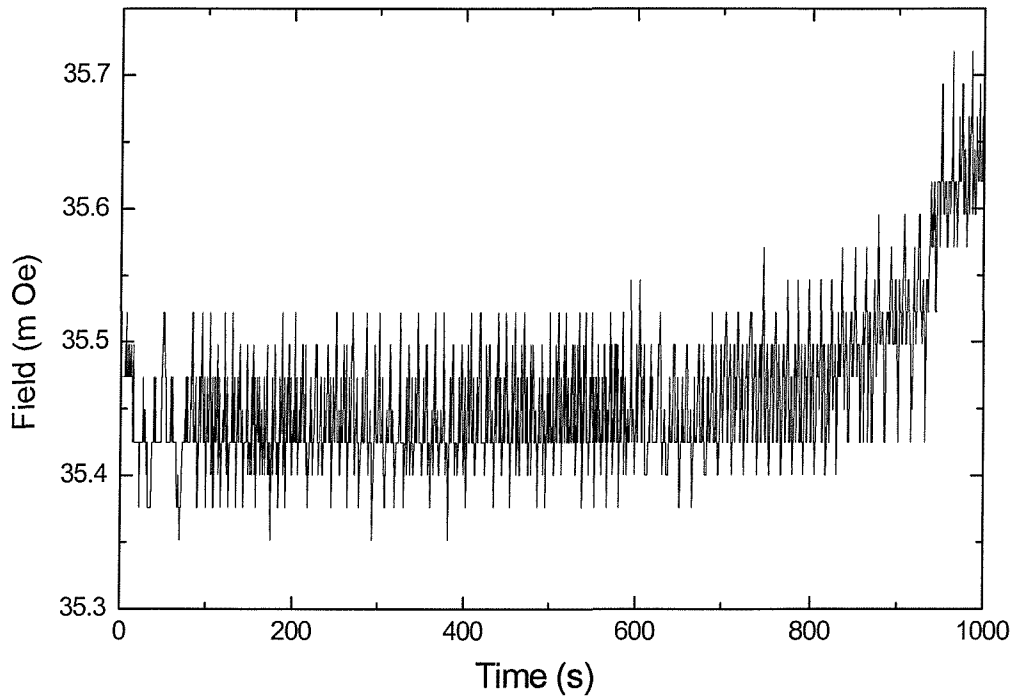

Graph 7.14- Fluxgate magnetometer with one mu metal shield.

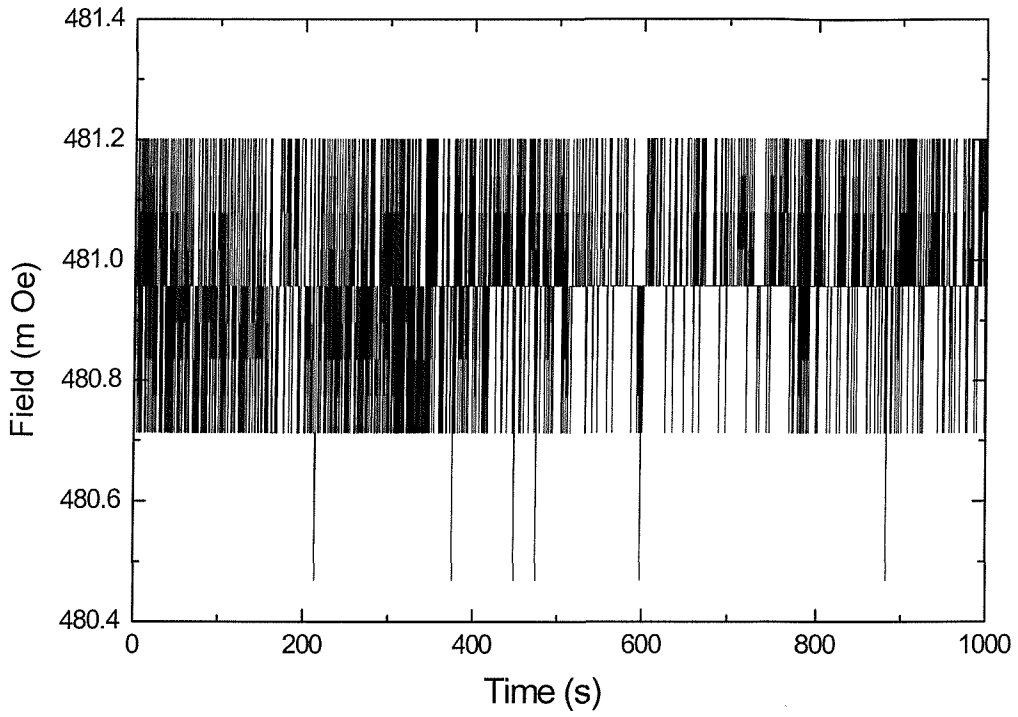

Graph 7.15- Fluxgate magnetometer with one mu metal shield and 100 μT magnet.

Graphs 7.13, 7.14 and 7.15 show the digitisation of the fluxgate magnetometer that was used. The instrument could not measure the required fields with enough sensitivity combined with the appropriate scale. The digitisation in graph 713 is approximately 250 pT with a variation of approximately 4-5 digitisation bands, or about 1 nT. The digitisation in graph 7.14 increases to around 2.5 nT with a variation of 5-6 bands over the initial 800 seconds of the run, or 15 nT. Graph 7.15 shows digitisation of around 10 nT per band, varying by around 8 bands, or 80 nT. Although this does not provide an accurate value of the noise associated with the three different conditions, it does show an upward trend in the noise of the magnetometer as the shields are removed and magnet introduced.

7.3.2 LAND MINE DETECTION.

Figure 6.1A shows the set-up initially used in the land mine detection experiments. During the set-up of the equipment a small steel screw was stuck with blu-tac to the end

of a wooden ruler. When screw was waved under the SQUID a signal was clearly detected. The amplitude of the signal was approximately 3-4 V, with the SQUID controller set to a gain of 500. This meant that a small screw waved about 5 cm below the sensor induced a signal of around100 pT into the SQUID.

When the land mine arrived for detection the cryostat had sprung a leak in the vacuum chamber. The nitrogen was boiling off vigorously, hence only giving a short time to run the system. The SQUID controller was set to a gain of 500 and the land mine swiped within 5 cm of the sensor. As a result of this experiment the signal went completely off the scale. Hence the SQUID was detecting a source of many hundreds of pT.

To reduce the scale deflection, the gain on the control electronics was decreased to a factor of 20. When the mine was passed beneath the sensor, full scale deflection was again very easily achieved.

The only way to prevent full scale deflection was to remove the large mu metal shield and wave the magnet at a distance of approximately 1 m from the sensor. This produced an amplitude variation of 3 – 4 V. On a gain of 20, the calculated calibration showed that 1 V corresponded to 783 pT

This meant that the landmine waved at a distance of 1 m produced a magnetic signal of approximately 2.5 – 3 μT.

It was unfortunate that no data could be taken of the runs, but it showed without doubt that a landmine was easily detected by a high temperature SQUID.

7.3.3 TRISTAN HTM1_2 MAGNETOMETERS.

All the measurements to this point had been made with single sensor magnetometers. It was planned that the final system would be a gradiometer system because of the advantages gained with such a set up. A two sensor gradiometer system would provide greater rejection of distant noise sources and greater sensitivity to the measured gradient. The greater sensitivity is created because two magnetometer sensors can be placed further apart than a single sensor gradiometer. Two new HTM1 sensors replaced the previous

single sensor system, along with a pair of small mu metal shields that were only slightly larger than the sensors themselves. The mu metal shields were approximately 20mm in diameter and 50 mm long. The system set up now consisted of two separate magnetometers, both now capable of being triply shielded. The new sensors came with their own noise curve as seen in graph 7.16.

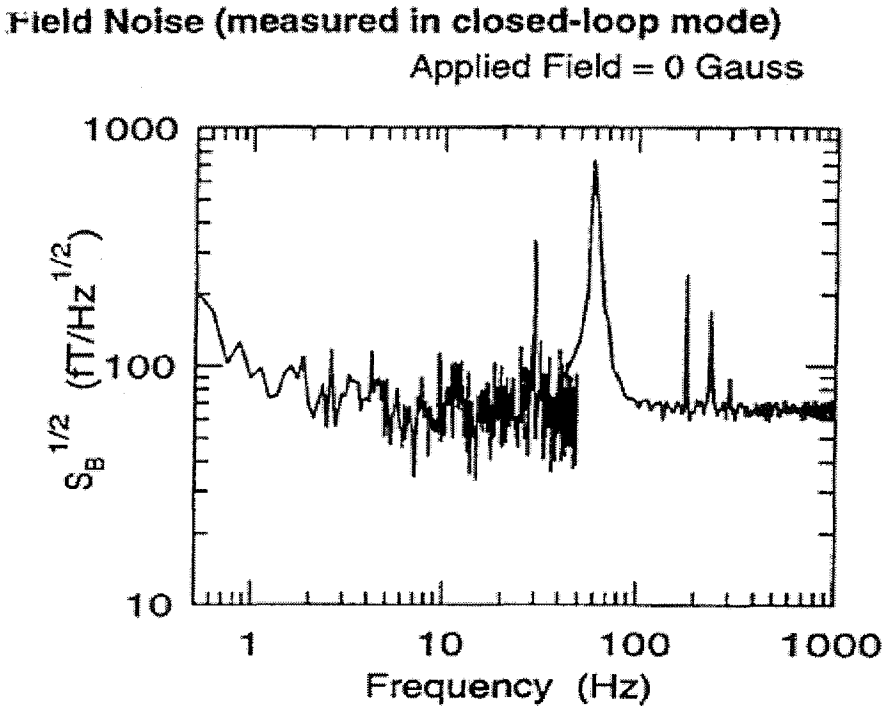

Graph 7.16- Noise curve of second HTM1 sensor.

A new way of graphing the new double set up was utilised to demonstrate their performance. The voltage output from the two sensors was collected in two data columns. That data was then corrected so that both sensors began at zero and calibrated into Tesla from Volts. The two columns of individual calibrated data were than subtracted from each other to form a single 'field difference' column. The field difference data could then be plotted to give a result that showed the relative gradient between the two sensors. The difference being proportional to the difference in intrinsic noise between the two sensors and the actual gradient detected between the two sensors. The resolution of what was noise and what was gradient being the primary objective.

A very long 14-hour run was conducted with graph 7.17 demonstrating the relative stability over the first 8 hours with a field difference figure of around 200 pT. Over the full 14-hour run the difference was around 1 nT. This was the first triple shielded run and demonstrated stability not seen before.

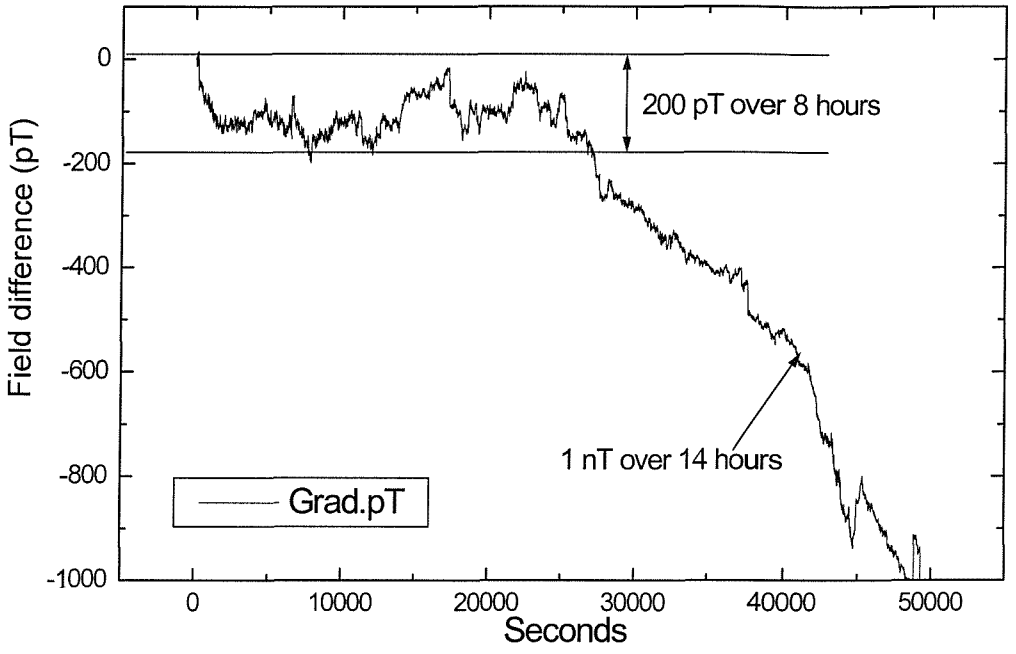

Graph 7.17- Field difference between two HTM1 sensors in three mu metal shields.

The unparalleled performance of the new sensors was reinforced in graph 7.18(a). The sensors are within three shields and run for 1700 seconds, it is possible to see the digitisation of the equipment as the analogue to digital converter reaches its limit of accuracy. It shows very clearly that two mu metal shields were not enough to expose the intrinsic noise of the SQUIDs within the laboratory environment. Graph 7.18(b) shows the field difference of the 1700 second three shield run resulting in a smoothed field difference of about 15 pT. The field to voltage calibration of these new sensors, when set on full sensitivity was 389 pT/V and 684 pT/V.

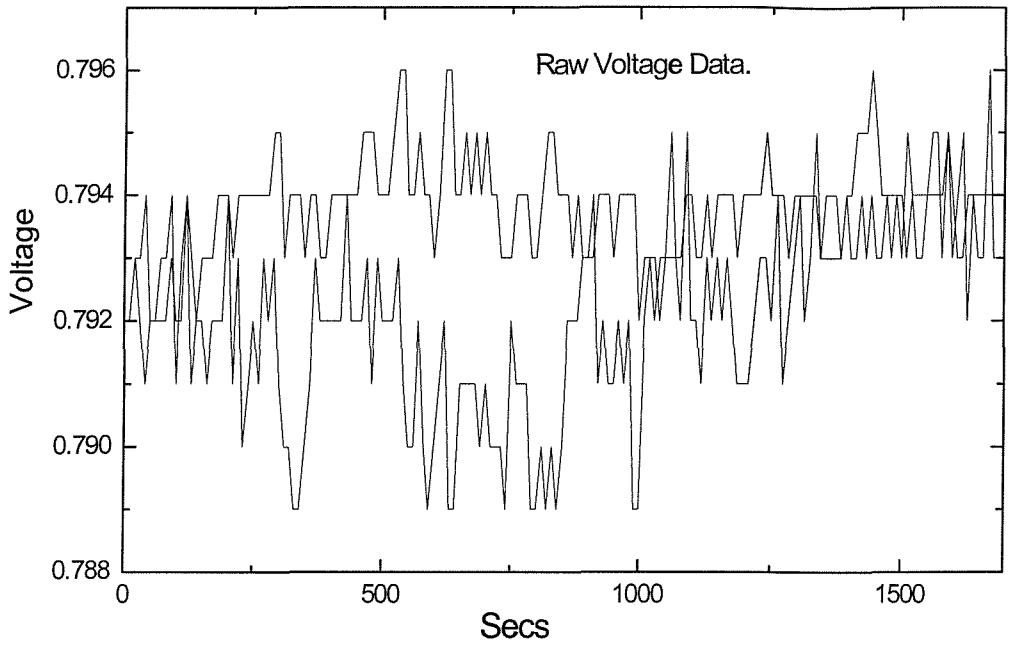

Graph 7.18a- Raw voltage data of field difference of triply shielded SQUIDs.

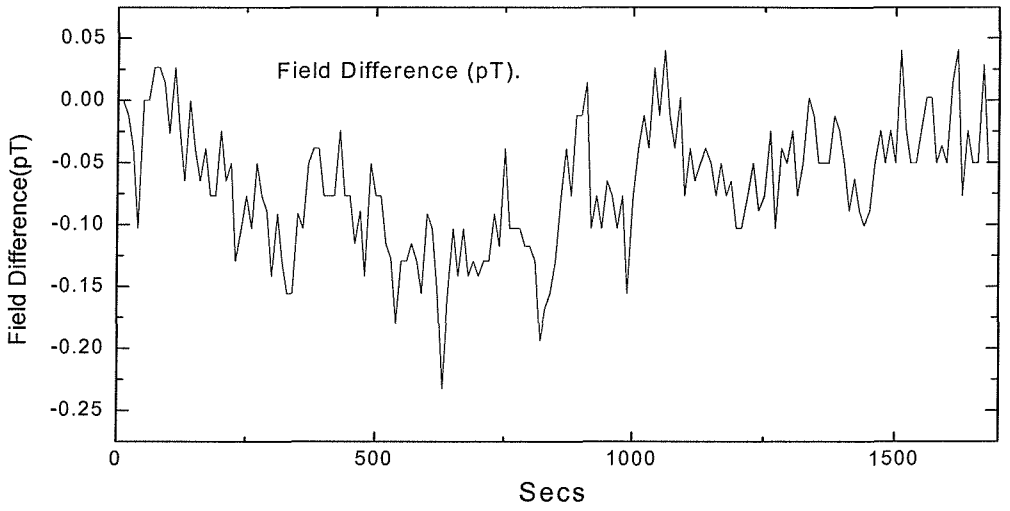

Graph 7.18b- Smoothed field plot of voltage data of triply shielded SQUIDs.

Graph 7.19 demonstrates the effect of the mu metal shields, where the voltage output of the sensor on channel A was protected by two mu metal shields but channel B sensor was only protected by one. There is easily an order of magnitude difference in the output between the two sensors, a detail that has been implied before in separate runs, but never proven in a simultaneous measurement. Both sensors were placed in the cryostat the same way up, but graph 7.20 shows that they output voltage and hence detects magnetic field in the opposite sense. This could mean that the pick-up coils are wired up in the opposite sense on the sensor.

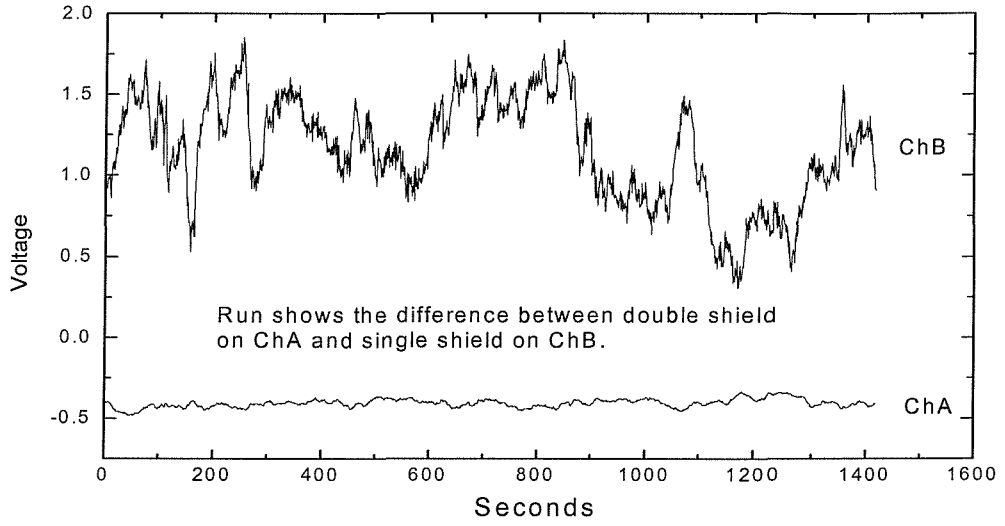

Graph 7.19- One SQUID in one mu metal shield and the other in two.

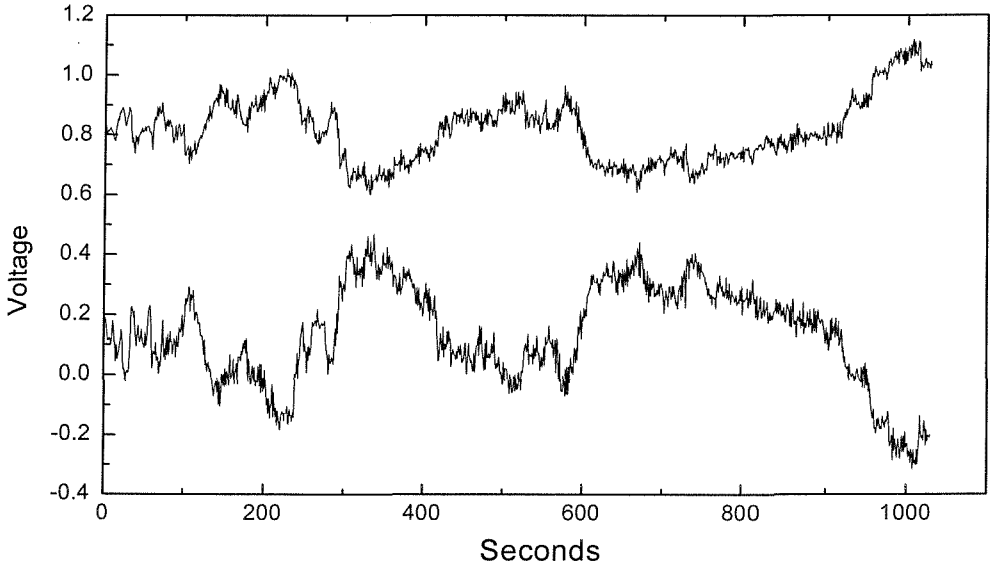

Graph 7.20- Both SQUIDs in one shield sensing magnetic field in the opposite direction.

The longest run of the entire project was undertaken to confirm the long-term stability of the SQUID sensors. The run shown in graph 7.21 lasted for over 14 hours and resulted in some interesting observations. The stability of the sensors was less than 800pT for a 40,000 second period of time, between 10,000 and 50,000 seconds. Unfortunately the output of the sensors had the tendency to jump, at random intervals by random amounts. Although this aspect could be corrected for in post run processing by removing these jumps, it was clear to see that the long term field drift of the HTM1 sensors were around the 1 nT mark.

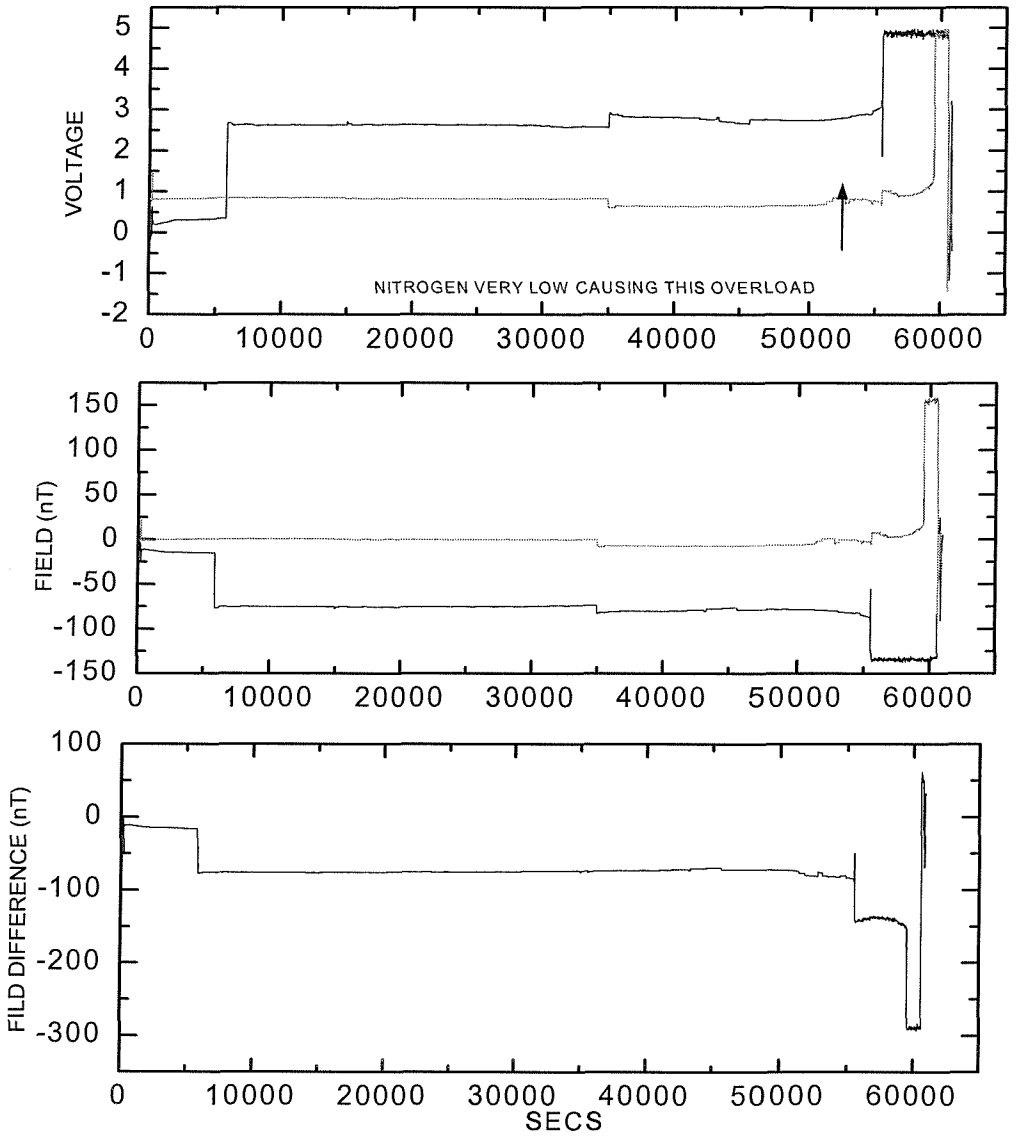

Graph 7.21- The longest three shield run.

It was believed that the focus of the project should start to look at much shorter timed runs so that all aspects of the SQUID performance could be assessed. To this end a collection of 700 second runs were completed, a typical example of which is shown in graph 7.22. The field output of the two individual channels averaged to around 25 pT over the 700 seconds. And more importantly the outputs appeared completely uncorrelated, indicating that it was the internal noise of the sensors that was being measured and not the signal from external sources. The graph shows the true output of each sensor and the 50 point average, which is the smoothed line on each channel.

Graph 7.23 shows data obtained from a leading fluxgate manufacturer on their best performing magnetometer within three layers of mu metal shielding. The average smoothed data from this fluxgate was over 100 pT, which is inferior to the performance of the HTM1 SQUIDs by a factor of around 5 times.

These final laboratory tests on the HTM1 system confirmed their performance relative to a top fluxgate magnetometer.

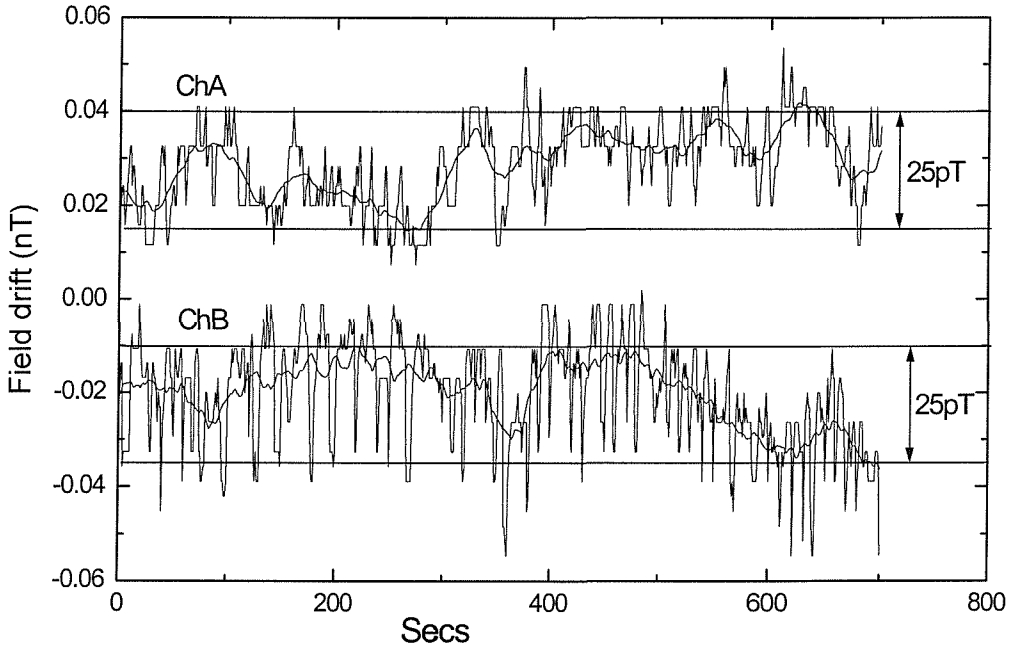

Graph 7.22- Triply shielded SQUID run for 700 seconds. Raw data and 50 point average smoothed data shown for each channel.

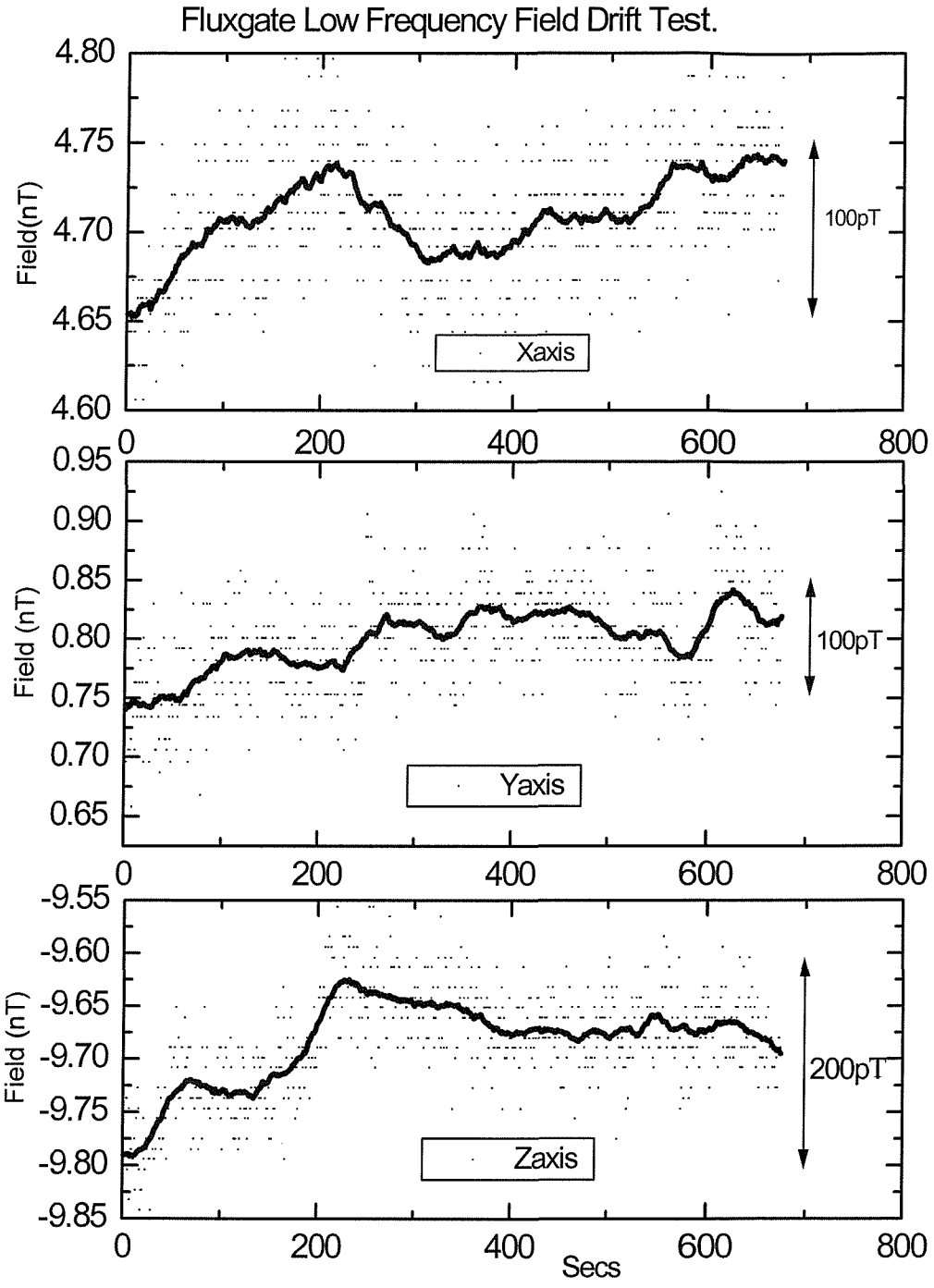

Graph 7.23- Triply shielded fluxgate run for 700 seconds.

7.4 COMMON MODE REJECTION TESTING

A signal generator was used to input the same wave into channels A and B of the ADC100. The resultant difference between the output of the two channels would be equal to zero in an ideal analogue to digital converter. As the ADC100 was not a perfect ADC it was useful to gain an estimation of the common mode rejection of the unit. This could then give an estimation of the resultant resolution of the ADC100 at different frequencies and durations as follows:

GENERATED SIGNAL INPUTTED INTO ADC100.			RESULTING ADC100 RESOLUTION	
FREQ.	AMPL. (V pk-pk)	LENGTH (S)	AT GAIN 100	AT GAIN 500
50 Hz	1	10	1pT	200fT
33 Hz	1	10	400fT	80fT
33 mHz	0.4	10	20fT	4fT
33 mHz	0.4	10	10fT	2fT
111 Hz	0.1	1000	40fT	8fT
33 Hz	1	1000	60fT	12fT
33 mHz	1	1000	40fT	8fT

The resultant sensitivities were calculated from the average power taken from the Origin power spectrum. The power spectra plot taken from the subtraction between channels A and B (i.e. the resultant from the ADC100.) The average power is provided by Origin in terms of volts per root Hertz. This figure was then multiplied by the respective calibration factors of the SQUID sensors to calculate the resultant sensitivity.

Spikes were observed from the output of the ADC100 when the signal generator was set close to 50 Hz. This means that the resolution the converter may be reduced at frequencies close to that of the mains.

7.5 TRISTAN HTM100 MAGNETOMETERS.

The sensors specifically designed for use in the earth's magnetic field were received and immediately replaced the HTM1_2 low field sensors. The noise curves of the two HTM100 sensors as completed by the Jülich group who manufactured them can be seen in graphs 7.24 and 7.25. A lower frequency noise spectrum was taken by Tristan Technologies, the sensor suppliers, at a much lower frequency range, and can be seen in graphs 7.26 and 7.27.

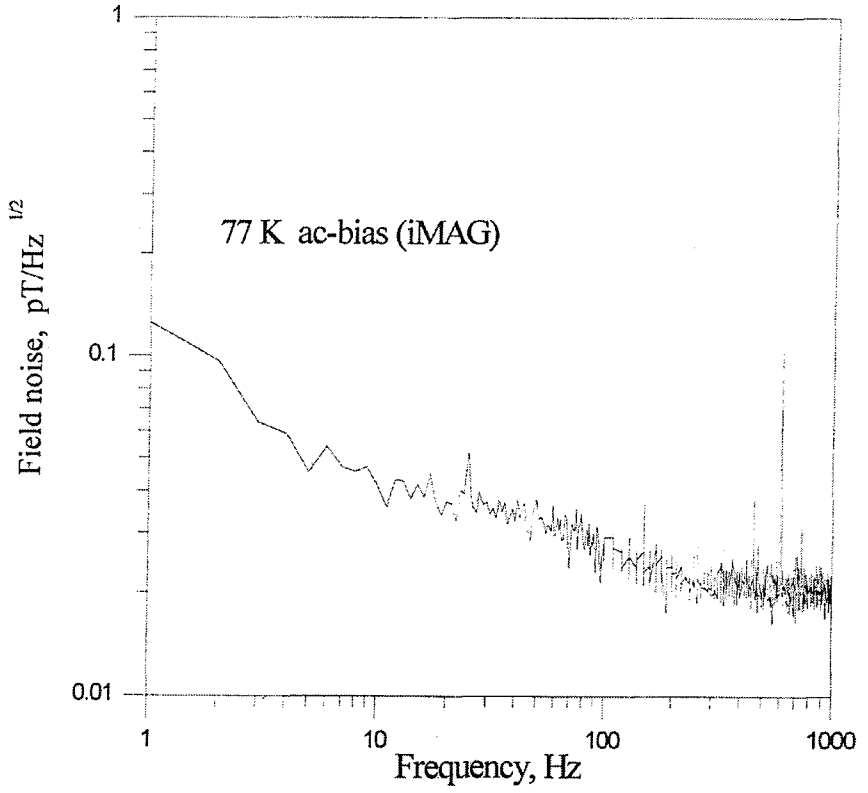

Graph 7.24- Jülich noise spectrum of the first HTM100 'channel A' sensor.

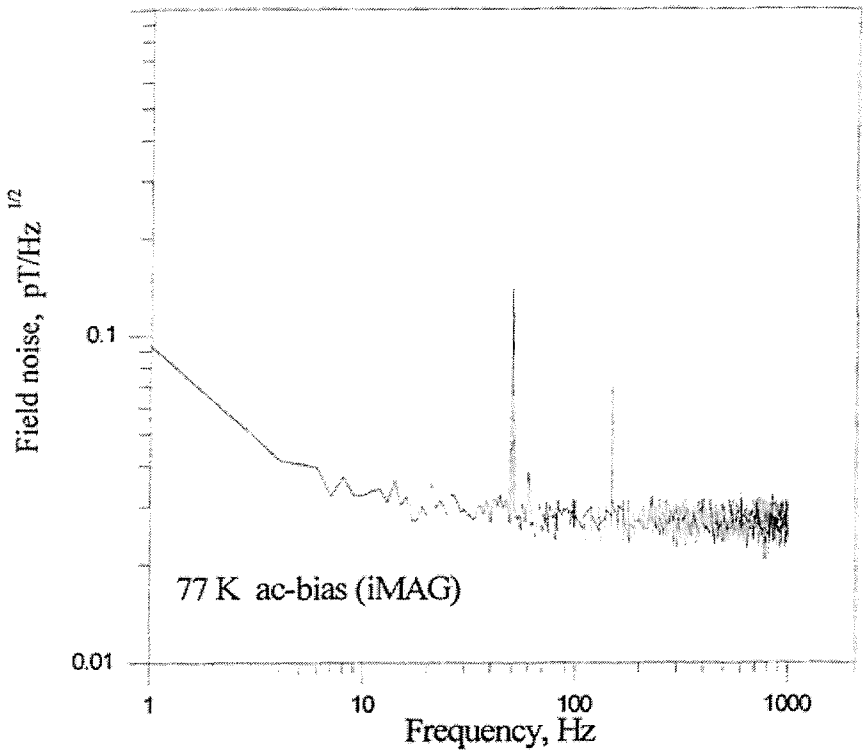

Graph 7.25- Jülich noise spectrum for other HTM100 'channel B' sensor.

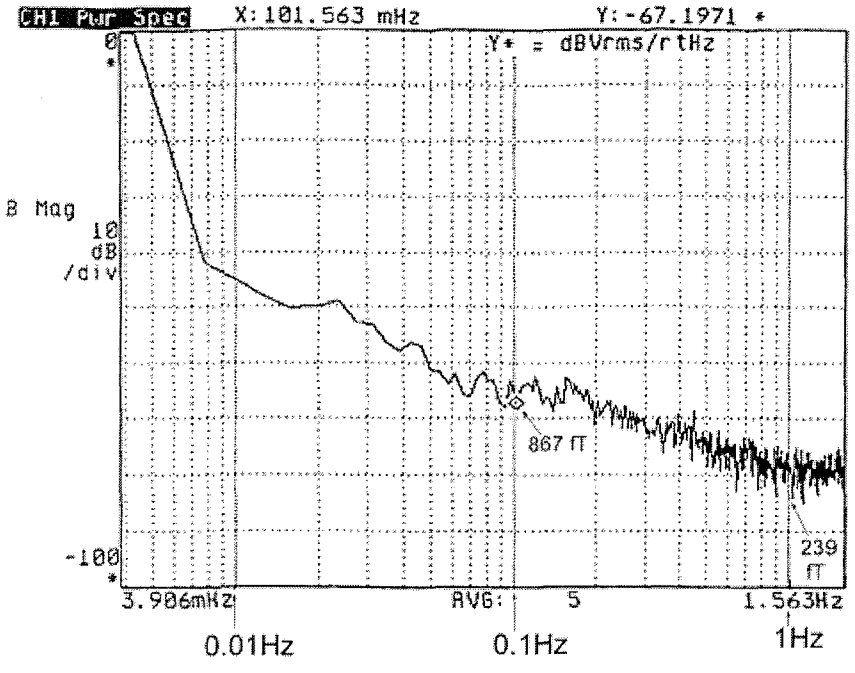

Graph 7.26- Tristan noise spectrum for channel A sensor.

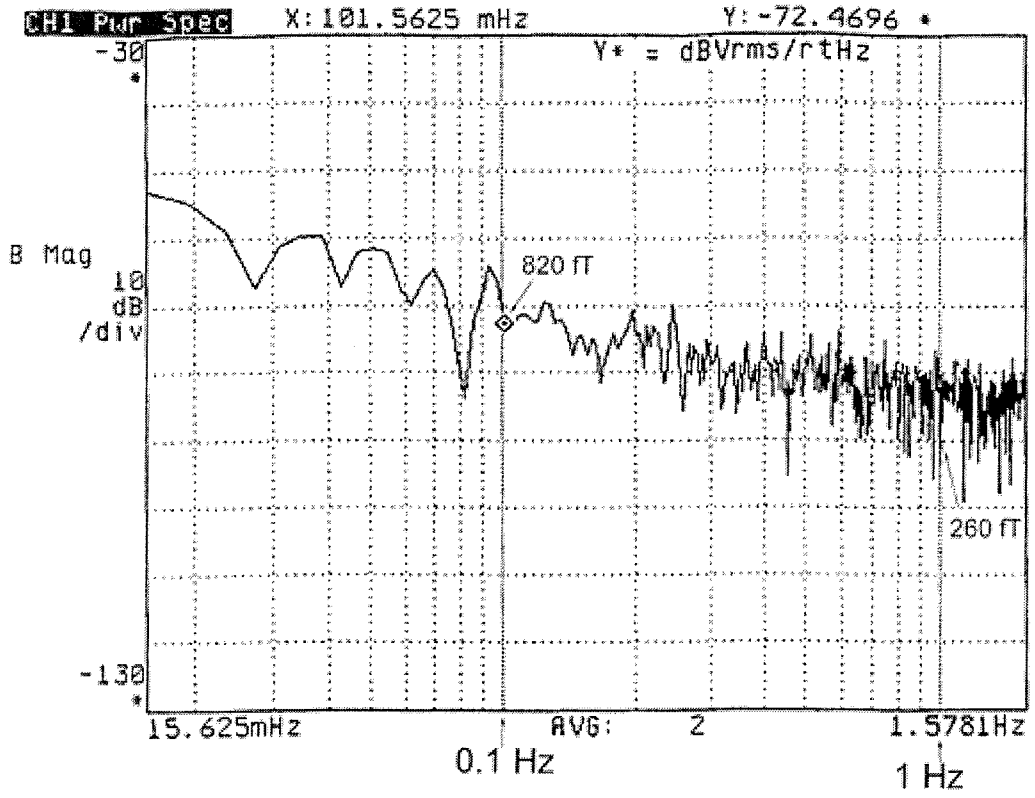

Graph 7.27- Tristan noise spectrum for channel B sensor.

The initial tests of the new HTM100 sensors were conducted in the laboratory with the sensors in three mu metal shields. The result of these initial runs is shown in graph 7.28, where a 30 pT per 1500 second peak to peak field difference is observed. This level of noise is very similar to the HTM1_2 noise observed previously. To ensure consistency, ten consecutive 1000 second runs were completed with all ten shown in graph 7.29. The field difference was consistently below 50 pT per 1000 seconds.

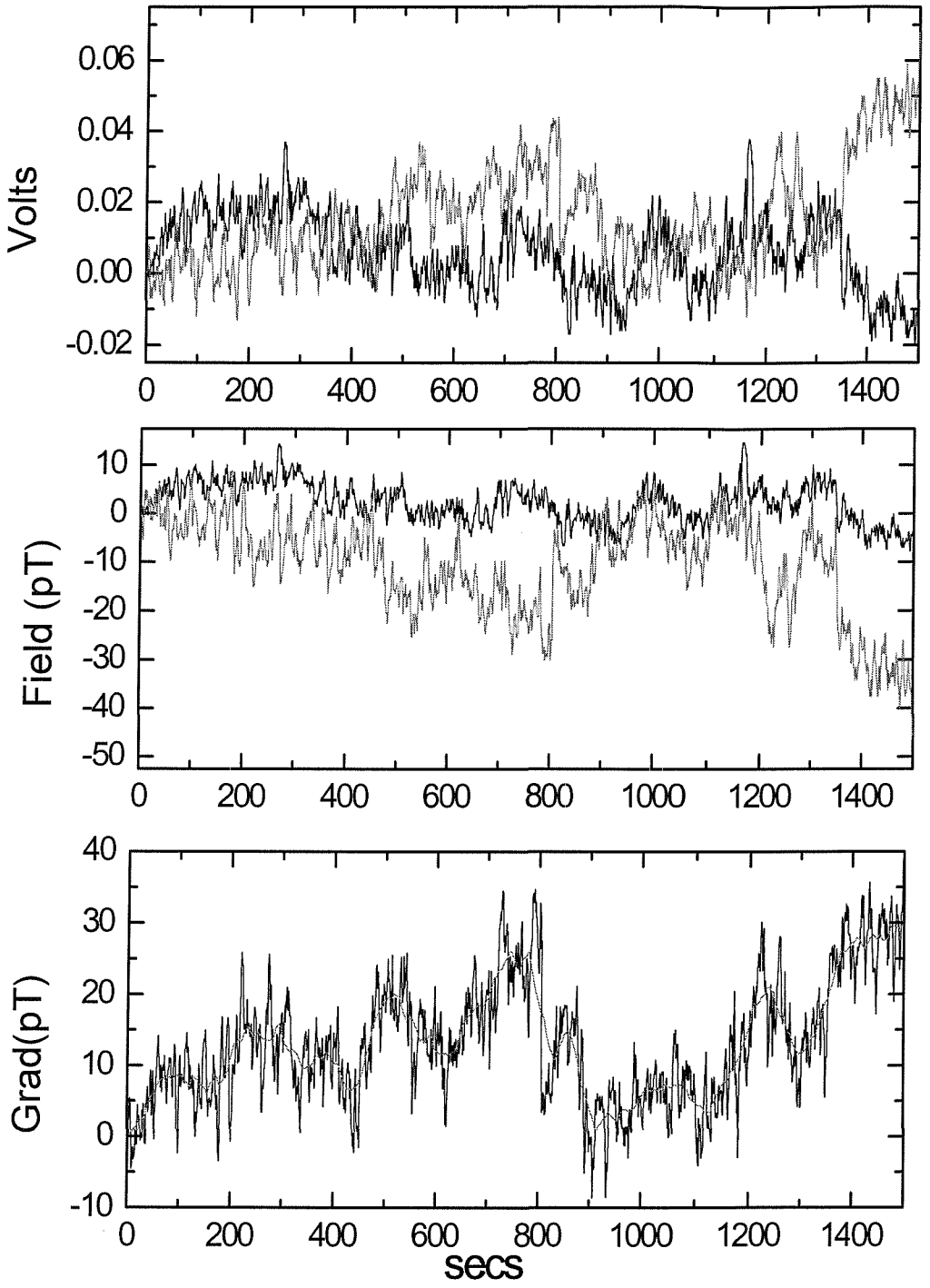

Graph 7.28- Initial three shield runs with new high field sensors.

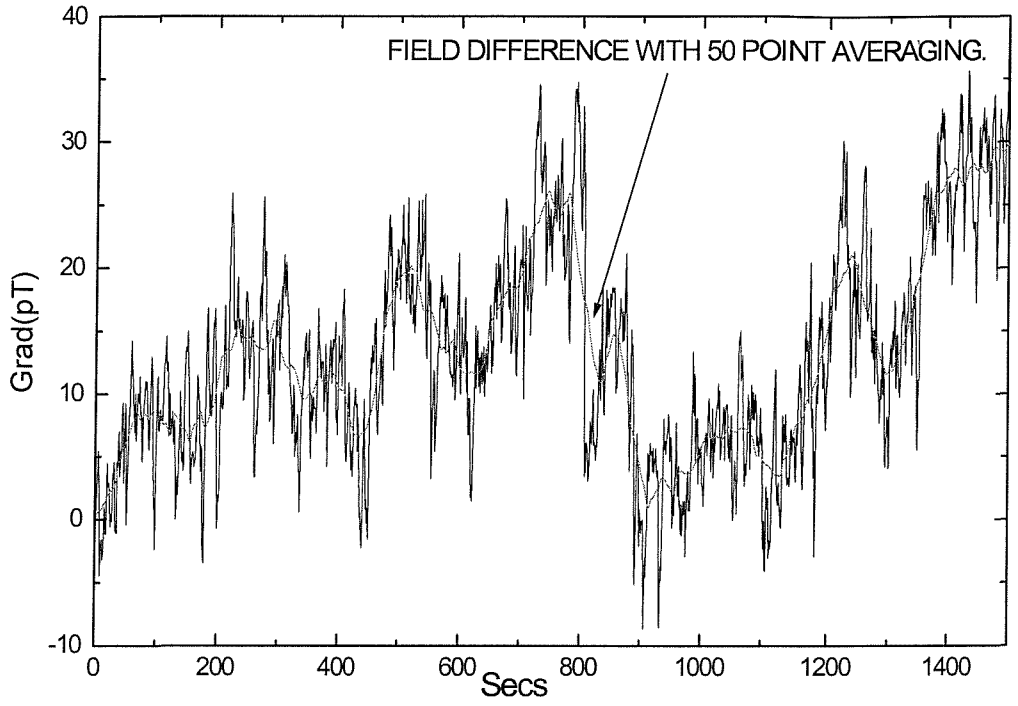

Graph 7.29- Comparative successive triply shielded runs.

To check the manufacturers specification of the sensors, data was collected with the sensors triple shielded. From which a power spectrum was created for each channel, as shown in graphs 7.30 and 7.31. These graphs confirmed that the sensors worked to specification in a fully shielded environment. In fact the results in graphs 7.30 and 7.31 are better than the low frequency noise spectrums collected by the suppliers as detailed in graphs 7.24 and 7.25

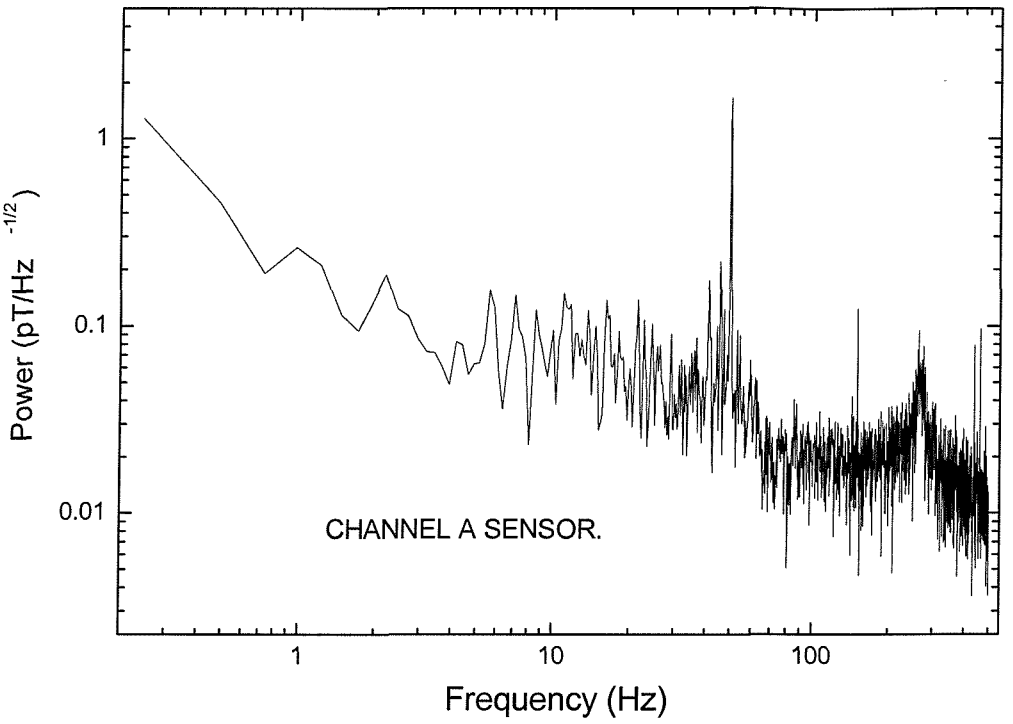

Graph 7.30- Power spectrum for channel A HTM100.

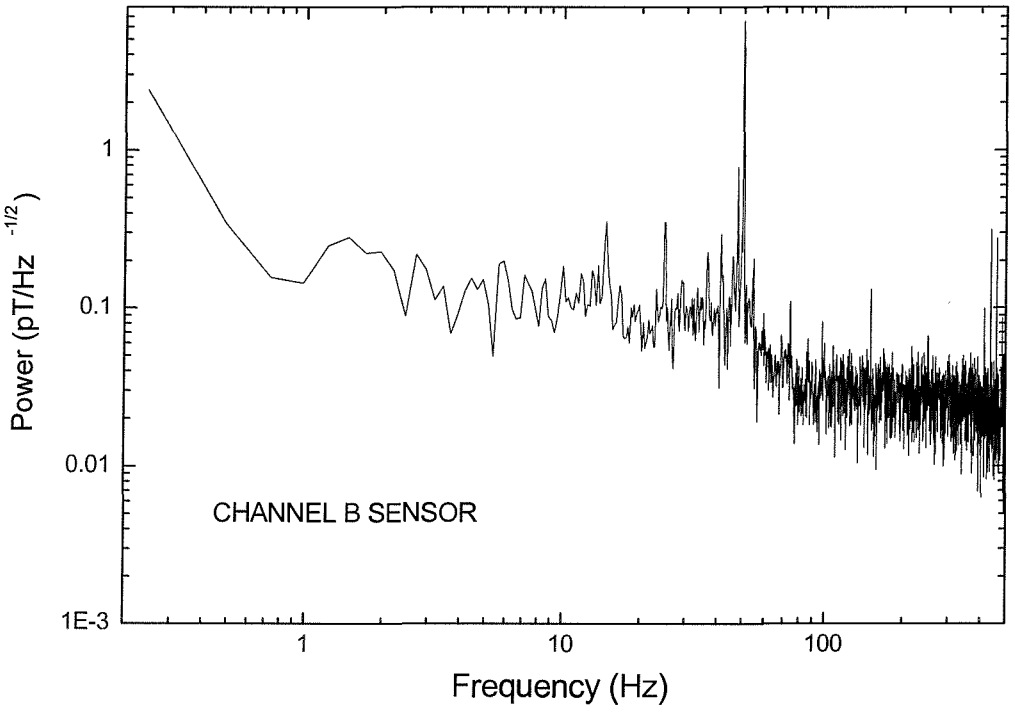

Graph 7.31- Power spectrum for channel B HTM100.

7.6. FIELD TESTS AND RESULTS.

7.6.1 HTM1_2 FIELD TESTS.

The first sensors that were used unshielded out of the laboratory were the HTM1_2 sensors. They were taken on to a piece of ground on Southampton common approximately 500 m from the nearest building or motor vehicle. The first outdoor run is shown in graph 7.32a, over 10 seconds, the field difference between the two sensors is several hundred picotesla. A contributing factor of this large noise is the abundant 50Hz signal as shown in graph 7.32(b).

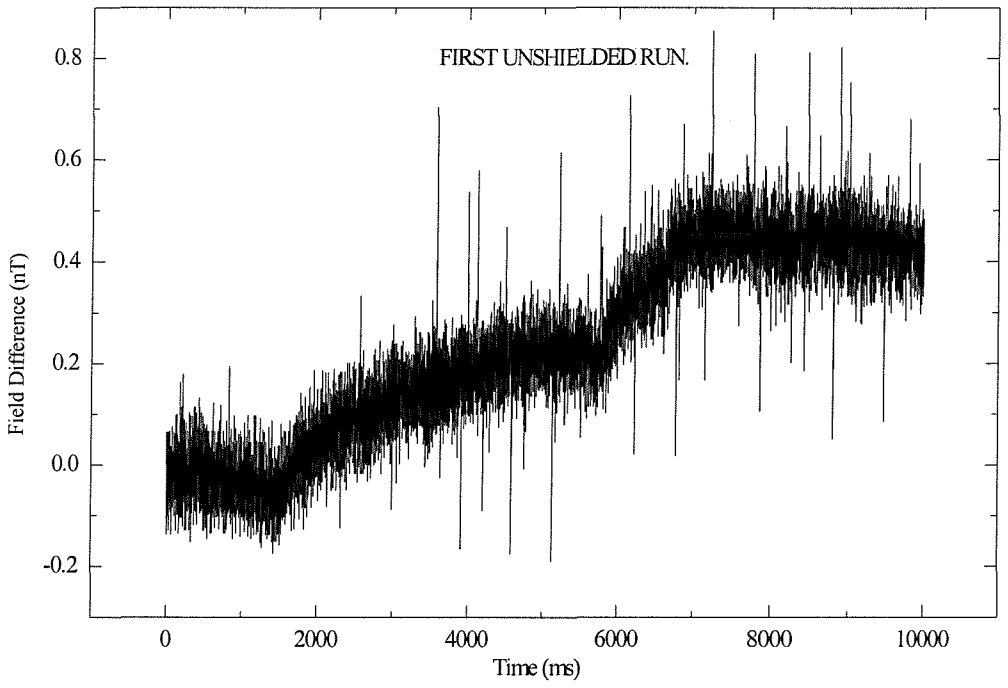

Graph 7.32a- Initial run taken in the field.

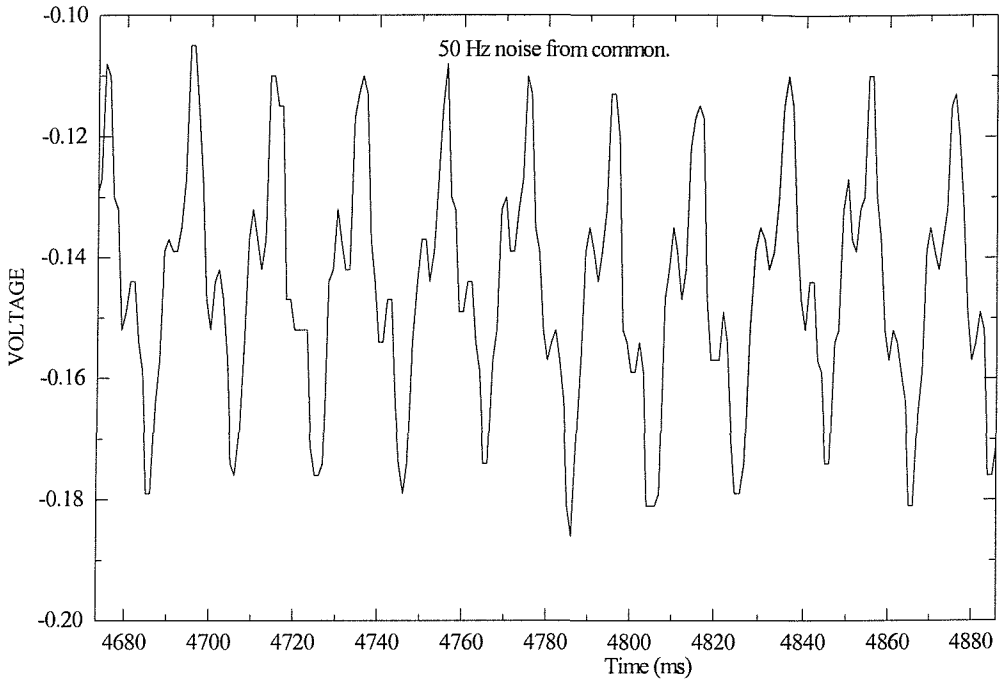

Graph 7.32b- 50 Hz component in initial run.

A longer run was achieved on the common, although the sensitivity of the SQUID had to be reduced to prevent it from saturating the voltage output. Graph 7.33 shows this run, demonstrating the fact that the sensors are mounted in the opposite sense as the external signals cause the voltage output to vary with the opposite sign. Just after the 2500 second mark, a bicycle passed the system causing it to jump. It is evident to see from the graph that one of the sensors returns to its initial voltage level immediately, whereas the other one moves to a new level. Again this fact can be corrected for in the post run processing. One fact that can be gained from the run shown in graph 7.34; observation of the field difference of the first 2500 seconds shows the following. The field difference continually increases with time. Due to the nature of the way the post processing is calculated with the raw data being effectively zeroed at the start of the run, the observed slope in the field difference is indicative of a calibration error. Graph 7.35 shows how the apparent field difference of nearly 3 nT can be reduced to a few hundred picotesla just by adjusting the

voltage to magnetic field calibration of one of the sensors by around 15%. This situation had not been observed before in the laboratory runs, and could be due to the HTM1 sensor calibration being dependent upon ambient magnetic field.

To confirm the effect that external field had on the sensor, if any, it would have been necessary to calibrate the sensors before and after each run in the field. It was not possible to calibrate the sensors in the field due to external interference. As a result the effect of external field strength on calibration of the sensor remains unanswered.

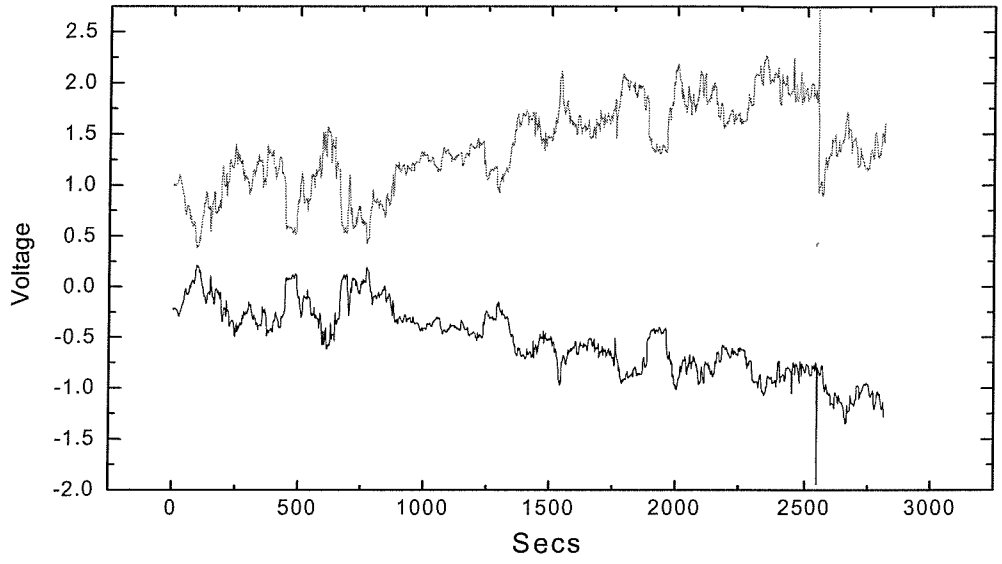

Graph 7.33- Longer run in field showing sensors detecting in opposite direction.

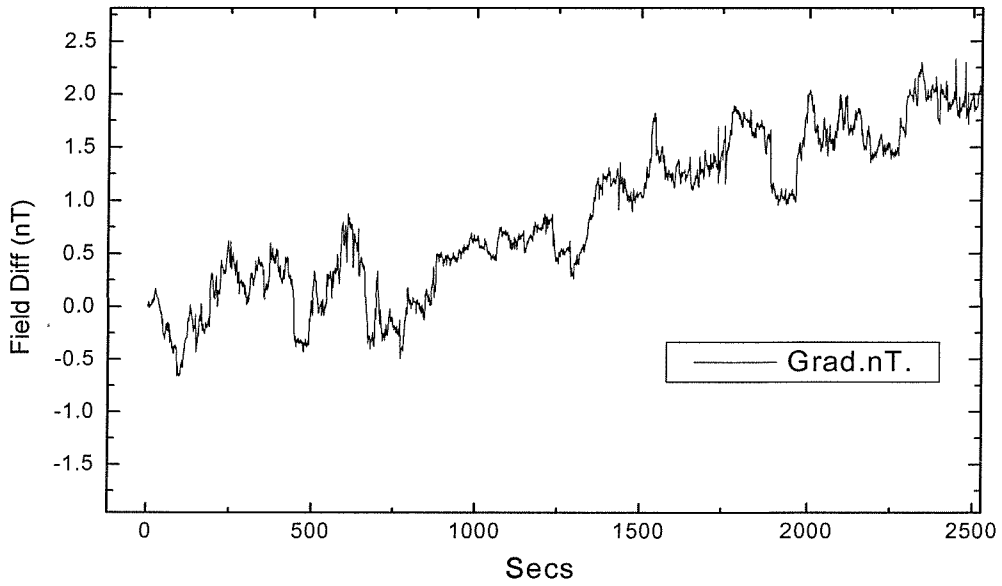

Graph 7.34- Constant gradient in noise drift between sensors.

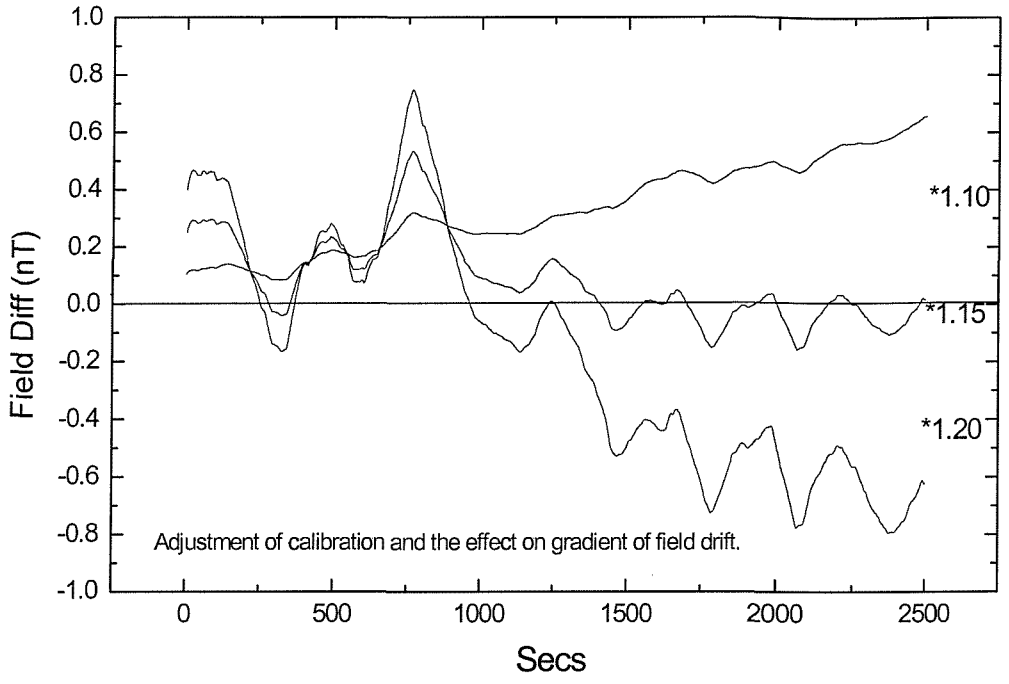

Graph 7.35- Reduction in noise gradient with adjustment of sensor calibration.

Another test that was conducted in the park was to tip the cryostat into and out of the earth's magnetic field to see if this affected the overall noise of the system. Because the low frequency noise of a SQUID is affected by the ambient field in which it is immersed. Graph 7.36 shows a 1000 second run of the SQUIDs in a vertical position. The resulting field difference being a little over 2 nT. In graph 7.37 the cryostat was then tipped 11 degrees in a northerly direction, which had the effect of reducing the earth's magnetic field incident upon the sensors. Even though the field is reduced in the sensors, the field difference is not; in fact it appears to increase slightly. Graph 7.38, where the sensors are placed in the higher field southerly direction, the net result on the field difference is similar to the last two results. It would appear therefore that the city park provides too much interference and external signal to allow the intrinsic noise of the sensors to be observed.

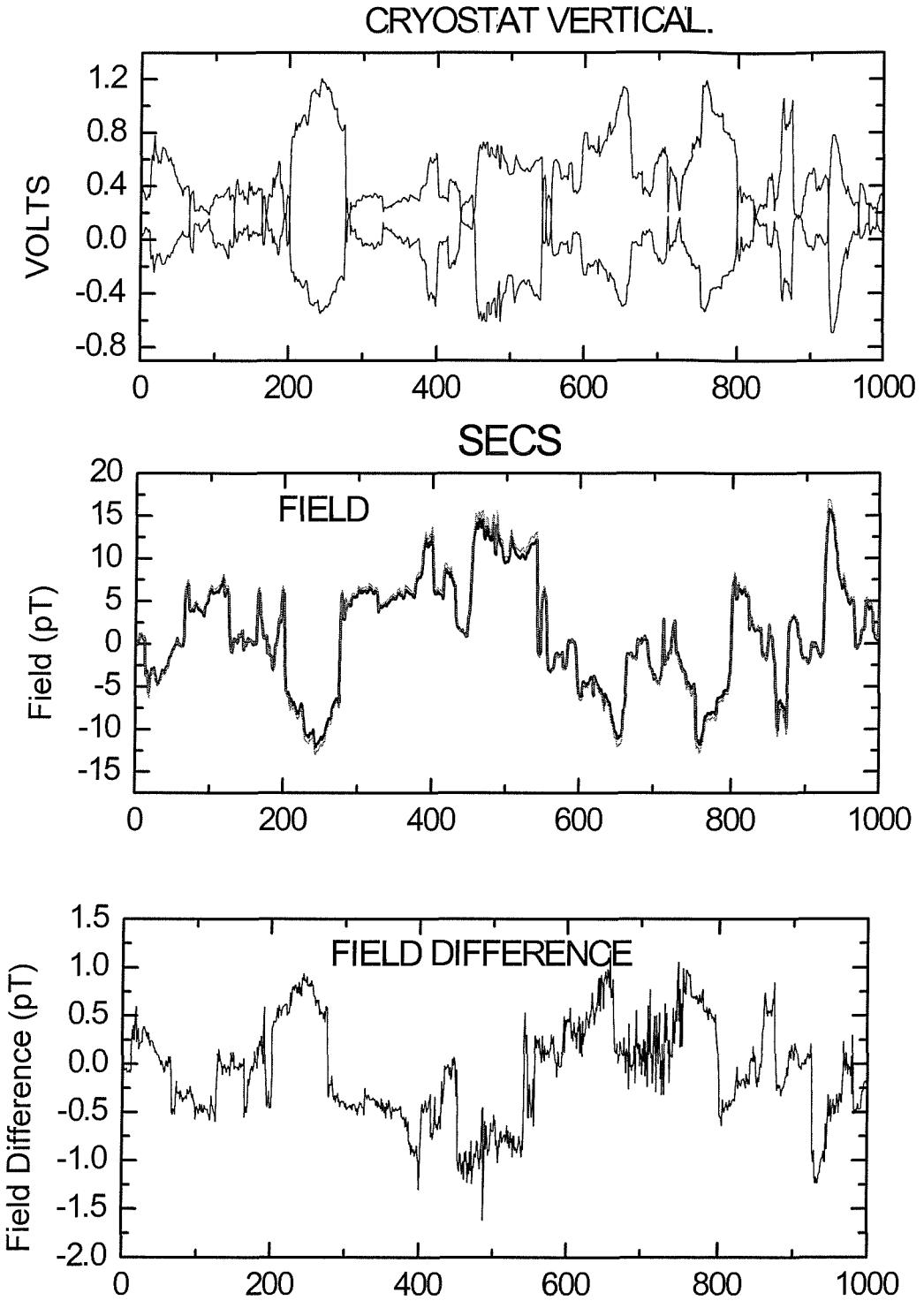

Graph 7.36- Field run with sensors and cryostat vertical.

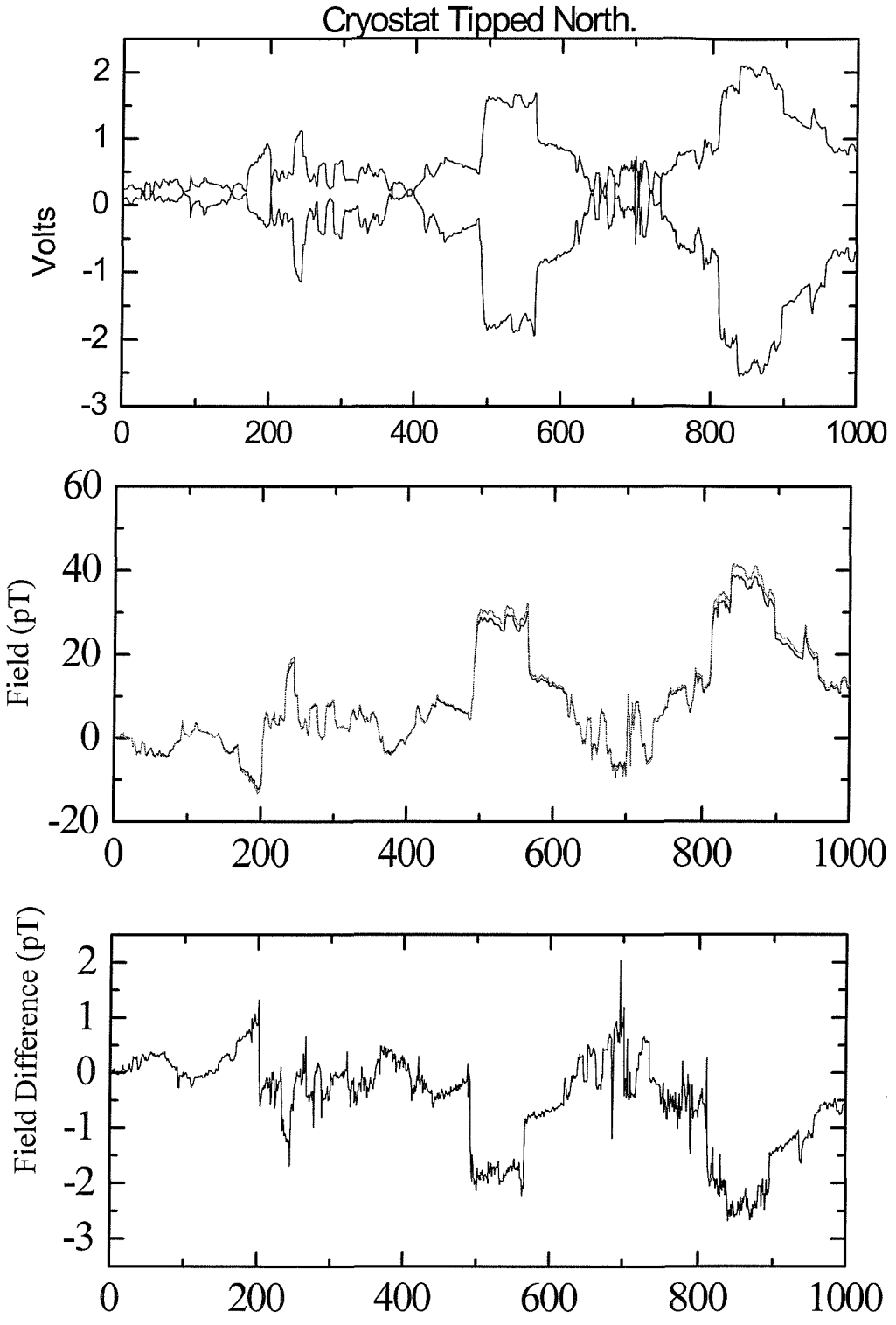

Graph 7.37- Field run with sensors tipped 11 degrees north.

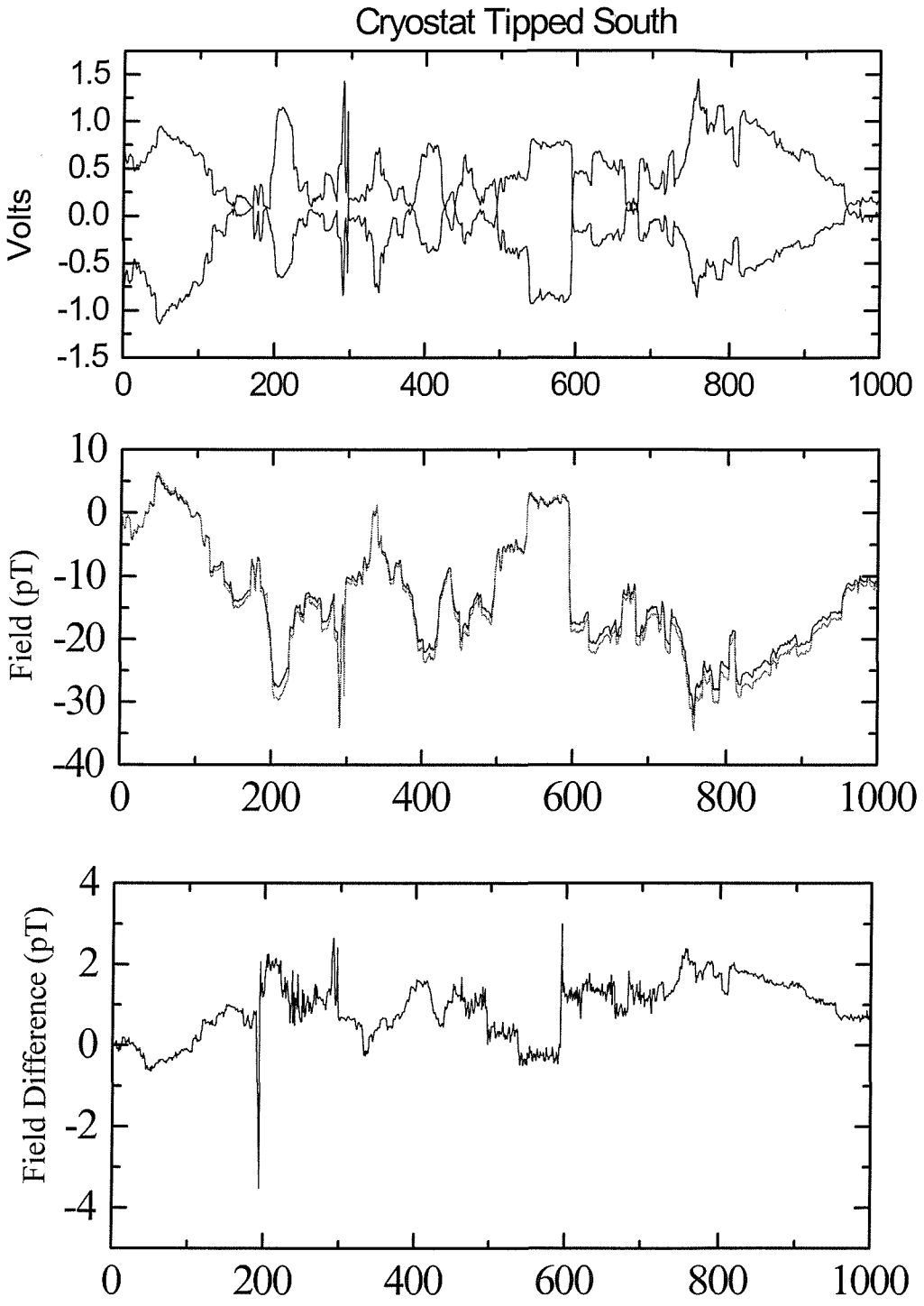

Graph 7.38- Field run with sensors tipped 11 degrees south.

7.6.2 HTM100 FIELD TESTS.

An environment more remote than a park in a city was sought to conduct tests with the new HTM100 sensors when they arrived to replace the HTM1_2 SQUIDs. An area in west Wales called the Gower was chosen because of its remoteness combined with accessibility. Figure 7.1 shows the general area in south Wales which Pembrey is set. A more detailed view of the test area is shown in figure 7.2.

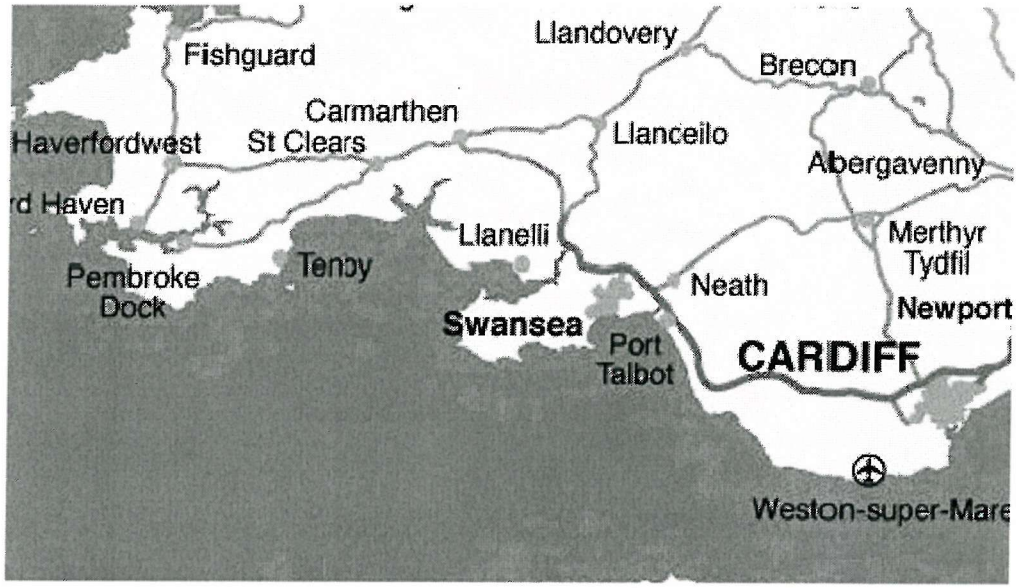

Figure 7.1. Map of southwest Wales, Pembrey is located just west of Llanelli.

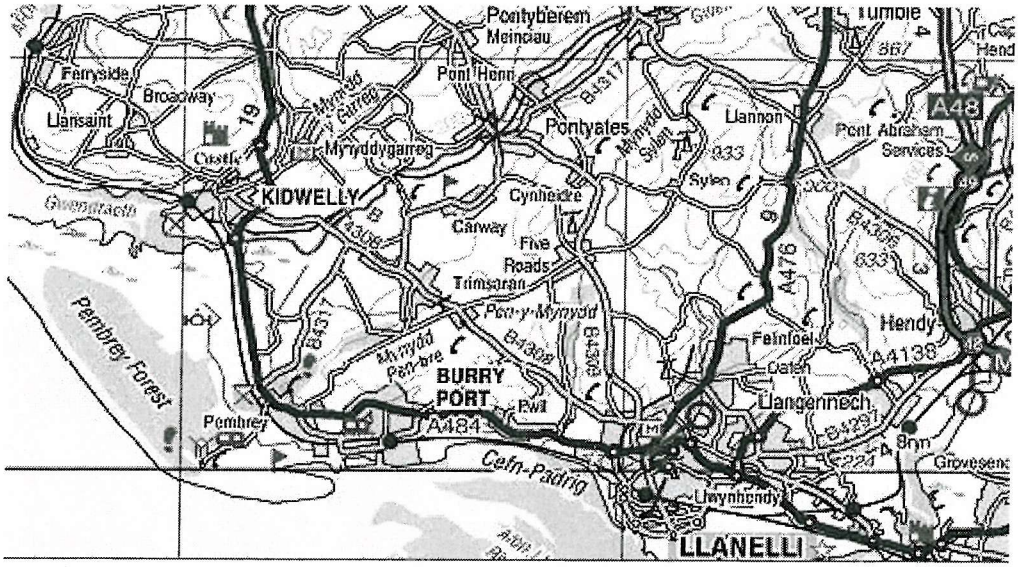

Figure 7.2. Map showing the beach area of Pembrey.

A twenty second segment of a run in this remote environment is displayed in graph 7.39, the two calibrated outputs from the SQUIDs being displayed along with their difference. The rejection of noise looks quite encouraging, except for the jumps in signal of about 10 pT that happens at fairly random intervals. On close inspection of graph 7.39 it is possible to note that the cause of these jumps is due solely to one of the sensors. Data was also collected that was suitable for use in calculating a power spectrum for the unshielded sensors. The field spectrum of the difference between the two sensors is shown in graph 7.40. The spectrum of the difference between the two sensors is shown because it is the only way to represent the actual intrinsic noise of the sensors in an open field environment because most of the external noise should be removed by the subtraction of the two sensors. A field noise of just less than 1 pT is achieved at 1 Hz for the combination. Graphs 7.30 and 7.31 show the noise spectra of the two HTM100 sensors in three shields in the laboratory. The noise at 1 Hz is around 0.2-0.3 pT. This demonstrates that the HTM100 in the field worked very close to its optimum in the laboratory.

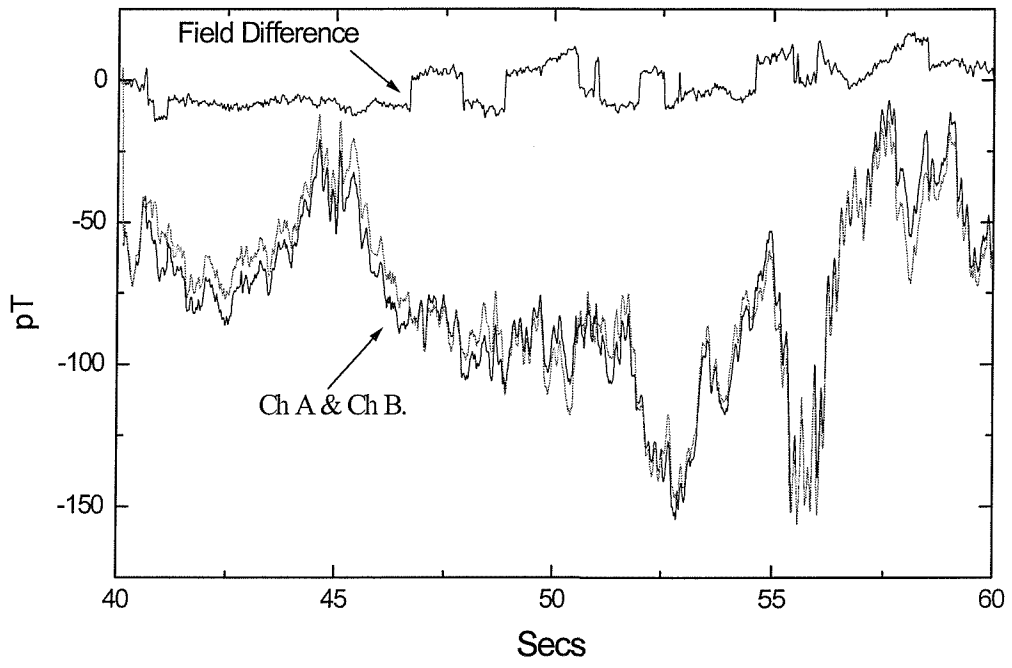

Graph 7.39- Field run on the Gower.

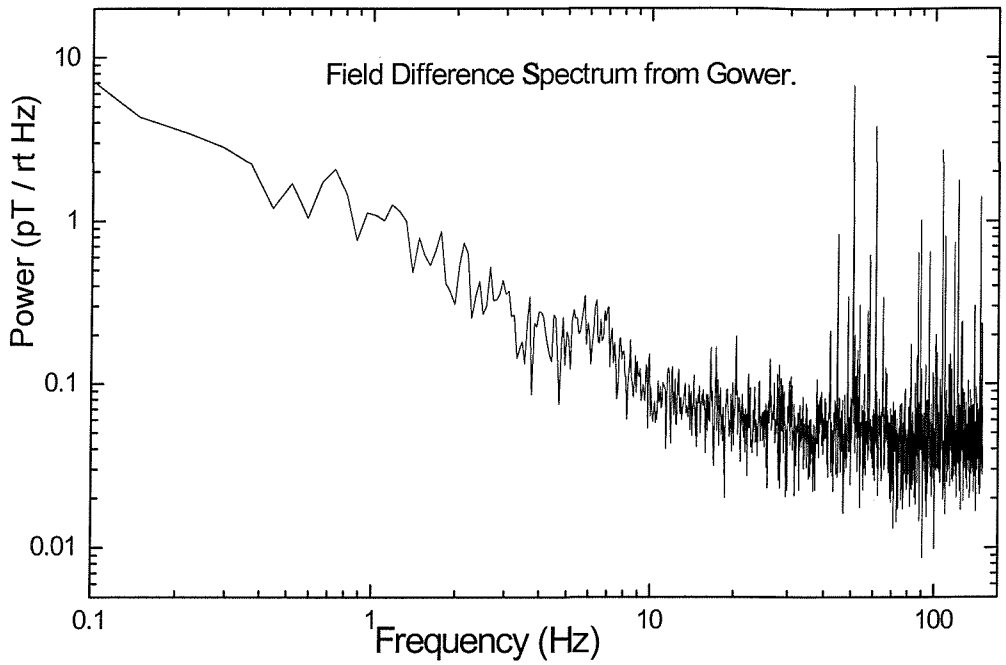

Graph 7.40- Power spectra resulting from run on Gower.

A 5 Hz magnetic dipole was activated as shown in figure 7.3. Graph 7.41, shows the detected signal by the two sensors and their difference, which represents a true changing gradient detected by the SQUIDs. The five hertz peak can be clearly seen in the power spectrum in graph 7.42 whilst a good overall noise level is maintained elsewhere.

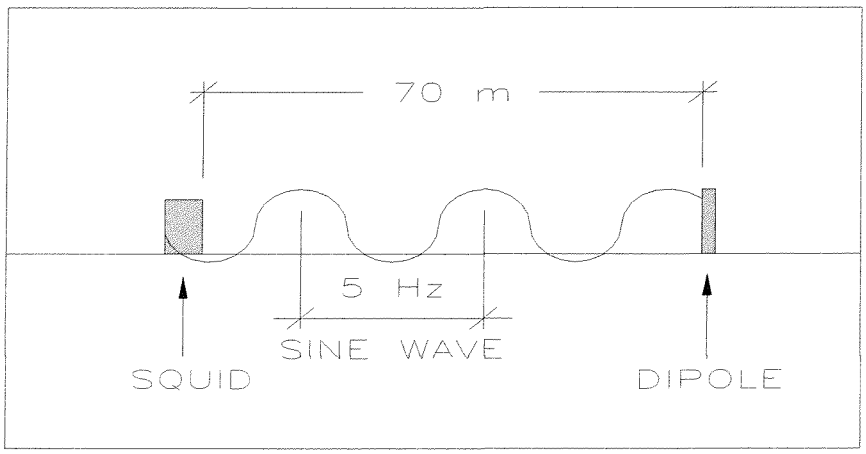

Figure 7.3. Field test to detect 5 Hz magnetic dipole.

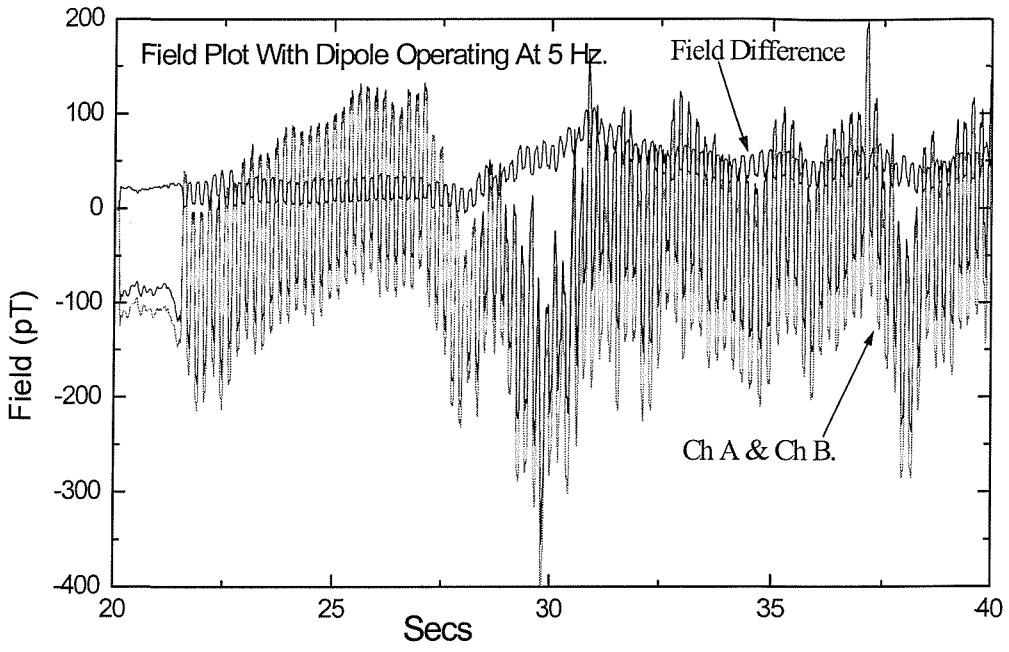

Graph 7.41- Detected gradient from dipole on the Gower.

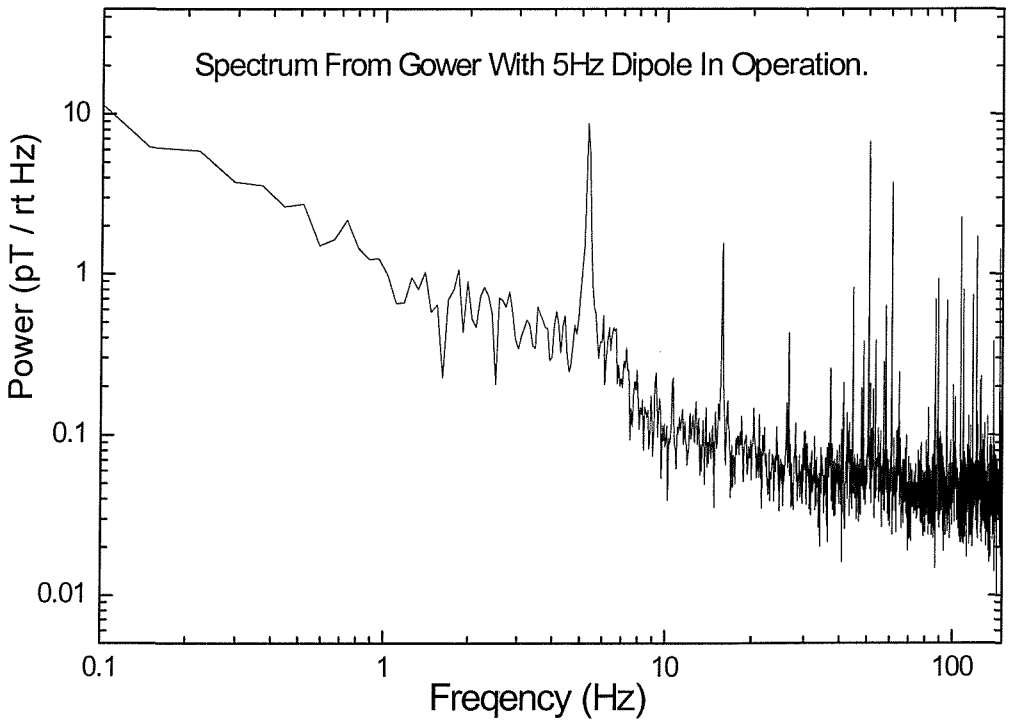

Graph 7.42- Power spectra showing the 5 Hz peak resulting from dipole run on Gower.

The design of the dipole is commercially sensitive and in the process of having a patent applied to its design. The dipole run enabled us to calibrate the dipole with the aid of the SQUIDs using the following equation:

$$B = m / 4\pi R^3$$

The magnetic dipole moment, m, of the dipole was calibrated by the Swansea group and found to be 6.5 x 10^{-4} Wb m. With the sensors 70 m away, the magnetic field incident upon the SQUIDs was easily calculated. This calculation gives an expected field strength at the sensors of 1.5x10^{-10} T. Close inspection of graph 7.41 gives good agreement with the calculated value, showing an amplitude in the region of 170 pT.

Much work has been conducted in the past with low T_c SQUIDs and it is well documented that the 1/f noise is much lower than high T_c SQUIDs. Graph 7.43 shows a comparison run taken in the open field between a low and high T_c device. We have assumed that the low temperature SQUID represented the actual ambient magnetic field. Hence any difference between the two sensors represents the noise of the high T_c SQUID.

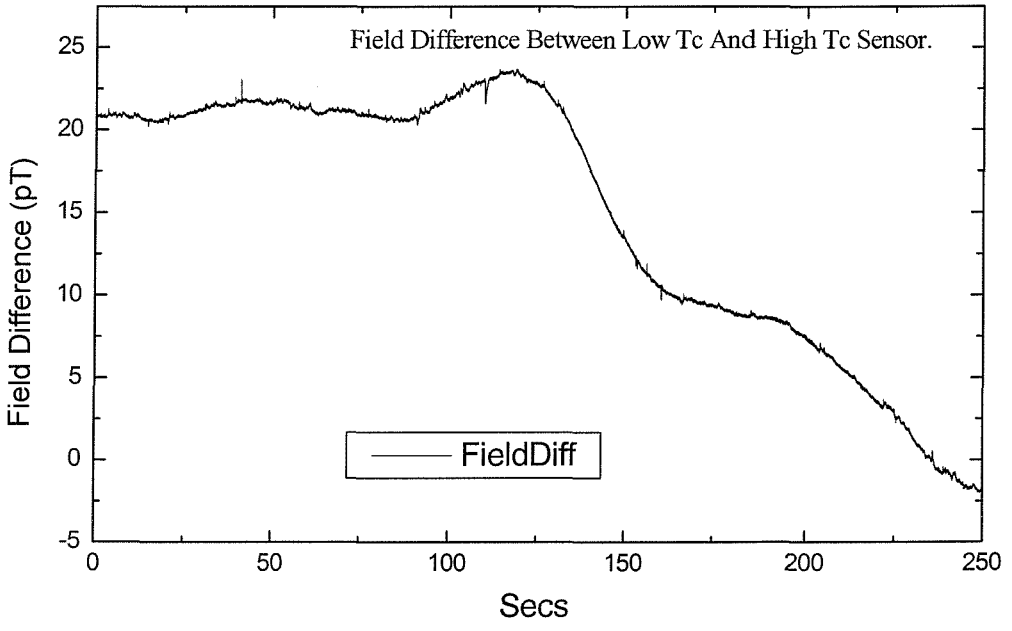

Graph 7.43- Field run on Gower to compare high and low T_c SQUIDs.

The final part of the project involved taking some magnetotelluric measurements. These were also taken in west Wales in the remote location near Pembrey. The beach in Pembrey has a very large flat bay that is potentially ideal for magnetotelluric measurements.

The set-up of this experiment is shown in figure 7.4. Copper pipes of approximately 500 mm in length were driven into the sand to ensure good electrical contact between the signal wire and the ground below. There were approximately ten copper rods hammered into the ground at each end of the signal wire as shown on the diagram as dots. The wire was energised with an a.c. current and the SQUID system took measurements of the magnetic component of the transmitted and reflected signals at various locations as shown by the X's in figure 7.4. Measurements were taken at as many locations as possible before the tide came in and ended the experiment.

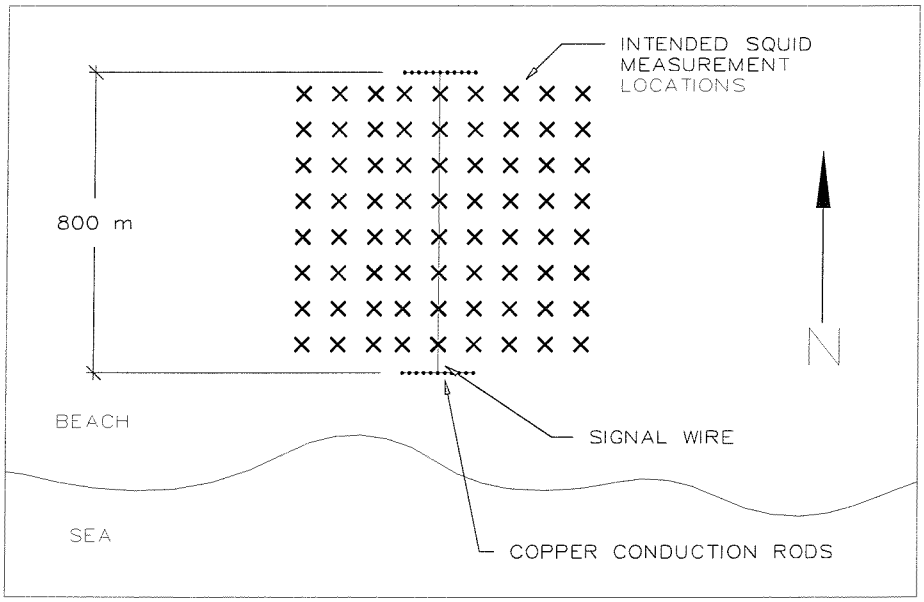

Figure 7.4. Aerial view of magnetotelluric measurement set-up on Pembrey beach.

The same alternating signal was transmitted into the ground on each occasion with the SQUID placed in various locations as indicated in the figure. The magnitude of the reflected signal was measured and stored in the computer. Graph 7.44 shows the magnetic field distribution that was measured from the reflected pulse that was transmitted into the ground. From this work it was possible to plot a graph of the magnetic profile of the earth in this region.

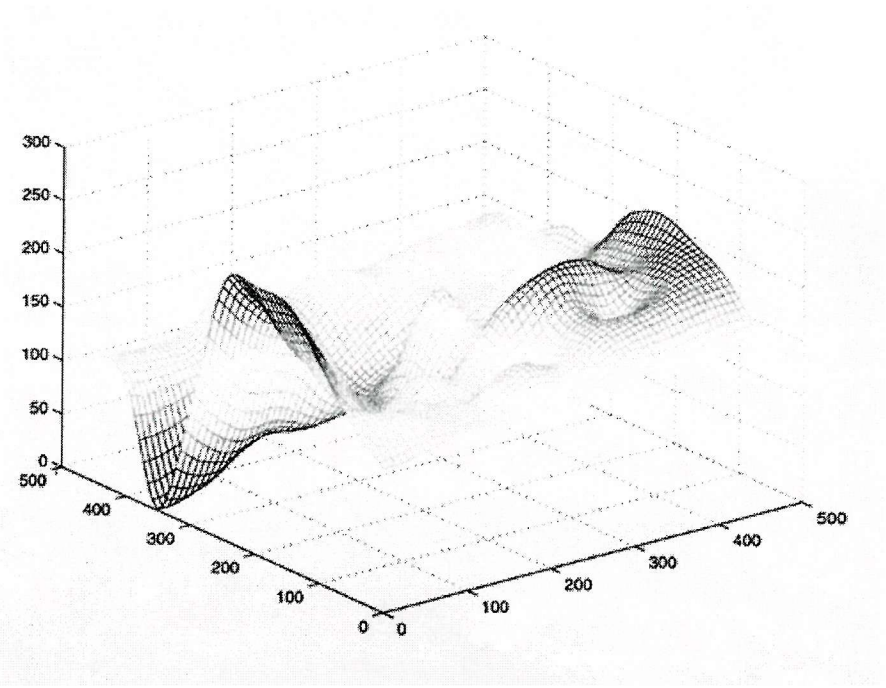

Graph 7.44- Magnetic field distribution in Z direction over test area.
(Z-axis units – Field in pT. X & Y-axis units – metres.)

CHAPTER 8.

8. CONCLUSIONS.

In this project we have optimised the operation of high temperature superconducting quantum interference devices, both in the laboratory and in the field. We have designed and built a fully integrated battery operated system suitable for operation in both locations. The voltage output from the SQUID was collected via an analogue to digital converter and stored on a laptop computer. The data was processed and then plotted in several forms, showing the voltage output, field drift, field difference and power spectrum.

The ability of a high temperature SQUID was demonstrated with the Oxford Instruments system, showing the ability of an unshielded SQUID to operate with great sensitivity in the unshielded laboratory. However we found that the Oxford Instruments system did not work reliably.

Reliable operation was achieved from the Tristan Technologies sensors. All the results gained in this project, including the detection of land mines were collected from these sensors. There were two different types of Tristan sensor used, the low field HTM1 and high field HTM100, which are designed for use in low and high ambient magnetic fields respectively. The low field sensors were designed for use in magnetic fields of less than 1 μT, and the high field sensors in fields up to around 100 μT.

Tests with a permanent magnet used to create a constant 100 μT magnetic field at the sensor showed that the noise increased by around an order of magnitude, compared to the SQUID in a single mu metal shield in the laboratory. Some unusual behaviour of the SQUID was discovered during the magnet runs. The normal stability of the sensor was compromised, replaced with an apparent periodic behaviour. One explanation that was posed for this behaviour was changes in atmospheric pressure. The periodic behaviour

had only been observed during magnet runs, but a test was undertaken in which the ambient pressure was varied when the SQUID was magnetically shielded. The result of this run showed that an increase in pressure did not give any noticeable effect on the performance of the SQUID. It was concluded that the operation of HTM1 sensors was affected by magnetic fields close to the earth's field strength.

The quoted performance of the SQUID sensors used in this project were checked and confirmed. The HTM100 SQUID sensors matched and sometimes exceeded the manufacturers and suppliers quoted performance within the laboratory.

When a third mu metal shield was obtained for the SQUIDs it was possible to observe their performance more closely. Runs using three shields showed the limit of the analogue to digital converter. A three shield run of 2000 seconds provided a graph that appeared very coarse. The coarseness was caused as a result of the voltage changes from the SQUID being close to the limit of the ADC, which had a resolution of 1 mV. Even with this digitisation of the signal it was possible to ascertain a field drift of around 10 pT over a 15 minute period. To confirm the effect of the third mu metal shield, a run with one sensor in two shields and one in three was performed. The noise level in the triple shielded sensor was lower by over an order of magnitude.

The long term stability of the SQUIDs was established with several runs of 24 hours being completed. In which time the sensors normally kept within their range of plus and minus five volts for 10 – 20 hours. During these runs the output would remain within a few hundred picotesla, although there would be periodic jumps from one level to another, possibly due to the movement of flux vortices entering or leaving the body of the superconductor.

In cooperation with the University of Southampton Institute of Transducer Technology we estimated the ability of a high temperature SQUID to detect land mines. Even though the cryostat was failing during the experiments, the HTM1 sensors easily detected two different types of land mine. At a distance of approximately 1 m the sensors detected a

signal of 2.5-3 μT. The two types of land mine were fairly old, similar to the type laid during the Vietnam war.

The initial field runs in the park in Southampton, demonstrated the massive 50 Hz noise that is present in urban environments. All noise spectra taken on the common were dominated by this frequency. The requirement of an area further from power lines and electrical power sources had been demonstrated. The Gower area in Wales was identified as being a suitable area, far enough from power lines and general civilisation but still accessible. The power spectrum from the Gower showed a significantly lower 50 Hz component.

It was discovered that the high temperature SQUIDs used in this project outperformed a leading edge fluxgate magnetometer. With the fluxgate in two mu metal shields, a run of 700 seconds returned a peak to peak field drift of just over 100 pT. Where as the same run for the SQUID gave a noise level of around 25 pT. Although the SQUID was consistently better than the fluxgate at low frequencies, fluxgate magnetometers are cheaper to purchase and easier to operate than a SQUID. Therefore we decided to investigate the higher frequency performance of the SQUID where it has a greater advantage.

The performance of induction coils was researched because they are extensively used in geophysical prospecting. It was found that their performance was mostly limited by physical dimension. Coils with sensitivities of less than 10 fT / √Hz were commercially available. The graphs show however that this sensitivity is gained above about several hundred hertz, i.e. as a white noise figure. The best high temperature SQUID white noise recorded was around 20 fT / √Hz. Below 100 Hz the performance of the SQUID was superior to that of induction coils. Coils measure the time derivative of the magnetic field, where as SQUIDs measure the magnetic field. Because the voltage decay across the coil is much quicker than the decay of the magnetic field, the SQUID can achieve lower noise levels at lower frequencies. As a result, the use of a SQUID can allow an increase in the depth of investigation in geomagnetic surveying, or a reduction in the

measurement time required to achieve the same data quality compared to that of an induction coil set.

As a result of this research, it became apparent that high temperature SQUIDs could be useful for frequencies between one and one thousand Hertz. Useful frequencies for geophysical prospecting start from around these values.

It appeared that the SQUID might have potential for application in this area. A geophysical prospecting run was undertaken in the remote Gower region. These runs were taken at the end of the project, and they showed great promise. Further research in this area is required to ascertain the suitability of high temperature SQUIDs, in geophysical prospecting.

REFERENCES.

[2.1] Clarke J, (1989) 'Principles and Applications of SQUIDs' Proceedings of the IEEE, **77**, No 8, 1208-1221.

[2.2] Bednorz J G and Muller K A, (1986) 'Possible High Temperature Superconductivity', Physik B, 189-193.

[2.3] Koch R H, Umbach C P, Clark G J, Chaudhari P and Laibowitz R B (1987) 'Quantum Interference Devices Made From Superconducting Oxide Thin Films' Appl. Phys Lett. **51**, 200-202.

[2.4] Face D W, Graybeal J M, Orlando T P and Rudman D A. (1990) 'Noise and dc Characteristics of Thin-film Bi-Sr-Ca-Cu-oxide dc SQUIDs', Appl. Phys. Lett. **56**, 1493-1495.

[2.5] Koch R H, Gallagher W J, Bumble B and Lee W Y (1989) 'Low-noise Thin-film TlBaCaCuO dc SQUIDs Operated at 77 K', Appl. Phys. Lett. **54**, 951-953.

[2.6] Simon R W, Bulman J B, Burch J F, Coons S B, Daly K P, Dozier W D, Hu R, Lee A E, Luine J A, Platt C E, Schwarzbek S M, Wire M S and Zani M J. (1991) 'Engineered HTS Microbridges' IEEE Trans. Magn. **MAG-27**, 3209-3214.

[2.7] Jia C L, Kabius B, Urban K, Herman K, Cui G J, Schubert J, Zander W, Braginski A I and Heiden C. (1991) 'Microstructure of Epitaxial $YBa_2Cu_3O_7$ Films on Step-edge $SrTiO_3$ Substrates' Physica C, **175**, 545-554.

[2.8] Dimod D, Chaudhari P, Mannhart J and LeGous F K, (1988) 'Orientation Dependence of Grain-boundary Critical Currents in $YBa_2Cu_3O_{7-\delta}$ Bicrystals' Phys. Rev. Lett. **61**, 219-222.

[2.9] Char K, Colclough M S, Garrison S M, Newman N and Zaharchuk G, (1991) 'Bi-epitaxial Grain Boundary Junctions in $Yba_2Cu_3O_7$' Appl. Phys. Lett. **59**, 733-735.

[2.10] Laibowitz R B, Koch R H, Gupta A, Koren G, Gallagher W J, Foglietti V, Oh B and Viggiano J M, (1990) 'All High-T_c Edge Junctions and SQUIDs' Appl. Phys. Lett. **56**, 686-688.

[2.11] Schwarz D B, Mankiewich P M, Howard R E, Jackel L D, Straughn B L, Burhat E G and Daymen A H, (1989) 'The Observation of the ac Josephson Effect in a $YBa_2Cu_3O_7$/Au/$YBa_2Cu_3O_7$ Junction', IEEE Trans. Magn. **MAG-25**, 1298-1300.

[2.12] DiIorio M S, Yoshizumi S, Yang K-Y, Yang J and Maung M, (1991) 'Practical High-T_c Josephson Junctions and dc SQUIDs Operating Above 85 K' Appl. Phys. Lett. **58**, 2552-2554.

[2.13] Rogers C T, Inman A, Hedge M S, Dutta B, Wu X D and Venkatesan T, (1989) 'Fabrication of Heteroepitaxial $YBa_2Cu_3O_{7-x}$-$PrBa_2CuO_{7-x}$-$YBa_2Cu_3O_{7-x}$ Josephson Devices Grown by Laser Deposition', Appl. Phys. Lett. **55**, 2032-2034.

[2.14] Gao J, Aarnink W A M, Gerritsma G J, Veldhuis D and Rogalla H, (1991) 'Preparation and Properties of All High-T_c SNS-type Edge dc SQUIDs' IEEE Trans. Magn. **MAG-27**, 3062-3065.

[2.15] Zani M J, Luine J A, Simon R W and Davidheiser R A, (1991) 'Focused Ion Beam High-T_c Superconductor dc SQUIDs' Appl. Phys. Lett. **59**, 234-236.

[2.16] Tinchev S S, Cui G, Zhang Y, Buchal C, Schubert J, Zander W, Hermann K, Sodtke E, Braginski A I and Heiden C, (1990) 'Properties of rf-SQUIDs Fabricated from Epitaxial YBCO Films' LT-19 Satellite Conference on High Temperature Superconductors, Cambridge, England, August 1990.

[2.17] Robbes D, Miklich A H, Kingston J J, Lerch P, Wellstood F C and Clarke J, (1990) 'Josephson Weak Links in Thin Films of $YBa_2Cu_3O_{7-x}$ Induced by Electrical Pulses' Appl. Phys. Lett. **56**, 2240-2242; erratum **57**, 1169.

[3.1] Whitmarsh, R B, Miles, P R, Sibuet, J-C and Louvel, V (1997) 'Geological and Geophysical Implications of Deep-Towed Magnetometer Observations Near Sites 897, 898, 899 and 901 on the West Iberia Continental Margin', Proceedings of the Ocean Drilling Program, Scientific Results, Vol. 149, 665-674.

[3.2] Murton, B J, Rouse, I P, Millard, N W and Flewellen, C G (1991) 'Multisensor, Deep-Towed Instrument Explores Ocean Floor', EOS, 225-226.

[3.3] Miklich, A H, Koelle, D, Shaw, T J, Ludwig, F, Nemeth, D T, Dantsker, E, Clarke, J, McN.Alford, N, Button, T W and Colclough, M C (1994) 'title', Appl. Phys Lett, vol 64, p3494.

[3.4] Keene, M N, Exon, N J, Horton, T, Humphreys, R G and Satchell, J S (1999) 'A HTS Gradiometer for Unshielded Operation from Moving Platforms', ISEC99 Extended Abstracts, 566-568.

[3.5] Clem, T R, Overway, D J, Purpura, J W, Allen, G I, Bono, J T,Koch, R H, Rozen, J R and Keefe, G A, (1999) 'A High T_c Superconducting Magnetic Gradiometer for Mobile Operation', ISEC99 Extended Abstracts, 569-571.

[3.6] Koch R H, Rozen J R, Sun J Z and Gallagher W J (1993) 'Three SQUID Gradiometer', Appl. Phys. Lett. **63**, 403-405.

[3.7] Kaufman, A A and Keller, G V, (1994) 'The Magnetotelluric Sounding Method', Elsevier.

[3.8] Vozoff K, (1997) 'The Magnetotelluric Method in the Exploration of Sedimentary Basins', Geophysics, **37**, No. 1, 98-141.

[3.9] Reedman, J H, (1995) 'Techniques in Mineral Exploration', Applied Science.

[3.10] Chwala A, Stolz R, Ramos J, Schultze V, Meyer H-G and Kretzschmar D (1999) 'A HTS dc SQUID System for Geomagnetic Prospection', ISEC99 Extended Abstracts, 598-600.

[3.11] Weidl R, Brabetz S, Schmidl F, Klemm F, Wunderlich S and Seidl P, (1997) 'Heart Monitoring with High-T_c d.c. SQUID Gradiometers in an Unshielded Environment.' Supercond. Sci. Technol. **10**, 95-99.

[3.12] Seidl P, Schmidl F, Wunderlich S, Dorrer L, Vogt T and Linzen S (1999) 'Different Applications of High T_c SQUID Sensors' ISEC99 Extended Abstracts, 578-580.

[3.13] Laudahn R, Kohlhoff H and Bromm B (1995) 'Magnetoencephalography in the Investigation of Cortical Pain Processing' Advances in Pain Research and Therapy, **22**, 267-282.

[3.14] Tavrin Y, Krause H-J, Wolf W, Glyantsev V, Schubert J, Zander W, Haller A and Bousak H (1996) 'Eddy Current Technique with High Temperature SQUID for Non-Destructive Evaluation of Non-Magnetic Metallic Structures' Cryogenics, **36**, 83-86.

[3.15] Haller A, Tavrin Y, Krause H-J, David P and Braginski A I, (1997) 'Eddy Current Tomography Using Rotating Magnetic Fields For Deep SQUID NDE' Supercond. Sci. Technol. **10**, 901-903.

[3.16] Krause H-J, Zhang Y, Hohmann R, Gruneklee M, Faley M I, Lomparski D, Maus M, Bousak H and Braginski A I, (1997) 'Eddy Current Aircraft Testing with Mobile HTS-SQUID Gradiometer System' Paper Presented at ASC 1997, 775-780.

[3.17] Krause H-J, Hohmann R, Gruneklee M, Maus M, Zhang Y, Lomparski D, Wolf W, Bousak H, and Braginski A I, (1998) 'Aircraft Wheel and Fuselage Testing with HTS SQUID' Paper Published in Proceedings of 4th Twente HTS Workshop, 6-7 May 1998.

[3.18] Krause H-J, Hohmann R, Gruneklee M, Maus M, Zhang Y, Lomparski D, Soltner H, Wolf W, Banzet M, Schubert J, Zander W, Bousak H, and Braginski A I, (1999) 'Aircraft Wheel and Fuselage Testing with Eddy Current and SQUID' To be Published in Proceedings of 7th European Conference on Non-destructive Testing.

[3.19] Hohmann R, Krause H-J, Zhang Y, Copetti C A, Bousak H, and Braginski A I, Faley M I, (1997) 'HTS SQUID System with Joule-Thomson Cryocooler for Eddy Current Non-destructive Evaluation of Aircraft Structures.' IEEE Trans. on Appl. Suprecond. **7**, No. 2, 2860-2865.

[3.20] McDermott R, Schlenga K, Clarke J, de Souza R E, Wong-Foy A and Pines A, (1999), 'Low-Field NMR and MRI of Room Temperature Samples Detected With a High T_c SQUID.' ISEC99 Extended Abstracts, 581-583.

[3.21] Tavrin Y and Siegel M, (1997), 'New Type of HTS-SQUID Microscope for Operation Without Shielding', ASC97 Extended Abstracts, 719-722.

[3.22] Macfarlane J, Peden D, Hao L, Gallop J and Romans E, (1997) 'Effect of Junction Noise in a Resistive High T_c SQUID Noise Thermometer', ASC97 Extended Abstracts, 723-726.

[3.23] Lockhart J M, Muhlfelder G M, Gutt G M, Luo M, Clappier R C, McGinnis T R and Smith G R, (1997), 'Optimisation of a SQUID System for Space', IEEE Trans. on Appl. Supercond. **7**, No. 2, 2534-2537.

[3.24] Wikswo J P, (1994), 'SQUID Magnetometers for Biomagnetism and Nondestructive testing: Important Questions and Initial Answers', IEEE Trans. on Appl. Supercond, **5**, No 2, 35-37.

[3.25] Reedman J H, (1989) 'Techniques in Mineral Exploration', Applied Science Publishers, 291-293.

[4.1] Foley C P, Leslie K P, Bink R E and Lewis C (1999) 'Excess low frequency noise in YBCO SQUIDs in weak magnetic fields' IEEE Trans. Appl. Supercond. **7**, No.2, 2334-2337.

[4.2] Deak J, Miklich A H, Slonczewski J and Koch R H. (1996) 'A Low-Noise Single-Domain Fluxgate Sensor.' Appl. Phys. Lett. **69**, (8), 1157-1159.

[4.3] Koch R H, Keefe G A and Allen G (1996) 'Room Temperature Three Sensor Magnetic Field Gradiometer' Rev. Sci. Instrumen. **67**, (1), 230-235.

[4.4] Bartington Instruments Ltd, 10 Thorney Leys Business Park, Witney, Oxford OX8 7GE, UK. Product code *Mag-03MSL80-5V.*

[4.5] Telford W M, Geldart L P and Sheriff R E (1996) 'Applied Geophysics' Second Edition, Cambridge University Press, 77-78.

[4.6] Geometrics UK, Kings Barn, Watling Street, Hockliffe, Leighton Buzzard, Bedfordshire, LU7 9NG, UK. Product code G-822A, mobile caesium magnetometer.

[4.7] Hood P, (1965) 'Gradient Measurements in Aeromagnetic Surveying' Geophysics, No.5, 891-902.

[4.8] www.zonge.com. Product code ANT/4.

[4.9] Chwala A, Stolz R, Ramos J, Schultze and Meyer H-G (1999) 'A HTS SQUID System for Geomagnetic Prospection' Proceedings of ISEC99, 598-600.

[4.10] Carr C and Macfarlane (1998) 'The Performance of Fluxgate Magnetometers for Non-Destructive Evaluation' Insight, **41**, No.1, 20-24.

[5.1] Clarke J (1989) 'Principles and Applications of SQUIDs.' Proceedings of the IEEE, **77**, No. 8, 1208-1221.

[5.2] Hao L, Macfarlane J C and Pegrum C M, (1996) 'Excess Noise in $YBa_2Cu_3O_7$ Thin Film Grain Boundary Josephson Junctions and Devices' Supercond. Sci. Technol., **9**, 678-687.

[5.3] Gallop J C (1991) 'SQUIDs, the Josephson Effects and Superconducting Electronics' Adam Hilger Press, 80-83.

[5.4] Ed. Weinstock H,(1996) 'SQUID Sensors: Fundamentals, Fabrication and Applications' NATO ASI Series E: Applied Sciences, **329**, 7-16.

[5.5] Rogers C T and Buhrman R A, (1983) 'Conductance Fluctuations and Low Frequency Noise in Josephson Junctions.' IEEE Trans. on Magnetics, **MAG-19**, 453-457.

[5.6] Rogers C T and Buhrman R A, (1984) 'Composition of 1/f Noise in Metal-Insulator-Metal Tunnel Junctions' Phys. Rev. Lett., **53**, No. 13, 1272-1275.

[5.7] Koch R H, Eidelloth W, Oh B, Robertazzi R P, Andrek S A and Gallagher W J, (1992) 'Identifying the Source of 1/f Noise in SQUIDs Made From High-Temperature Superconductors.' Appl. Phys. Lett. **60**, No.4, 507-509.

[5.8] Faley M I, Poppe U and Urban K (1995) 'Noise Properties of Direct Current SQUIDs with Quasiplanar $YBa_2Cu_3O_7$ Josephson Junctions' Appl. Phys. Lett. **67**, No. 14, 2087-2089.

[5.9] Milliken F P, Brown S L and Koch R H (1997) 'Magnetic Field-Induced Noise in Directly Coupled High T_c Superconducting Quantum Interference Device Magnetometers' Appl. Phys. Lett. **71**, (13), 1857-1859.

[5.10] Foglietti V, Koch R H, Sun J Z, Laibowitz R B and Gallagher W J (1995) 'Characterising, Modelling, and Optimising High-T_c Superconducting Quantum Interference Devices' J. Appl. Phys. **77**, (1), 378-381.

[5.11] Huber M E, Cromar M W and Ono R H (1997) 'Excess Low-Frequency Noise in DC SQUIDs' IEEE Trans. on Appl. Supercond. **7**, (2), 2882-2885.

[5.12] Tesche C D and Clarke J (1977) 'dc SQUID: Noise and Optimisation' Journal of Low Temperature Physics, **29**, No's 3 and 4, 301-330.

[5.13] Sloggett J, Dart D L, Foley C P, Binks R A, Savvides N and Katsaros A (1994) 'Noise in Thin-Film YBCO Step-Edge Junction RF SQUIDs' Supercond. Sci. Technol. **7**, 260-264.

[5.14] Muck M (1997) 'Practical Aspects for SQUID Applications' Superlattices and Microstructures **21**, No. 3, 415-421.

[5.15] Ferrari M J, Johnson M, Wellstood F C, Kingston J J, Shaw T J and Clarke J (1994) 'Magnetic-Flux Noise in Copper Oxide Superconductors' Journal of Low Temperature Physics, **94**, No. 1-2, 15-61.

[5.16] Brake H J M, Aarnink W A M, van den Bosch P J, Hilgenkamp J W M, Flokstra J and Rogalla H. (1997) 'Temperature Dependence of the Effective Sensing Area of High-T_c dc SQUIDs' Supercond. Sci. Technol. **10**, 512-515.

[5.17] Clarke J (1983) 'Geophysical Applications of SQUIDs' IEEE Trans. on Magnetics, **MAG-19**, No.3, 288-294.

[5.18] Lubkin G B, (1995) 'Applications of High-Temperature Superconductors Approach the Marketplace' Physics Today, March 1995.

[5.19] Dantsker E, Tanaka S and Clarke J (1997) 'High T_c Super Conducting Quantum Interference Devices with Slots or Holes: Low 1/f Noise in Ambient Magnetic Fields' Appl. Phys. Lett. **70**, (15), 2037-2039.

[5.20] Selders P, Castellanos A M, Vaupel M and Wordenweber R (1998) 'Reduction of 1/f Noise in HTS SQUIDs by Artificial Defects' Submitted to IEEE Trans. on Appl. Supercond.

[5.21] Koch R H, Sun J Z, Foglietta V and Gallagher W J (1995) 'Flux Dam, a Method to Reduce Extra Low Frequency Noise when a Superconducting Magnetometer is Exposed to a Magnetic Field' Appl. Phys. Lett. **67**, (5), 709-711

[5.22] Fife A A, Anderson G, Angus V, Backhouse C, Betts K, Burbank M B, Cragg R A, Ferguson K, Habib F, Kubik K R, Nomura J, Smith M, Spear P, Westera W, Zhou H and Vrba J (1995) 'Noise Performance of High-T_c DC SQUID Magnetometers' IEEE Trans. on Appl. Supercond. **5**, (2), 3113-3118.

[5.23] Leslie K E, Macks L D, Foley C P, Macfarlane J C, Muller K-H and Sloggett G J. (1997) 'Noise Performance of High T_c rf SQUIDs in Ambient Magnetic Fields With and Without a Flux Dam.' IOP conference series no. 158, Paper presented at Applied Superconductivity, The Netherlands June 1997, 715-718.

[5.24] Muck M, Schone S and Heiden C (1997) 'Reduction of Low Frequency Excess Noise and Temperature Drift of SQUIDs by "Degaussing" Using High Frequency Magnetic Fields' IEEE Trans. on Appl. Supercond. **7**, (2), 3263-3266.

[5.25] Koch R H, Clarke J, Goubau W M, Martinis J M, Pegrum C M and Van Harlingen D J, (1983) 'Flicker (1/f) Noise in Tunnel Junction DC SQUIDs' Journal of Low Temperature Physics, **51**, 207-224.

[5.26] Camerlingo C, Castellano M G, Granata C, Monaco A, Russo M, Sarnelli E and Torrioli G, (1997) 'Bias Reversal Reduction of 1/f Noise in Sputtered YBCO Bicrystal dc-SQUIDs', IOP conference series no. 158, Paper presented at ASC the Netherlands 30 June-3 July 1997, 647-650.

[5.27] Zhang Y, He D F, Wolters N, Otto R, Barthels K, Zeng X H, Yi H R, Krause H-J, Braginski A I and Faley M I (1998) 'Radio Frequency Bias Current Scheme for dc Superconducting Quantum Interference Device.' Presented at ASC, Palm Dessert, Ca, USA, Sept 1998.

[5.28] Koch R H, Rozen J R, Sun J Z and Gallagher W J (1993) 'Three SQUID Gradiometer' Appl. Phys. Lett. **63**, (3), 403-405.

[5.29] Ilichev E, Schultze V, Ijsselsteijn R P J, Stolz R, Zakosarenko V and Hoenig H E (1999) 'Peculiarities of RF SQUID Response in Finite Magnetic Fields' Presented at 7th international superconducting electronics conference, 140-142.

[6.1] Clem T R, Overway D J & Purpura J W (1999) 'A high T_c superconducting gradiometer for mobile operation' Presented at 7th international superconducting electronics conference, 569-572.

[6.2] Braginski A I, (1999) 'Superconducting Electronics Coming to Market' IEEE Trans. Appl. Supercond. (Proc. ASC'98), 1-12.